BAYESIAN-BASED METHODOLOGY FOR PROGRESSIVE STRUCTURAL HEALTH EVALUATION AND PREDICTION BY USE OF MONITORING DATA

YOUWU WANG

Ph.D

The Hong Kong Polytechnic University

2017

The Hong Kong Polytechnic University

Department of Civil and Environmental Engineering

Bayesian-based Methodology for Progressive Structural Health Evaluation and Prediction by Use of Monitoring Data

Youwu Wang

A thesis submitted in partial fulfillment of the requirements for the degree of

Doctor of Philosophy

July 2017

Certificate of Originality

I hereby declare that this thesis is my own work and that, to the best of my knowledge and belief, it reproduces no material previously published or written, nor material that has been accepted for the award of any other degree or diploma, except where due acknowledgement has been made in the text.

_____ (Signed)

Youwu Wang (Name of student)

To my parents

Abstract

Despite the continuous evolution and development in the field of structural health monitoring (SHM), interpreting the huge amount of monitoring data from an SHM system to obtain useful information on structural conditions remains a challenge. Furthermore, due to the complexity of structures, measurement noise, inherent uncertainties in measured data and analytical methods, precise models which reflect the actual structural systems are difficult to create. In this regard, this thesis presents novel model-free data-interpretation methodologies within the Bayesian framework for structural health evaluation and prediction.

The first part of the thesis is aimed at conducting SHM-based structural condition assessment using Bayesian linear model (BLM) and Bayesian generalized linear model (BGLM). For condition assessment of bridge expansion joints, the relationship pattern between thermal movement of expansion joints and effective temperature of bridge deck is quantified using BLM and long-term monitoring data. The model parameters, model error and their associated uncertainties are estimated by analytical and simulation algorithms. With the established BLM, an anomaly index is defined to evaluate the failure probability of the expansion joints. The maximum and minimum displacements of the expansion joints under design extreme temperatures are predicted and compared with the design allowable values for validation. Then the BLM is extended to BGLM for assessing

wind-induced displacement responses of instrumented bridge. With the monitoring data of displacement and wind during typhoons, the correlation pattern between wind-induced displacement and wind speed/direction is explored. The crucial issue of optimizing model structure is dealt with by employing Bayesian model class selection, in terms of maximizing the log-likelihood function. Based on the established model, the bridge displacement responses and the associated confidence intervals under wind speed at serviceability limit state (SLS) are predicted and compared with the design allowable values for validation.

In the second part, Bayesian inference-based dynamical linear models (BDLM) are developed for prognosis and damage detection by using the time series of structural response. Firstly, different step ahead predictions by various models considering different component forms, such as trend, seasonal and regression components, are evaluated and compared in accordance with three model criteria. After the most suitable model is determined, a novel detection technique based on the forecasting of BDLM is proposed for local anomaly diagnosis. An index called Bayes factor is introduced for outlier detection. It is carried out by checking the current observation against the forecasting distribution (yielded from the BDLM at current moment) as well as against an alternative model (whose mean value is shifted by a prescribed offset). The detection rule is that if the alternative model better fits the actual observation, a potential outlier is detected. Then,

the logic of outlier detection is extended to distinguish between the single outlier and the appearance of a change through defining the cumulative Bayes factors, which can diagnose the anomaly of local component under extreme events or due to structural damage. Finally, Bayesian hypothesis testing is conducted by comparing the time series of structural response before and after the change point to make a judgement on whether the structure is healthy. Two case studies using the in-service monitoring data from a high-speed train and the data from a bridge benchmark problem are provided to show the applicability and effectiveness of the proposed method.

Publications

Journal Papers

Ni, Y. Q, and Wang, Y. W. (2017). "Bayesian structural model for damage diagnosis and prognosis under unknown noisy." *Engineering Structures*, under review.

Wang, Y. W., and Ni, Y. Q. (2017). "Bayesian approach for charactering and predicting wind-induced displacement response of bridge using structural health monitoring data." *Journal of Wind Engineering and Industrial Aerodynamics*, under review.

Ni, Y. Q., Lin, K. C., Wu, L. J., and Wang, Y. W. (2017). "Visualized spatiotemporal data management system for lifecycle health monitoring of large-scale structures." *Journal of Aerospace Engineering*, 30(2), B4016007-1-14.

Zhang, F. L., Ni, Y. Q., Ni, Y. C., and Wang, Y. W. (2016). "Operational modal analysis of Canton Tower by a fast frequency domain Bayesian method." *Smart Structures and Systems*, 17(2), 209-230.

Ni, Y. Q., Wang, Y. W., and Xia, Y. X. (2015). "Investigation of mode identifiability of a cable-stayed bridge: comparison from ambient vibration responses and from typhoon-induced dynamic responses." *Smart Structures and Systems*, 15(2), 447-468.

Niu, Y., Fritzen, C. P., Jung, H., Buethe, I., Ni, Y. Q., and Wang, Y. W. (2015). "Online simultaneous reconstruction of wind load and structural responses–theory and

application to Canton Tower." *Computer-Aided Civil and Infrastructure Engineering*, 30, 666-681.

Conference Papers

Wang, Y. W., Ni, Y. Q., and Wang, X. (2017). "Detection of performance of high-speed train wheels based on Bayesian dynamic model." *Proceedings of the 11th International Workshop on Structural Health Monitoring,* 12-14 September 2017, Stanford, California, USA.

Wang, Y. W., and Ni, Y. Q. (2017). "Bayesian dynamic linear model for real-time condition prediction." *Proceedings of the 8th Cross-Strait Summer School Workshop on Structural Monitoring and Vibration Control in Civil Engineering*, 21-26 August 2017, Hangzhou, China. (**Excellent Student Paper Award**)

Ni, Y. Q., and Wang, Y. W. (2016). "Bayesian approach for characterizing wind-induced displacement responses of bridge using structural health monitoring data." *Proceedings of the 24th Australian Conference on the Mechanics of Structures and Materials*, 6-9 December 2016, Perth, Australia.

Wang, Y. W., and Ni, Y. Q. (2016). "Bayesian approach for charactering the temperature-induced displacement of expansion joint." *Proceedings of the 7th Cross-Strait Summer School Workshop on Structural Monitoring and Vibration Control in Civil*

Engineering, 5-8 July 2016, Taipei, Taiwan.

Wang, Y. W., and Ni, Y. Q. (2015). "Correlation between displacement response and wind speed for an instrumented long-span bridge." *Proceedings of the 7th International Conference on Structural Health Monitoring of Intelligent Infrastructure*, 1-3 July 2015, Torino, Italy.

Ni, Y. Q., Wang, Y. W., and Xia, Y. X. (2015). "Using weigh-in-motion data to identify traffic loading on a long-span suspension bridge." *Proceedings of the 7th International Conference* on Structural Health Monitoring of Intelligent Infrastructure, 1-3 July 2015, Torino, Italy.

Ni, Y. Q., Wang, Y. W., and Song, S. D. (2014). "Field measurement of wind pressure distribution at a supertall structure above maximum gradient wind level." *Proceedings of SPIE 9061, Sensors and Smart Structures Technologies for Civil, Mechanical, and Aerospace Systems*, 11-12 March 2014, San Diego, California, USA.

Acknowledgements

First of all, I would like to express my sincere gratitude to my chief supervisor, Prof. Yi-Qing Ni, for his constant encouragement, valuable guidance and support throughout the whole study. I am lucky to share his vision, insight and passion in research. It is my honor to have the opportunity to have Prof. Ni as my advisor. I am very grateful to my co-supervisor, Dr. Dan Wang, for his generous support in my research.

I am grateful to Prof. Ka-Veng Yuen at University of Macau for his valuable suggestions on my research. I also wish to thank the members of the Examination Board, Prof. Chul-Woo Kim at Kyoto University (Japan), Dr. Peter W. Tse at City University of Hong Kong, and Dr. Songye Zhu at The Hong Kong Polytechnic University, for giving valuable comments to my thesis.

My appreciation also goes to Dr. Kai-Yuen Wong, formerly a senior engineer at the Highways Department of HKSAR Government, for providing valuable structural health monitoring data; Prof. Hui Li and Prof. Shun-Long Li at Harbin Institute of Technology (China) for generous sharing of their benchmark data and other research resources; colleagues at the National Rail Transit Electrification and Automation Engineering Technology Research Center (Hong Kong Branch) who provided the in-service monitoring data of a high-speed train.

My thanks also give to many friends met during my study in Hong Kong, and the

previous and current members of Prof. Ni's research group, whose warm friendship and kind support kept me going in my PhD study.

Finally, my deepest thanks go to my parents and sister, for their great love, support and encouragement.

This research is sponsored and supported by the PolyU PhD studentship and the RGC-GRF funding (project No. B-Q37Q). The financial supports are greatly acknowledged.

Contents

List of Figures

List of Tables

List of Abbreviations

AASHTO	American association of state highway transportation officials
ANN	Artificial neural network
BBN	Bayesian belief network
BDLM	Bayesian dynamic linear model
BGLM	Bayesian general linear model
BLM	Bayesian linear model
BPIC	Bayesian predictive information criterion
CD	Convergence diagnostic
CDF	Curvature damage factor
CPDF	Cumulative probability distribution function
DBN	Dynamic Bayesian network
DIID	Damage-induced inter-story deflection
DLV	Damage locating vector
ETDR	Electrical time domain reflectometry
FBG	Fibber Bragg grating
FE	Finite element
GPS	Global positioning system
GPS-OSIS	GPS on-structure instrumentation system
HKO	Hong Kong Observation
LANL	Los Alamos national laboratory
LLH	Log-likelihood
MAPE	Absolute percentage error
MC	Model curvatures

MCMC	Markov chain Monte Carlo
OLS	Ordinary least squares
PDF	Probability density function
RMSE	Root mean squared error
SD	Standard deviation
SHM	Structural health monitoring
SLS	Serviceability limit state
SMC	Structural monitoring and control
SNL	Sandia national laboratory
TKB	Ting Kau Bridge
TMB	Tsing Ma Bridge
TOC	Time of occurrence
TON	Time of notification
UCL	Uncertainty limit
WASHMS	Wind and structural health monitoring system

Chapter 1

Introduction

1.1 Research Motivation

The main objective of structural health monitoring (SHM) is to track the health condition of structures in order to prevent any catastrophic failure as well as to prolong the service life of engineered structures. The practical applications of the SHM technology to critical civil structures (such as high-rise buildings, long-span bridges), and transportation systems (such as rail and aircraft), have been increased in the past decades because of (i) the ability of SHM systems in offering continuous monitoring for detecting any adverse condition and evaluating structural durability, reliability and integrity; and (ii) the advances on sensing, communication and signal processing technologies (Dirbaz 2013). Successful implementations of long-term SHM systems to critical infrastructure systems have been increasingly reported. Most examples are on long-span bridges and high-rise buildings, such as the Confederation Bridge in Canada (Cheung *et al.* 1997), the Great Belt Bridge in Demark (Henrik and Denmark 2002), the Tsing Ma Bridge, Ting Kau Bridge, and Kap Shui Mun Bridge in Hong Kong (Wong 2004, 2007), and the Canton Tower (Ni *et al.* 2009) in the Chinese mainland. More applications can be found in the literature (Chang *et al.* 2003; Li *et al.* 2014; Annamdas *et al.* 2015; Seo *et al.* 2015; Li

and Hao 2016). A viable SHM system enables continuous measurement of loading environment and structural responses, providing a valuable tool for condition assessment and performance prediction of the instrumented structure. Research efforts have been made on damage detection, structural load-carrying capacity evaluation and remaining service life estimation with the use of long-term SHM data. These efforts span a broad range of research from tracking the change of structural characteristics for damage detection, to developing codified approaches for structural load-carrying capacity estimation, and to SHM-based reliability evaluation for forecasting structural remaining life (Seo *et al.* 2016). Simply put, all the efforts are made for structural health evaluation and prediction.

Structural condition assessment techniques can generally be categorized into physics-based and data-based methods, though a combination of them is usually employed (Farrar and Lieven 2007). The physics-based techniques are especially useful for making a prediction of structural responses to new system configurations or new loading conditions, while their computations are more complicated than data-based methods. Data-based assessment approaches depend on the previous measurements from the system to evaluate the current structural condition, typically by use of pattern recognition methods. Although the data-based assessment approaches are able to indicate the change in the presence of new system configurations or varying loading conditions, their performance on

classifying the nature of the change is poor. So perfecting the balance between the two assessment techniques is critical, whose principle will depend on the amount of available data and the level of confidence in forecast accuracy. After the current status of a structure is assessed, the prognosis problem will be addressed according to the goal of the prognosis. The most types of prognosis estimate how long the structure can continue in its safe use or how the structure will respond to the anticipated and unanticipated environments/loading such as extreme earthquakes.

However, most condition assessment and forecast methods may produce inexact and limited results in conjunction with field measurements because of (i) incompleteness of measured data, (ii) inherent uncertainties in measured data and analytical methods, (iii) measurement noise (Dirbaz 2013). These internal and external uncertainties created during design, construction and use, pose a great challenge to engineers/operators in charge of structure safety, operation and maintenance.

Stimulated by the challenges and limitations stated above, the efforts of this PhD work are to explore structural health evaluation and prediction of in-service structures using the measured responses and environments from the SHM systems, with an emphasis on dealing with uncertainty from a Bayesian perspective. This study starts with developing a Bayesian linear model (BLM) for condition assessment of bridge expansion joints with the use of long-term monitoring data of displacement and temperature. After

that, BLM is extended to Bayesian generalized linear model (BGLM), for the purpose of assessing wind-induced displacement with the monitoring data of displacement and wind data acquired during typhoons. Finally, Bayesian dynamic linear model (BDLM) is formulated for modeling the time-dependent structural responses. Based on the BDLM and Bayesian forecasting, a novel on-line change/damage detection method is developed and verified.

1.2 Research Objectives

This study is intended to investigate structural health evaluation and prediction of in-service structures based on SHM data in the Bayesian framework. The research objectives are as follows:

1. To formulate a Bayesian linear model (BLM) for condition assessment of bridge expansion joints. Using the long-term monitoring data from an SHM system, the relationship pattern between the thermal movement of expansion joints and the effective temperature of bridge deck is established, where the uncertainty is quantitatively described. It is then applied to forecast future movement of the expansion joints.
2. To formulate a Bayesian general linear model (BGLM) for assessing wind-induced displacement responses of bridges. With the monitoring data of displacement and

wind during typhoons, the correlation pattern between wind-induced displacement and wind speed/direction is developed for bridge condition assessment and prediction. In particular, model class selection approach is explored to determine the optimal model among numerous candidate models.

3. To propose a Bayesian dynamic linear model (BDLM) framework for modeling time-dependent structural response. The time series of structural response is modelled by assembling combinations of generic components, including local level/trend component, periodic component, and regression component. Then the formulated model is applied to forecast the structural behavior at one or several steps ahead beyond the current time.
4. To develop an on-line change/damage detection method based on BDLM and Bayesian forecasting. The change detection is carried out by checking the current observation against the current model (forecast distribution) and against an alternative model (whose mean value is shifted by a prescribed offset). To determine whether the observation is an outlier or the occurrence of change/damage, a special logic is developed. Then Bayesian hypothesis testing is conducted through comparing the time series of structural response before and after the change point to make a judgement on whether the structure is healthy.

1.3 Thesis Outline

This thesis consists of the following seven chapters:

Chapter 1 introduces the motivation for the present research, makes clear the objectives of research to be pursued, and states the structure of the thesis.

Chapter 2 presents the background of this research. The applications of the structural health monitoring (SHM) technology to civil structures are reviewed. Research efforts employing Bayesian probabilistic approaches to SHM are summarized and the limitations in these attempts are addressed.

Chapter 3 proposes a Bayesian linear model (BLM) for condition assessment of bridge expansion joints. Using the long-term monitoring data from an SHM system, Bayesian relationship between the thermal movement of bridge expansion joints and the effective temperature of bridge deck is formulated, in which the uncertainty is quantitatively characterized. With the formulated Bayesian model, an anomaly index is defined to evaluate the failure probability of the expansion joints. The maximum and minimum displacements of the expansion joints under design extreme temperatures are predicted and compared with the design allowable values for validation.

Chapter 4 presents a Bayesian generalized linear model (BGLM) for assessing wind-induced displacement response of bridges. With the monitoring data of displacement and wind during typhoons, the correlation pattern between wind-induced displacement and

wind speed/direction is formulated. The most suitable class of models is determined by the Bayesian model class selection techniques, which is then applied for bridge response prediction.

Chapter 5 presents a Bayesian dynamic linear model (BDLM) framework for modeling time-dependent structural response. The monitoring data of strain response is modelled by assembling combinations of generic components, such as local level/trend component, periodic component, and regression component, to account for the missing physical phenomena. Kalman filter, Kalman smoother and Gibbs sampling algorithms are applied to estimate the hidden state variables and model parameters for each component. Finally, the performance of the proposed model in forecasting structural behavior at different steps ahead are examined.

Chapter 6 presents a novel on-line change/damage detection method based on BDLM and Bayesian forecasting. The change/damage detection is carried out by checking the current observation against the current model (forecast distribution generated from the BDLM at current moment) and against an alternative model (whose mean value is shifted by a prescribed offset). The detection rule is that if the alternative model better fits the actual observation, a potential change/damage is indicated. To determine whether the current observation is an outlier or the beginning of a structural change, a special logic is developed by defining Bayes factors and cumulative Bayes factors. Then Bayesian

hypothesis testing is conducted through comparing the time series of structural response before and after the change point to make a judgement on whether the structure is healthy. The performance of the proposed method is verified with the monitoring data from an in-service bridge and an in-operation high-speed train.

Chapter 7 summarizes the major conclusions of this thesis and gives the recommendations for further research.

Chapter 2

Literature Review

2.1 Structural Health Monitoring of Civil Structures

Structural health monitoring is essential to evaluate the safety of critical infrastructure systems, such as high-rising buildings, larger-scale space structures and long-span bridges. It refers to the use of continuous field monitoring and analyses of environmental and structural parameters under operation conditions, for the purpose of warning abnormal states or accidents at an early stage to avoid casualties and providing maintenance advice (Hoursner *et al.* 1997; Li *et al.* 2014). Over the past decades, long-term SHM systems had been increasingly implemented on civil structures worldwide. Most applications were on long-span bridges, such as the Confederation Bridge in Canada (Cheung *et al.* 1997), the Commodore Barry Bridge in United States (Barrish *et al.* 2000), the Akashi Kaikyo Bridge in Japan (Kashima *et al.* 2001), the Singapore-Malaysia second link bridge (Brownjohn and Moyo 2001), the Great Belt Bridge in Demark (Henrik and Denmark 2002), the Tsing Ma Bridge, Ting Kau Bridge, and Kap Shui Mun Bridge in Hong Kong (Wong 2004, 2007), the Sutong Bridge in the Chinese of mainland (Ni *et al.* 2004), the Jindo Bridge in South Korea (Jang *et al.* 2010). Applications of SHM systems to high-rise buildings were also widely reported. For example, the Republic Plaza in Singapore

(Brownjohn *et al.* 1998), the Marco Polo tension leg platform in United States (Dijk and Boom 2007), the Canton Tower (Ni e*t al.* 2009) and Shanghai Tower (Zhang *et al.* 2015) in the Chinese mainland, the San Siro Meazza stadium in Italy (Cigada *et al*. 2010), the Toyosu Building in Japan (Takao and Takao 2015). The applications of the SHM technology to other infrastructure systems can be found in the literature (Chang *et al.* 2003; Li *et al.* 2014; Annamdas *et al.* 2015; Seo *et al.* 2015; Li and Hao 2016). Different from traditional non-destructive evaluation techniques, SHM systems enable real-time and long-term monitoring of a structure. In connection with SHM systems, research efforts have been mainly focused on damage detection, structural load-carrying capacity evaluation, and remaining service life estimation of structures. These efforts span a broad range of data processing approaches from tracking the change of structural characteristics to SHM-based reliability assessment for forecasting structural remaining life (Seo *et al.* 2016). Typical SHM methods are reviewed in the following.

2.1.1 Damage detection

Damage can be defined as changes in structural characteristics that make adverse effects to structural integrity (Farrar and Worden 2007). The structural characteristics parameters are functions of the physical properties of a structure, including structural mass, stiffness and damping. Therefore, change in those physical properties will cause

the change of structural characteristics parameters. Based on this principle, the damage detection algorithms are devoted to detecting the change in structural characteristics parameters through the structural responses measured from an array of sensors linked into the SHM system. There have been a great number of investigations on developing damage detection algorithms in line with on vibration and strain measurement (Peeters *et el.* 2001; Lee *et al.* 2007; Magalhães *et al.* 2008, 2010; Phares *et al.* 2013 a, b).

2.1.1.1 Vibration-based damage detection

1) Natural frequencies

Based on the vibration measurement by an SHM system, extensive research works have been devoted to damage detection based on detecting changes of the dynamic characteristics parameters, such as natural frequency, modal shape curvature, modal strain energy, dynamic flexibility and others (Seo *et al.* 2016). Among the dynamic characteristic parameters, natural frequency is recognized as one of the most obvious indicators in detecting damage occurrence. Over the past decades, many investigators have studied using the change in natural frequencies to detect damage of structures (Gawley and Adams 1979; Kato and Shimada 1986; Farrar *et al.* 1994; Peeters and De Roeck 2001; Kullaa 2003; Teughels and De Roeck 2004; De Roech and Reynders 2009; Mekjavić 2015).

Gawley and Adams (1979) were among pioneers to develop vibration-based damage detection procedures. They developed a damage detection method coupled with analytical techniques to detect, locate and quantify damage by using the change in natural frequencies.

In 1986, Kato and Shimada performed the first vibration-based SHM test on a prestressed concrete bridge. During the bridge failure test, vibration measurement was carried out in vertical and horizontal directions and the change of natural frequencies at each damage stage was examined. It was found that the natural frequency of the first vertical bending mode decreased rapidly as the static load increased to the ultimate load.

Another important work on damage detection using vibration monitoring data was carried out on I-40 Bridges over the Rio Grande (Farrar *et al.* 1994). Because the I-40 Bridge was to be razed, the investigators were able to introduce simulated fatigue cracks into this structure in order to verify various damage identification methods and observe the change in load paths. Researchers from Los Alamos National Laboratory (LANL) and Sandia National Laboratory (SNL) carried out this SHM test. They introduced four different damage states on the bridge by continually cutting the web and bottom flange of the steel girder at the mid-span of the bridge and investigated the change in nature frequencies. It was observed that the frequency changes were not precisely proportional

to the changes in structural stiffness. A large number of follow-up studies have utilized the data obtained from the bridge to assess the capabilities of various damage detection algorithms (Farrar and Jauregui 1998; Kim and Stubbs 2003; Wang and Ong 2010).

Another significant work on modal and damage identification based on vibration data from the Z24 bridge in Switzerland was performed by Peeters and De Roeck (2001). They established black-box models to describe the variation of natural frequencies as a function of temperature based on the data from the bridge. If the measured frequency exceeds certain confidence intervals, it is more likely another cause than temperature that drives the frequency variation, which implies a damaged status. After that, many other follow-up studies have used the data from this bridge to assess the capability of various damage detection methods (Kullaa 2003; Teughels and De Roeck 2004; De Roech and Reynders 2009).

Mekjavić (2015) developed a structural damage detection approach for bridges using only the change of natural frequencies. To demonstrate the capability of the proposed method, numerical simulation and experiment of a concrete girder bridge were carried out through incrementally applying static load. It was shown that the proposed method can accurately locate damage and predict the extent of damage using the high-frequency vibrational responses.

2) Mode shape curvature

Mode shape curvature has been recognized as a good candidate for damage detection of structures. Abdel Wahab and De Roeck (1999) investigated using the change in modal curvature (MC) to detect damage in a prestressed concrete bridge, the Z24 bridge. At first, a theoretical study using simulated data for a simple continuous beam was conducted and a damage indicator called "curvature damage factor (CDF)" was defined. Then the technique was further applied to the Z24 bridge.

Guan *et al.* (2007) performed the implementation of a long-term SHM system on a FRP highway bridge and used vibration-based techniques for damage detection. The mode shape curvature was extracted from the ambient vibration to detect localized damage in the structure. In addition to damage detection, finite element model was updated by using measured frequencies to better represent the true properties of the structure.

Recently, Frans *et al.* (2017) made a comparative study of the mode shape curvature and damage locating vector methods for diagnosing structural damage. In their study, three type of structures (shear building, beam-type and plane truss structures) and several damage scenarios were considered in numerical simulation. The simulation result showed that mode shape curvature was suitable for beam structures but not for truss structures, while the damage locating vector method was appropriate to locate damage of truss

structures.

3) Modal strain energy

Structural damage detection using modal strain energy is one of the most efficient and reliable structural health evaluation techniques (Doebling *et al.* 1997; Shi *et al.* 1998, 2000; Yan *et al.* 2010, 2012; Moradipour e*t al.* 2015). Doebling et al. (1997) proposed an approach based on modal strain energy in conjunction with finite element (FE) model to select the subset of identified vibration modes for structural damage detection. It was shown that using the maximum modal strain energy provides more accurate updating results than using the minimum modal frequency.

Shi *et al.* (2000) presented a modal strain energy change-based method to realize structural damage location identification and damage magnitude quantification. The performance of the proposed method was validated by numerical simulation and experiment on a single-bay, and two-story portal steel frame structure. Their results indicated that the modal strain energy change is noise sensitive, but it can localize single and multiple damage and quantify the damage.

Moradipour *et al.* (2015) proposed an improved modal strain energy method and investigated its effectiveness by applying it to a fix-end beam and a three-story frame with single and multiple damage. The derived mode shapes of the intact structure and damaged structure at each damage level were separately used in the improved formulation to

determine the damage location and magnitude.

4) Dynamic flexibility

Apart from the aforementioned modal parameters, the change in dynamic flexibility is also capable of detecting the presence of damage. Pandey and Biswas (1994, 1995) proposed an approach based on changes in the flexibility matrix of a structure, which can be easily and accurately estimated from the several lowest modes of vibration of the structure, to identify and locate damage. The difference in flexibility matrix before and after the occurrence of damage was treated as an indicator to locate the damage.

Catbas *et al.* (2006) presented the modal flexibility-based displacement profile as an index for damage detection. Firstly, the modal flexibility was determined from the frequency response function measurements of the structure, and then it was employed to obtain the deflection profile. To demonstrate the effectiveness of this approach, two real-life bridges (a steel stringer bridge in Cincinnati and a posttensioned concrete box girder bridge in Switzerland) with different damage scenarios were selected as test beds.

Ni *et al.* (2008) proposed an index in terms of relative flexibility change coupled with three-dimensional (3D) finite element model to locate damage. The capability of this approach for damage location on the Ting Kau Bridge (a cable-stayed bridge in Hong Kong) was examined by investigating various damage scenarios, and taking into account measurement noise as well as two ambient factors (temperature and traffic loading).

Scianna and Jang (2011) presented a model-free modal flexibility procedure to identify structural damage and investigated its capability by application to a laboratory scale girder bridge under constant temperature and an in-service highway bridge under ambient loading conditions.

Sung *et al.* (2014) applied a damage detection algorithm for cantilever beam-type structures, which used the damage-induced inter-story deflection (DIID) derived from modal flexibility matrix to locate damage. This approach has a clear theoretical base and can locate the damage without need of a finite element model. For validating its effectiveness, a series of numerical and experimental studies on a 10-story building were carried out. It was observed that the proposed approach can successfully detect the damage locations for both single- and multiple-damage scenarios.

2.1.1.2 Strain-based damage detection

In parallel with the development of vibration-based identification techniques, recently emerged some studies which use time domain approaches coupled with strain measurements for structural damage detection. The basic principle of strain-based detection techniques is that the change of structural physical properties will cause a change in magnitude of strain responses. Although there have been a significant number of studies on vibration-based damage detection, only a few studies have attempted to

detect structure damage using strain-based identification methods (Seo *et al.* 2015).

Lin and Thaduri (2005) investigated the electrical time domain reflectometry (ETDR) distributed strain sensing technique for damage detection. Its capability was demonstrated by application to a small-scale concrete beam with an imbedded ETDR distributed strain sensor. It was shown that the embedded ETDR sensor not only can identify load-induced damage at early stage, but also locate single and multiple damage positions simultaneously along a single sensing line.

Jang *et al.* (2007) developed a strain damage locating vector (DLV) method combing static strain measurement and DLV to identify possible damage location. A series of numerical simulations and experiments were carried out to verify the effectiveness of the proposed strain DLV method and the results showed that it can locate the damage successfully.

Phares *et al.* (2013) performed a field validation for a strain-based statistical damage detection algorithm on the Iowa Bridges in U.S. In place of actual damage on the bridge, two sacrificial specimens that simulate damage-sensitive locations were installed on the bridge, and diverse levels and types of damage were imposed on the specimens. It was shown that the algorithm was able to accurately identify the damage by using strain data collected from sensors on the sacrificial specimens.

Xu *et al.* (2013) performed a damage detection strategy based on distributed strain

responses measured by long-gauge fiber Bragg grating (FBG) sensors. The distributed strain mode was first derived via the frequency response function of the distributed strain responses and then an index named strain mode residual trend was developed using strain statistical tendency analysis and confidence probability.

Recently, Hong *et al.* (2016) proposed a damage-assessment method based on long-gauge strain response resulting from moving vehicular loads on bridges. Numerical simulation, laboratory experiments and field testing of a real bridge (Kawane Bridge in Japan) were carried out to demonstrate the applicability of the proposed method. The macrostrain-based damage index was sensitive to local damage covered by gauge length of the long-gauge strain sensors and less affected by measurement error.

2.1.2 Structural load-carrying capacity and remaining life estimation

In addition to SHM-based damage detection algorithms, SHM systems have also been used to evaluate structural load-carrying capacity and remaining life in real time. One of the typical methods for structural load carrying capacity estimation is using load rating concept. For example, the American Association of State Highway Transportation Officials (AASHTO) Manual for Bridge Evaluation (2010) provides guidelines to engineers on how to evaluate the bridge load rating for determination of the live load carrying capacity. Based on the documented guidelines, the calculation load rating relies

on using a sophisticated finite element model calibrated with field data or reliability analysis using SHM data.

Turer and Shahrooz (2011) investigated the different levels of analytical modeling (1D, 2D and 3D models) on the sensitivity of load rating in conjunction with experimental studies conducted on an actual bridge. Both dynamic data and static deformed profile information were collected to calibrate the analytical model at different stages, and the finding showed that 2D-grid models can successfully simulate the critical members.

Davids *et al.* (2012) presented an approach based on finite element analysis specifically for load rating of flat slab concrete bridges. The designed FE software formulation and convergence were verified by comparing with the known analytical solutions and the predictions from commercial FE software under realistic loading scenarios. To assess the applicability of the FE modeling strategy, the load ratings obtained by FE model analysis were compared with the results of load tests and the predictions from AASHTO approximate analysis.

Seo *et al.* (2013) described a load rating protocol coupled with a strain-based SHM system for the generation of multiple rating distributions for highway steel I-girder bridges. The strain time history data were used to calibrate finite element models according to two load scenarios: known and unknown trucks, and then the refiled FE models were adopted to calculate the multiple load rating distributions, which finally

were combined into a single holistic distribution. For verification of the proposed protocol, the distribution was compared with the results calculated from a rating package that was in use in Iowa Department of Transportation.

In addition to the evaluation of load rating based on finite element models, newly emerging methods using various reliability techniques in conjunction with load test data or field monitoring data from SHM systems have been reported (Akgül and Frangopol 2003, 2004; Bhattacharya *et al.* 2005). Akgül and Frangopol (2004) investigated the interaction between the reliability index and rating factor for various bridge types at different limit states and applied the reliability-based evaluation technique to a group of 14 bridges in a bridge network. Bhattacharya *et al.* (2005) presented a probability-based method for determination of bridge load rating using site-specific structural response. This method is able to eliminate a majority of live-load modeling uncertainties, and can be applied to determine load rating for various projected time intervals and limit states (yield and ultimate).

Estimating the remaining life of bridges is a significant element in long-term bridge performance management. However, only a few researches have focused on estimating the remaining life of bridges by using long-term monitoring data from SHM systems. Frangopol *et al.* (2008) presented an approach for incorporating the monitoring data from an SHM system to assess structural reliability and illustrated it on Lehigh River Bridge

SR-33 (a steel truss bridge). Recently, Hajializadeh *et al.* (2017) presented a framework for virtual monitoring of steel bridges and applied it in a cable-stayed bridge in Netherlands to calculate the fatigue damage and assess the remaining life. The virtual SHM system refers to that all components of the bridge are not monitored directly, but rather using the load information and a calibrated FE model. The validated numerical model coupled with actual site traffic loading can provide a satisfactory prediction of the accumulative fatigue damage.

2.2 Bayesian Approach

2.2.1 Overview of Bayesian approach

Probability is a useful tool to express the likelihood of an occurrence of an event. It has been extensively applied in many areas of science, such as natural sciences, social sciences and medical science, for decision making, forecasting and stochastic structure exploration. In the field of probability theory, there are two kinds of interpretations for the probability of an event. One is called "frequency" probability, the other is "Bayesian" probability (Ando 2010). The core difference is that frequency consider probability to be a property of the physical world, whereas Bayesians consider probability to be a measure of uncertainty regarding their knowledge of the physical world (Stone 2013). More

detailed discussions on the differences between the Bayesian and frequentist approaches can be found in Gill (2014).

Bayesian estimation and inference has a number of advantages in statistical modeling and data analysis. It provides a rational approach for updating beliefs in light of new information. The process of inductive learning via Bayes' rule is referred to as Bayesian inference. The result of combining the prior information and observed data in this way is the posterior distribution. In other words, the posterior is proportional to the prior times likelihood (function for observed data). If the prior information is vague, then it will have negligible weight in the posterior, and the posterior will in effect be dominated by the data information. Similarly, as more and more data obtained, the weight of data information relative to the prior increases, and again the posterior effectively relies on the information in data. Once the data provide conclusive evidence, there is essentially no room left for subjective opinion (prior information) (O'Hagan 2004).

In addition to the formal interpretation as a means of induction, Bayesian approach also provides: (i) parameter estimates with good statistical properties; (ii) parsimonious descriptions of observed data; (iii) predictions for missing data and forecasts of future data; and (iv) a computational framework for model estimation, selection and validation (Hoff 2009).

2.2.2 Bayesian methods in SHM

Bayesian methods have been widely used in a variety of areas since the pioneering work by Thomas Bayes (1763) and the significant contribution by Jeffreys (1961), Cox (1961) and Jaynes (1968, 1974, 2003). In diverse disciplines of social sciences, natural sciences and engineering, Bayesian methods have been developed and widely applied, especially in statistical physics (Jaynes 1974, 2003), finance (Rachev 2008), social and behavioral sciences (Gill 2014), marketing (Rossi *et al.* 2012), econometrics (Zellner 1996), medical sciences (Woodworth 2004), computer sciences (Lee 2007), and civil engineering (Yuen 2010) among others.

Bayesian approach is very useful for civil structures because there are many types of modeling and parametric uncertainty in structural problems. Since the first trial of combination of Bayesian approach and SHM conducted by Beck (1989), Bayesian approach began to attract the attention of researchers in SHM. The studies have mainly focused on two purposes: model updating and system identification (Yuen 2010). One goal is to identify structural parameters, such as stiffness, frequencies, mode shapes. These identified parameters can be used as an indicator for the status of the structure or a damage index. For example, the frequencies of a structure can be monitored from time to time and an abnormal value indicates possible damage of the structure. However, this change may be caused by uncertainty. So it is necessary to quantify the uncertainty and

narrow the distributions of the frequencies to distinguish whether the change is due to deterioration of the structure. Another purpose is to obtain a mathematical model to represent the underlying system for future prediction. There are also parameters to be identified, but these parameters may not be physical, such as the coefficients of regress models. These identified parameters are used only to provide an accurate prediction of system output. Nevertheless, quantifying the uncertainty of parameters is also necessary for further processing.

The first application of Bayesian approach in SHM can be traced back to Beck (1989), where a Bayesian statistical framework was applied to system identification that selects the optimal model from a series of candidate models based on its input/output measurement. Sohn and Law (1997) presented a Bayesian probability approach for damage detection which was not only able to detect the most likely damage locations but also the number of damage locations in a structure. Beck and Katafygiotis (1998) addressed the problem of updating a structural model and its associated uncertainties by using dynamic response data. In the Bayesian statistical framework, the most probable/optimal model was selected for response predictions at prescribed dynamic loadings. Vanik *et al.* (2000) presented a Bayesian probabilistic method for structural health monitoring, where the probability density function for the model stiffness parameters conditional on measured modal data was developed and then applied to

calculate the damage probability.

Lam *et al.* (2006) proposed an artificial neural network (ANN) design method based on Bayesian probabilistic approach, where the number of hidden layers and neurons was selected by the Bayesian model class selection approach. Then the Bayesian ANN design algorithm in conjunction with pattern recognition method formed a practical SHM strategy. Later, Lam and Ng (2008) extended the Bayesian ANN design method to cover the selection of activation functions for neurons in the hidden layers. In the case study, damage-induced changes in Ritz vectors and modal parameters were separately utilized as pattern features to train ANNs and the Bayesian ANN design method was employed to select the most suitable class of ANN models.

Arangio and Beck (2012) developed a two-step Bayesian procedure in which the probability logic approach was applied to neural network models for identification and quantification of damage in a suspension bridge. In the first step, the occurrence of damage was detected; and in second step, the specific damage element was identified and the intensity of damage was quantified.

Sankararaman and Mahadevan (2013) developed a Bayesian approach to continuously quantify and update the uncertainty in terms of three steps, that is damage detection, damage localization, and damage quantification. Finally, the uncertainties in the three steps were combined to determine the PDF of the damage parameter. The

method was illustrated in regard to a frame structure and a hydraulic actuation system.

Au (2011, 2012) proposed a Fast Bayesian FFT method and its improved version for output-only modal identification, in which uncertainties associated with the modal parameters can be quantitatively assessed. Au *et al.* (2011, 2012a, 2012b, 2013) assessed the most probable values of the identified mode shapes by the Bayesian approach, addressed the uncertainties of modal properties from both frequentist and Bayesian perspectives, and discussed the implementation issues of the proposed Fast Bayesian FFT method for field applications.

Arangio and Bontempi (2015) presented a Bayesian neural network for damage detection and investigated its applicability to a cable-stayed bridge which was proposed as a benchmark problem by Asian-Pacific Network of Center for Research in Smart Structure Technology. The proposed method was able to detect anomalies of the structure with the monitoring vibration data acquired before and after damage.

Huang and Beck (2015) proposed a hierarchical sparse Bayesian learning methodology for computing the probability of localized stiffness loss induced by damage, which employs modal parameters as extra variables for Bayesian model updating.

Dzunic *et al.* (2017) applied the recently developed switching Bayesian model to the problem of automatic damage detection. Based on a state-space approach, the model was derived from a set of measurement data without the corresponding physical information,

and the change of the model parameters served as an indicator of damage.

In addition to the aforementioned Bayesian methods for modal identification and damage detection, Bayesian model updating has been addressed for structural strength and reliability predictions (Geyskens *et al.* 1998; Enright and Frangopol 1998, 1999; Zhang and Mahadevan 2000; Ching and Leu 2009; Stewart 2010; Ma *et al.* 2013, 2014). Geyskens *et al.* (1998) proposed a predictive model for a specific concrete mix based on Bayesian theory, which accounted for all sources of model uncertainty and dealt with the important issue of model-induced correlation. Enright and Frangopol (1998, 1999) proposed a time-variant bridge reliability estimation algorithm for deteriorating concrete bridges in a Bayesian framework. Through combining the information from both inspection data and engineering judgment, the approach can be used in a rational manner to better predict future bridge conditions. Zhang and Mahadevan (2000) proposed a Bayesian procedure to quantify the modeling uncertainty using nondestructive inspections and applied it to a fatigue reliability problem. Ching and Leu (2009) developed a Bayesian framework for estimating time-varying reliabilities of civil infrastructure facilities under the circumstance that only condition-state data of components were available, and applied it to assess the reliability of a hydraulic gate system. Yuen and Kuok (2010) developed a systematic approach for reliable health assessment of reinforced concrete buildings by modeling and quantifying the

environmental influence on modal frequencies using the Bayesian spectral approach and the Bayesian modal class selection approach. Ma *et al.* (2013, 2014) proposed an approach for predicting the remaining bridge strength by integrating Bayesian network and in-situ load testing, which accounted for uncertainty of important factors on corrosion damage, stiffness degradation, and load-deflection response. Rafiq *et al.* (2015) presented a condition-based deterioration modeling methodology for bridges using Bayesian belief network (BBN) and dynamic Bayesian network (DBN), in which the predictions of the deterioration rates for the bridges were able to be updated in light of data obtained from the monitoring, inspection or maintenance actives.

2.3 Remarks

In summary, a significant number of studies have focused on structural damage detection, structural load-carrying capacity estimation, reliability analysis and remaining life prediction, etc., based on the obtained data from SHM systems. No matter what kind of methodology applied in these studies, most of them are related to structural elements or structural parameters. It is well known that a precise structural model accurately reflecting the real behavior of an in-service structure is difficult to create due to the uncertainty inherent in complex civil structures. Moreover, model-based methods may not identify structural damage successfully. By contrast, there is limited literature on

developing completely data-driven models in the context of Bayesian methodology for structural health evaluation and prediction, especially the model-free data interpretation methods which accommodate time-series response data. The model-free data interpretation methodology is applicable to diverse types of structures since no geometrical and material information is required.

Chapter 3

SHM-based Condition Assessment of Bridges Using BLM

3.1 Introduction

A lot of research efforts have been given on model updating by use of a mass of measurement data acquired from SHM systems (Beck *et al.* 2001; Sohn and Law 2001; Figueiredo *et al.* 2014; Lam *et al.* 2015). Among various model updating techniques, Bayesian model updating techniques can not just find the most plausible model but also quantify the probability of the model parameters conditional on the measurement data. Inheriting this appealing advantage, Bayesian model updating methods are robust and suitable to characterize modeling uncertainties of structural systems (Ching *et al.* 2005). However, the application of Bayesian methods in civil engineering are still in its infancy; there is great potential for exploration (Yuen 2010). Herein, we focus on applying Bayesian approach for condition assessment of bridge expansion joints with the use of long-term monitoring data from an SHM system.

Expansion joints are important components in bridge structures, which are designed to accommodate the relative movement between bridge deck and abutments, ensuring the serviceability of bridges. Due to the direct and repetitive impact of vehicle loads, expansion joints often become the weakest part of bridges, especially for long-span

bridges with observed premature failures, resulting in considerable repair and maintenance costs (Roeder 1998; Chang and Lee 2002; Lima and Brito 2009; Guo *et al.* 2014). For example, the expansion joints in the Runyang Suspension Bridge in China (1,490 m) had been repaired only two years after the bridge was opened to traffic; for the Jiangyin Suspension Bridge in China (1,385 m), excessive wear and transversal shear failure of bearings in expansion joints were observed after 3 to 4 years of service (Guo *et al.* 2014); the expansion joints in the Martinus Nijhoff Bridge had been repaired several times in recent years (Coelho *et al.* 2013). These premature failures of expansion joints call for a better understanding of the mechanism of failure.

The implementation of structural health monitoring (SHM) systems enable to gain substantial information of the field performance of bridges, and to foresee the possible failure of expansion joints in an early stage. Based on the long-term monitoring data from an SHM system, research efforts have been devoted to condition assessment of bridge expansion joints. Ni *et al.* (2007) established a normal correlation pattern between the effective temperature and thermal movement for predicting the extreme displacement. Ding and Li (2011) assessed the bridge expansion joints using the long-term displacement under changing environmental conditions (considering changes in temperature and traffic load). Guo *et al.* (2014) analyzed the expansion joints displacement of a long-span steel bridge equipped with viscous dampers, with an emphasis on the influence of viscous

dampers. In these studies, the relationship models between temperature and displacement were formulated with certain coefficients. However, there are various uncertainties involved in the movement of expansion joints; so a more feasible approach is to formulate an optimal model with uncertainty coefficients based on the system input-output data. Bayesian approach is the best choice. In this chapter, Bayesian linear regression model is developed to explore the correlation pattern between the displacement of expansion joints and effective temperature of bridge deck for condition diagnosis and prognosis.

3.2 Bayesian Linear Model (BLM)

3.2.1 Modeling framework

Suppose we have n sets of independent observations $\{(y_{\alpha,}\ x_{\alpha}), \alpha = 1,2,\dots,n\}$, where y_{α}'s are random response variables and x_{α}'s are vectors of k-dimensional explanatory variables $(x_{\alpha 1},\dots,x_{\alpha k})$. The linear regression model of the relationship between the response variables and explanatory variables is expressed as

$$y_{\alpha} = \beta_1 x_{\alpha 1} + \beta_2 x_{\alpha 2} + \cdots + \beta_k x_{\alpha k} + \varepsilon_{\alpha}\ , \qquad \alpha = 1,\cdots,n \tag{3.1}$$

where ε_{α} is an error term. This model can be expressed compactly in matrix form by defining the following vectors and matrix

$$y = \begin{bmatrix} y_1 \\ y_2 \\ \vdots \\ y_n \end{bmatrix}, \qquad \beta = \begin{bmatrix} \beta_1 \\ \beta_2 \\ \vdots \\ \beta_k \end{bmatrix}, \qquad X = \begin{bmatrix} x_{11} & x_{12} & \cdots & x_{1k} \\ x_{21} & x_{22} & \cdots & x_{2k} \\ \vdots & \vdots & \ddots & \vdots \\ x_{n1} & x_{n2} & \cdots & x_{nk} \end{bmatrix}, \qquad \text{and } \varepsilon = \begin{bmatrix} \varepsilon_1 \\ \varepsilon_2 \\ \vdots \\ \varepsilon_n \end{bmatrix}$$

and written as

$$y = X\beta + \varepsilon \tag{3.2}$$

3.2.2 Likelihood function

Assume the error term ε has a multivariate normal distribution with mean 0_n and covariance matrix $\sigma^2 I_n$, where 0_n is an *n*-vector with all elements being 0 and I_n is a $n \times n$ identity matrix. Its notation is $\varepsilon \sim N(0_n, \sigma^2 I_n)$. Using the definition of multivariate normal distribution, the likelihood function can be written as

$$f(y|X, \beta, \sigma^2) = \frac{1}{(2\pi\sigma^2)^{n/2}} \exp\left[-\frac{(y - X\beta)^T (y - X\beta)}{2\sigma^2}\right] \tag{3.3}$$

Here the likelihood function is expressed as the joint probability density function for all data conditional on the unknown parameters β and σ^2.

For convenience of further derivations, we rewrite the likelihood in a different form. It can be shown that (Koop 2003)

$$(y - X\beta)^T (y - X\beta) = as^2 + \left(\beta - \hat{\beta}\right)^T X^T X (\beta - \hat{\beta})$$

where

$$a = n - k$$

$$\hat{\beta} = (X^T X)^{-1} X^T y$$

$$s^2 = \frac{(y - X\hat{\beta})^T (y - X\hat{\beta})}{a}$$

$$b = as^2$$

It is noted that $\hat{\beta}$, s^2 and a are the Ordinary Least Squares (OLS) estimator for β, standard error, and degrees of freedom, respectively. As such, the likelihood function can be written as

$$f(y|X,\beta,\sigma^2) = \frac{1}{(2\pi)^{n/2}} \left\{ \frac{1}{\sigma^k} exp\left[-\frac{1}{2\sigma^2} \left((\beta - \hat{\beta})^T X^T X (\beta - \hat{\beta}) \right) \right] \right\} \times \left\{ \frac{1}{\sigma^a} exp\left[-\frac{b}{2\sigma^2} \right] \right\} \tag{3.4}$$

3.2.3 Prior selection

The prior information is a basic aspect of Bayesian inference, which reflects the prior knowledge of the phenomenon before seeing the data. Though there are numerous forms of priors, it is common to use the specific priors that are easy for calculation. Natural conjugate prior has such advantages. A conjugate prior distribution, when combined with the likelihood, can yield a posterior that keeps the same type of distribution with the prior.

In the linear regression model, we elicit a prior for β and σ^2 which is denoted by $p(\beta, \sigma^2)$. The posterior density for β and σ^2 will be denoted by $p(\beta, \sigma^2|y, X)$, which means the posterior density is conditional on the data. The form of Equation (3.4) suggests that the natural conjugate prior is Normal Inverted-Gamma distribution. More specifically, a prior for β conditional on σ^2 is a normal distribution and a prior for σ^2 is an

Inverted-Gamma distribution. It proves convenient to write

$$p(\beta, \sigma^2) = p(\beta|\sigma^2)\ p(\sigma^2) \tag{3.5}$$

with

$$p(\beta|\sigma^2) = N(\beta_0, \sigma^2\sum_0) = \frac{1}{(2\pi\sigma^2)^{k/2} \cdot |\sum_0|^{1/2}} \exp\left[-\frac{(\beta-\beta_0)^T\sum_0{}^{-1}(\beta-\beta_0)}{2\sigma^2}\right]$$

$$p(\sigma^2) = IG\left(\frac{a_0}{2}, \frac{b_0}{2}\right) = \frac{\left(\frac{b_0}{2}\right)^{a_0/2}}{\Gamma\left(\frac{a_0}{2}\right)} (\sigma^2)^{-a_0/2-1} \exp\left(-\frac{b_0}{2\sigma^2}\right)$$

where $\sum_0$ is a symmetric positive definite matrix of size $k \times k$.

3.2.4 Posterior distribution

The posterior distribution for the unknown parameters can be derived by multiplying the likelihood (Equation (3.3)) and the prior distribution (Equation (3.5)),

$$\begin{aligned} p(\beta, \sigma^2|y, X) = &\ p(y|X, \beta, \sigma^2) \cdot\ p(\beta, \sigma^2) \\ &\propto (\sigma^2)^{-n/2} \exp\left[-\frac{(y-X\beta)^T(y-X\beta)}{2\sigma^2}\right] \\ &\times (\sigma^2)^{-k/2} \exp\left[-\frac{(\beta-\beta_0)^T\sum_0{}^{-1}(\beta-\beta_0)}{2\sigma^2}\right] \\ &\times (\sigma^2)^{-a_0/2-1} \exp\left(-\frac{b_0}{2\sigma^2}\right) \end{aligned} \tag{3.6a}$$

Combining these densities and the joint posterior gives

$$\begin{aligned} p(\beta, \sigma^2|y, X) \propto &\ (\sigma^2)^{-k/2} \exp\left\{-\frac{1}{2\sigma^2}\left(\beta^T\left[X^TX + \sum_0{}^{-1}\right]\beta\right.\right. \\ &\left.\left. - 2\beta^T\left[X^Ty + \sum_0{}^{-1}\beta_0\right] + y^Ty + \beta_0{}^T\sum_0{}^{-1}\beta_0\right)\right\} \\ &\times (\sigma^2)^{-(a_0+n)/2-1} \exp\left(-\frac{b_0}{2\sigma^2}\right) \end{aligned} \tag{3.6b}$$

Completing the square obtains the following expression of posterior distribution

$$p(\beta,\sigma^2|y,X) \propto (\sigma^2)^{-k/2}\ \exp\left\{-\frac{(\beta-\beta^*)^T(\sum^*)^{-1}(\beta-\beta^*)}{2\sigma^2}\right\} \times (\sigma^2)^{-a^*/2-1}\exp\left(-\frac{b^*}{2\sigma^2}\right) \tag{3.6c}$$

where

$$\sum^* = (X^TX + \sum_0{}^{-1})^{-1}$$

$$\beta^* = (X^TX + \sum_0{}^{-1})^{-1}(X^Ty + \sum_0{}^{-1}\beta_0)$$

$$\hat{\beta} = (X^TX)^{-1}X^Ty$$

$$a^* = a_0 + n$$

$$b^* = b_0 + \left(y - X\hat{\beta}\right)^T\left(y - X\hat{\beta}\right) + (\beta-\hat{\beta})^T[(X^TX)^{-1} + \sum_0]^{-1}(\beta-\hat{\beta})$$

Note that Equation (3.6c) is again the kernel Normal Inverted-Gamma distribution, and can be factored as the conditional posterior distribution β multiplied by the marginal posterior distribution of σ^2

$$p(\beta,\sigma^2|y,X) = p(\beta|\sigma^2,y,X) \times p(\sigma^2|y,X) \tag{3.7}$$

where

$$\beta|\sigma^2,y,X \sim N(\beta^*,\sigma^2\sum^*)$$

$$\sigma^2|y,X \sim IG\left(\frac{a^*}{2},\frac{b^*}{2}\right)$$

Since the posterior distribution of parameters is obtained, we can summarize the characteristics of the posterior distribution, such as posterior mean, posterior median, and posterior credible intervals.

3.2.5 Marginal posterior density

In regression modeling, the coefficients on the explanatory variables, β, are usually the primary concern. The expression in Equation (3.7) describes the joint posterior distribution. If we are interested in the marginal posterior distribution for the parameters β, the variance parameter σ^2 has to be integrated out through

$$\begin{aligned} p(\beta|y,X) &= \int_0^\infty p(\beta,\sigma^2|y,X)d\sigma^2 \\ &\propto \int_0^\infty (\sigma^2)^{-(k+a^*)/2-1} \exp\left\{-\frac{(\beta-\beta^*)^T(\sum^*)^{-1}(\beta-\beta^*)+b^*}{2\sigma^2}\right\} d\sigma^2 \\ &= \int_0^\infty (\sigma^2)^{-(k+a^*)/2-1} \exp\left\{-\frac{B}{2\sigma^2}\right\} d\sigma^2 \end{aligned} \quad (3.8a)$$

where $B=(\beta-\beta^*)^T(\sum^*)^{-1}(\beta-\beta^*)+b^*$. Let $u=\frac{B}{2\sigma^2}$, then $\sigma^2=\frac{B}{2u}$ and $\frac{d\sigma^2}{du}=-\frac{B}{2}u^{-2}$.

$$\begin{aligned} p(\beta|y,X) &\propto \int_0^\infty \left(\frac{B}{2u}\right)^{-(k+a^*)/2-1} \cdot \exp\{-u\} \cdot \left(-\frac{B}{2}u^{-2}\right) du \\ &= \left(\frac{B}{2}\right)^{-(k+a^*)/2} \int_0^\infty u^{(k+a^*)/2-1} \exp\{-u\} du \end{aligned} \quad (3.8b)$$

The definition of Gamma function is $f(u)=\frac{1}{\Gamma(\alpha)}u^{\alpha-1}\lambda^\alpha\exp(-\lambda u)$. When $\lambda=1,\alpha=(k+a^*)/2$, then $f(u)=\frac{1}{\Gamma((k+a^*)/2)}u^{(k+a^*)/2-1}\exp(-u)$. From the properties of Gamma distribution, it follows that $\int_0^\infty u^{(k+a^*)/2-1} \exp\{-u\}d\mathrm{u}=\Gamma((k+a^*)/2)$.

Equation (3.8b) can be re-written as

$$\begin{aligned} p(\beta|y,X) &\propto \left(\frac{B}{2}\right)^{-(k+a^*)/2} \Gamma((k+a^*)/2) \propto B^{-(k+a^*)/2} \\ &= [(\beta-\beta^*)^T(\sum^*)^{-1}(\beta-\beta^*)+b^*]^{-(k+a^*)/2} \\ &= [1+(\beta-\beta^*)^T(b^*\sum^*)^{-1}(\beta-\beta^*)]^{-(k+a^*)/2} \end{aligned} \quad (3.8c)$$

$$= \left[1 + \frac{1}{a^*}(\beta - \beta^*)^T (\frac{b^*}{a^*}\Sigma^*)^{-1}(\beta - \beta^*)\right]^{-(k+a^*)/2}$$

which is the kernel for the density of a multivariate Student-*t* distribution (Ando 2010). Thus, the marginal posterior distribution for β is Student-*t* distribution, whose form is

$$\beta|y, X \sim t(\beta^*, \frac{b^*}{a^*}\Sigma^*, a^*) \tag{3.9}$$

with

$$E(\beta|y, X) = \beta^*$$

and

$$Var(\beta|y, X) = \frac{b^*}{a^* - 2}\Sigma^*$$

3.2.6 Prediction distribution

Suppose we have the linear regression model as in Equation (3.1), with likelihood and prior given in Equations (3.3) and (3.5), and the posterior distribution given in Equation (3.7). We want to make a prediction about a set of unobserved data ($y^\# = y_1^\#, \dots, y_m^\#$), which can be generated by

$$y^\# = X^\#\beta + \varepsilon^\# \tag{3.10}$$

where $y^\#$ is unobserved, β in Equation (3.10) is the same as the β in Equation (3.2) and $\varepsilon^\#$ is independent of ε but follows $N(0, \sigma^2 I_m)$. We assume that the explanatory variable $X^\#$ is observed and is a $m \times k$ matrix.

The Bayesian prediction is conducted by calculating

$$p(y^{\#}|\ X^{\#}) = \int p(y^{\#}|\ X^{\#},\beta,\sigma^2)p(\beta,\sigma^2|y,X)\ \ d\beta d\sigma^2$$

$$= \frac{\Gamma(\frac{a^*+m}{2})}{\Gamma(\frac{a^*}{2})(\pi a^*)^{m/2}}|\sum^{\#}|^{-1/2}\left\{1 + \frac{1}{a^*}(y^{\#}-\mu^{\#})^T\sum^{\#^{-1}}(y^{\#}-\mu^{\#})\right\}^{-(a^*+m)/2} \quad (3.11)$$

where $\mu^{\#} = X^{\#}\beta^*$, and $\sum^{\#} = \frac{b^*}{a^*}\left(I + X^{\#}\sum^{*^{-1}} X^{\#^T}\right)$. This turns out to be the multivariate Student-*t* distribution (Ando 2010; Koop 2003), whose mean and covariance are $E(y^{\#}|\ X^{\#}) = X^{\#}\beta^*$ and $var(y^{\#}|\ X^{\#}) = \frac{b^*}{a^*-2}\left(I + X^{\#}\sum^{*^{-1}} X^{\#^T}\right)$, respectively.

3.3 Computational Scheme for Parameter Estimation

3.3.1 Gibbs sampler

Posterior inference about β and σ^2, and prediction for unobserved data can all be done analytically using the results presented in the previous section. However, there are cases such as nonlinear function of β, linear regression model with other prior distributions, and more complex models with a larger set of unknown parameters, where analytical solutions are not possible. In such circumstances, it is appropriate to figure them out by using a simulation method. A number of simulation methods such as Markov chain Monte Carlo (MCMC) method, have been developed in the past two decades, which greatly simplify the integration calculation and make it possible to extend Bayesian analysis to a variety of complex models. Since Gibbs sampler was firstly introduced to

Bayesian statistics by Gelfand and Smith (1990), it remains in current and widespread use. Being one of the MCMC algorithms, Gibbs sampler is a special case of the more general Metropolis-Hasting algorithm and is useful when sampling from a multivariate posterior is not feasible, while sampling from the conditional distribution for each parameter is feasible (Feinberg *et al.* 2005). The idea in Gibbs sampler is to generate posterior samples by sweeping through each variable to sample from its conditional distribution with remaining variables being fixed to their current values. In this study, Gibbs sampler is used to obtain the marginal distributions for β and σ^2; its iterative process is summarized in Algorithm 3.1.

Algorithm 3.1 Gibbs sampler for marginal distributions

1. Initializing the parameters $\{\beta^{(0)}, \sigma^{2(0)}\}$ and let $k = 1$,
2. Sample $\beta^{(k)}$ from the conditional distribution $f(\beta|y, X, \sigma^{2(k-1)})$,
3. Sample $\sigma^{2(k)}$ from the conditional distribution $f(\sigma^2|y, X, \beta^{(k)})$,
4. Let $k = k + 1$, go back to (2) and (3) and repeat until L samples $\{\beta^{(k)}, \sigma^{2(k)}: k = 1, \dots, L\}$ are obtained.

As the number of Gibbs iterations increases to infinity, the draws from the conditional distributions converge to the joint posterior distribution $f(\beta, \sigma^2|y, X)$. Therefore, after a large enough number of iterations, the marginal distributions of β and σ^2 can be approximated by the empirical distributions of samplers. In other words, one repeats the

Gibbs iterations L times (large enough for convergence) and save the last L_1 samplers of $\beta^{(k)}$ and $\sigma^{2(k)}$ $(k = L_0, \dots, L)$ for estimating approximate marginal distributions of β and σ^2. Apart from that, the posterior means, the standard errors, and the 95% confidence intervals of the β and σ^2 can be calculated by using the last L_1 samplers. The 95% confidence interval is estimated using the 2.5% and 97.5% of the posterior samples. It is required to judge convergence of the process before using the samples obtained from Gibbs sampler for making inference, because it directly affects the accuracy of the statistical results. A concept of burn-in period (here referred to as $L_0 = L - L_1$) is introduced to estimate the time period required for the draws to reach its stationary state, and the criteria for convergence judgment will be discussed in the next sub-section.

The predictive density can also be estimated based on the Gibbs sampling output. By using the posterior samples $\{\beta^{(k)}, \sigma^{2(k)}: k = L_0, \dots, L\}$, the predictive density of future value $y^{\#}$, given $X^{\#}$, can be approximated as

$$\begin{aligned} f(y^{\#}|X^{\#}) &= \int f(y^{\#}|X^{\#}, \beta, \sigma^2) f(\beta, \sigma^2|y, X) \; d\beta d\sigma^2 \\ &\approx \frac{1}{L - L_0} \sum_{k=L_0}^{L} f(y^{\#}|X^{\#}, \beta^{(k)}, \sigma^{2(k)}) \end{aligned} \tag{3.12}$$

3.3.2 Convergence diagnostics

One important practical issue in application of MCMC algorithms is to check the

convergence of the sampling process before using the draws for parameters estimation. In contrast to convergence of optimizing algorithms (such as minimum least squares or maximum likelihood), the Markov chain converges to a density rather than deterministic points (Congdon 2003). Solution to the problem of determining convergence can be addressed in two approaches: the first is theoretical, wherein the Markov transition kernel of the chain is predetermined to insure convergence of the generated samples; the second approach is applying diagnostic tools to check the convergence issue (Cowles and Carlin 1996). In practice, the second approach is widely applied for convergence verification. In this study, the second approach is adopted and two common criteria are introduced for convergence checking.

In the process of examining the convergence of Gibbs sequences, trace plots would be useful and intuitive for detecting poorly sampled Markov chains. If the Markov chain has converged to the distribution, the trace plot will fluctuate smoothly without any trends. If some trends of Markov chain are observed, it is a clear sign of nonconvergence. Although this method is easily implemented, we have to be careful because the trace plot will tend to be stable even when the Markov chain is trapped in a local region (Ando 2010).

Geweke (1992) proposed a convergence diagnostic (CD) test statistic that measures the equality of the means of first and last part of the Markov chain. If the samples are

drawn from the stationary distribution, the means calculated from the first part and last part of the chain are equal. Divides the *L* draws from the Gibbs sampler into an initial L_0 which are discarded as burn-in replications and the remaining L_1 draws. Further, the latter draws are divided into three sets: a first set of L_A draws, a middle set of L_B draws and a last set of L_C draws. In practice, it has been found that setting $L_A = 0.1L_1$, $L_B = 0.5L_1, L_C = 0.4L_1$ works well in many applications (Koop 2003). For the purpose of calculating the convergence diagnostic, the middle set of draws are dropped out for making it likely that the first and last sets of draws are independent of one another. Let M_{L_A} and M_{L_C} be the average of the first and last set of draws, σ_{L_A} and σ_{L_C} be the standard error of these two parts. Then the test statistic is

$$CD = \frac{M_{L_A} - M_{L_C}}{\sigma_{L_A} + \sigma_{L_C}}, \tag{3.13}$$

which is asymptotically normal distribution as $N(0,1)$. Large value of *CD* means that there is a significant difference between M_{L_A} and M_{L_C}, hence the number of total Gibbs iterations should be increased to generate sufficient samples. If the convergence diagnostic indicates that enough draws have been obtained, then finial results can be calculated based on the complete set of L_1 draws.

3.4 Application: Expansion Joints in a Cable-Stayed Bridge

3.4.1 Ting Kau Bridge

The Ting Kau Bridge (TKB) in Hong Kong is a three-tower cable-stayed bridge with two main spans of 448 m and 475 m, respectively, and two side spans of 127 m each (Bergermann and Schlaich 1996). The bridge deck is separated into two carriageways with a width of 18.8 m each, between them being three slender single-leg towers with heights of 170 m, 194 m, and 158 m, respectively. The deck is supported by 384 stay cables in four cable planes. As part of a long-term SHM system devised by the Hong Kong SAR Government Highways Department, more than 230 sensors have been permanently installed on the TKB after completing the bridge construction in 1999 (Wong 2004; Ko and Ni 2005). The sensors deployed on the bridge include accelerometers, strain gauges, displacement transducers, anemometers, temperature sensors, GPS, and weigh-in-motion sensors (Wong 2007; Ni *et al.* 2011). Two displacement transducers have been used for the measurement of longitudinal movements of the expansion joints at the two ends of the continuous bridge deck (DSGAW01 and DSGPW01). There are a total of 83 temperature sensors in the SHM system; 51 of them are installed on a deck cross section for measurement of steel, concrete, asphalt and atmosphere temperature. The deployment of displacement transducers and temperature sensors on the TKB is illustrated in Figure 3.1 to Figure 3.3.

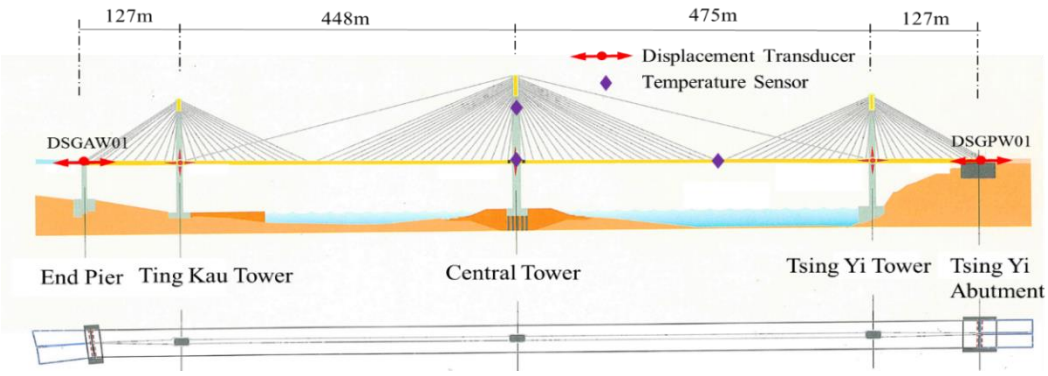

Figure 3.1 Deployment of displacement transducers and temperature sensors on Ting Kau Bridge (TKB)

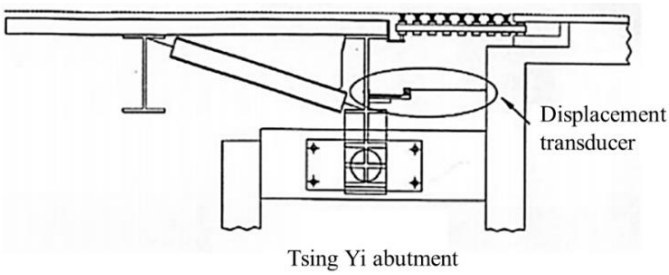

Figure 3.2 Displacement transducer at Tsing Yi abutment

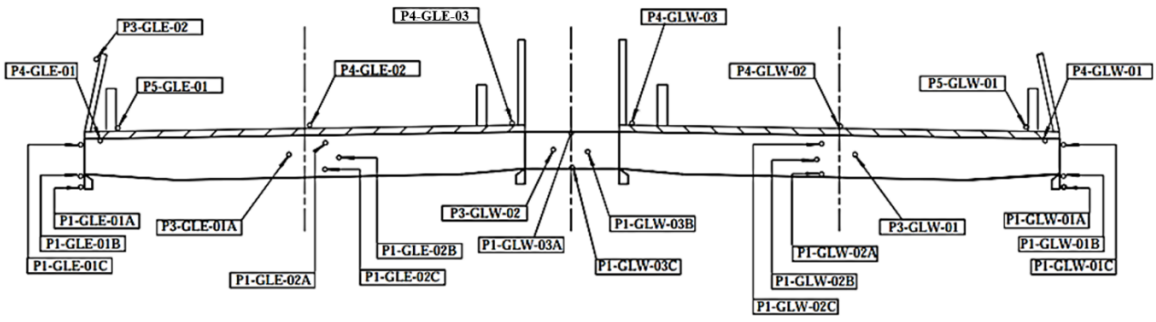

Figure 3.3 Temperature sensors on deck cross section

3.4.2 Processing of monitoring data

One-year continuous monitoring data (displacement and temperature) obtained from the TKB are used herein. The displacement and temperature measurement data were acquired with sampling rates of 2.56 Hz and 0.07 Hz, respectively, from which the hourly-average values of displacements and temperatures have been obtained.

In this study, the effective temperature is used to represent the average of temperature distributed across the cross section, which accounts for the thermal movements of the bridge deck. It is obtained by weighted average of temperatures measured at all subareas, where the weighting is the ratio of each subarea to the total area of the cross section (Ni *et al.* 2007). The effective temperature can be expressed as

$$T = \sum_{i=1}^{k} \frac{A_i}{A} \bar{T}_i \tag{3.14}$$

where $A_i = i$th subarea; A is the gross area of the cross section; $\bar{T}_i =$ measured temperature at the ith subarea; and $k =$number of subareas divided for the cross section. The measured temperatures from 39 sensors on the deck cross section, including 15 in steel and 24 in concrete, are used to calculate the effective temperature. Figure 3.4 illustrates the effective temperature of the bridge deck and the displacements of the expansion joints in one year. The positive direction of displacement is defined as towards the end of bridge deck along the bridge longitudinal direction.

After obtaining the effective temperature, a check on the relationship between the

displacement of the expansion joints and the effective temperature of the bridge deck is made. Figure 3.5 shows the deck effective temperature and expansion joint displacement at the Ting Kau and Tsing Yi abutments for 48 hours duration, where *DSGAW01* denotes the displacement at Ting Kau abutment while *DSGPW01* denotes the displacement at the Tsing Yi abutment. It is seen that the change of displacement coincides with effective temperature fluctuation very well. Furthermore, a good linear relationship between the expansion joint displacement and the deck effective temperature is observed, as shown in Figure 3.6. So it is concluded that the movement of the expansion joints is mainly caused by the temperature fluctuation. A Bayesian linear regression model will be formulated in following sub-section.

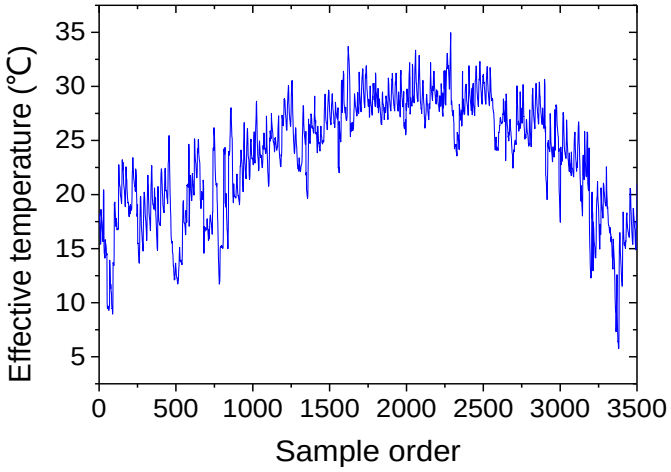

(a) Effective temperature

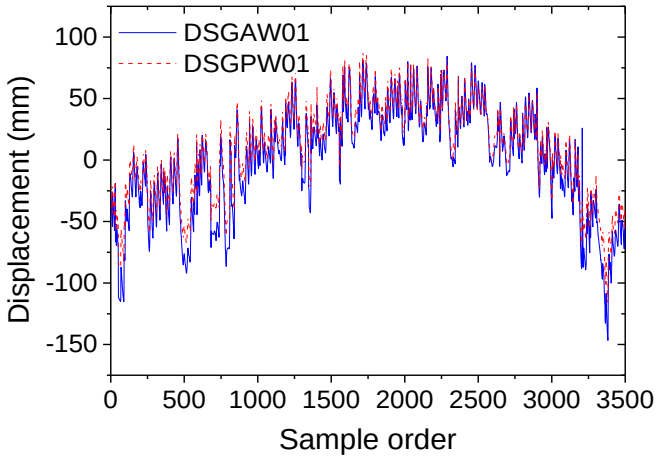

(b) Displacement

Figure 3.4 Sequences of measured effective temperature and displacement

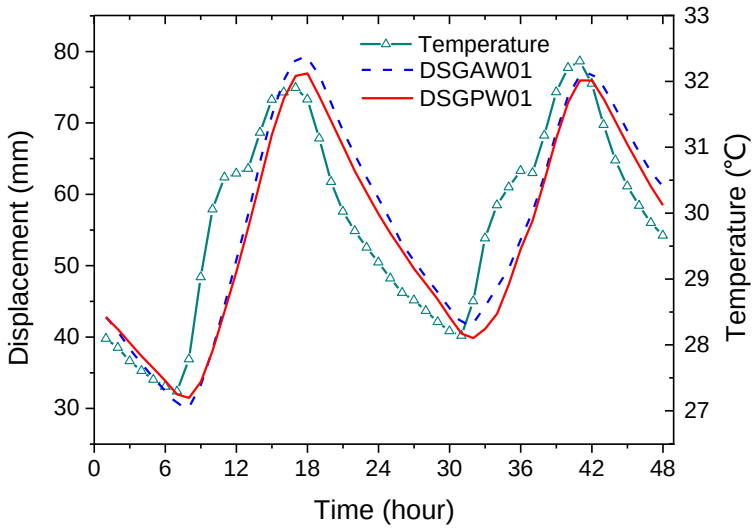

Figure 3.5 Time histories of displacement and effective temperature

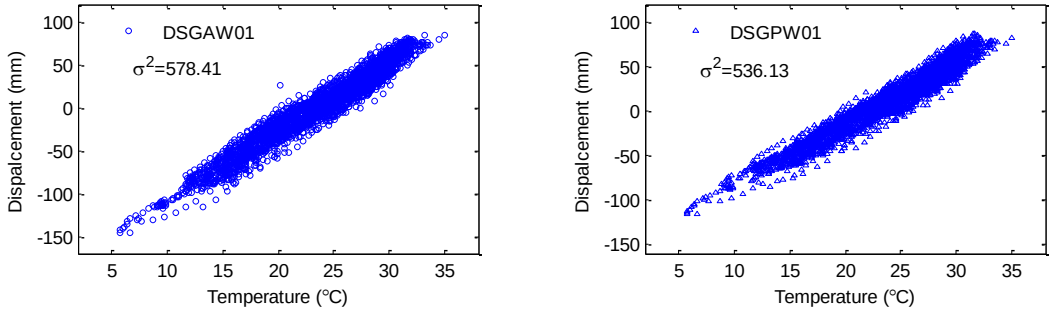

Figure 3.6 Relationship between displacement and temperature

3.4.3 Bayesian analysis and assessment

3.4.3.1 Problem description

A linear regression model is assumed for the correlation between the expansion joint displacement and the deck effective temperature. As specified in Equation (3.1), the response variable y represents the average displacement of the expansion joints per hour

and the covariates *x* denote the effective mean hour temperature. The data set, of sample size $n = 3602$, covers the whole year. Since only one variable, effective temperature, is considered in the linear regression model in this case, the model reduces to

$$y_\alpha = \beta_1 x_{\alpha 1} + \beta_2 x_{\alpha 2} + \varepsilon_\alpha \,, \qquad \alpha = 1, \cdots, n \tag{3.15}$$

where ε_α is the regression error, and $x_{\alpha 1}$ is implicitly set to 1 to allow for an intercept.

3.4.3.2 Selection of prior distribution

When using Bayesian method to formulate a regression model, prior distribution should be specified for each model parameter. The Normal Inverse-Gamma prior, expressed in Equation (3.16), is adopted

$$f(\beta, \sigma^2) = f(\beta|\sigma^2)\ \ f(\sigma^2) = N(0, \sigma^2 \sum_0)\ \ IG\left(\frac{a_0}{2}, \frac{b_0}{2}\right) \tag{3.16}$$

The level of (un)certainty in a prior is manipulated through the specified features of the prior distribution, and these features are called hyperparameters in the Bayesian context. For example, a normal distribution is defined through a mean and a variance and the amount of knowledge incorporated into normal distribution is directly controlled by the mean and variance hyperparameters. Figure 3.7 shows four normal distributions having different variance hyperparameters. It can be seen that the distributions with small variance (1 and 10) are illustrating much more certainty about the possible values of the parameter because the spread of these distributions covers a much smaller range of

possible values compared to those plots with large variance. In other words, the distributions with large variance (100 and 1000) show very little certainty about the possible values of the parameter because there is much larger spread of possible values that fall under this prior.

Akin to the normal distribution, the Inverse-Gamma distribution with different parameter values is also manipulated, as shown in Figure 3.8. In general, the parameters a and b indicate the possible range of values for the corresponding parameters being estimated. The smaller the values of a and b, the larger the spread of the possible values.

Because of very little certainty of the parameters, we choose reasonable values for the parameters of prior distribution covering a wide range of the possible values. Here, we set $\sum_0 = 1000 \times I_2$ (I_2 is second order identity matrix), and $a_0 = b_0 = 0.002$ (equivalent to $a = b = 0.001$ in Figure 3.8), which make the prior diffused.

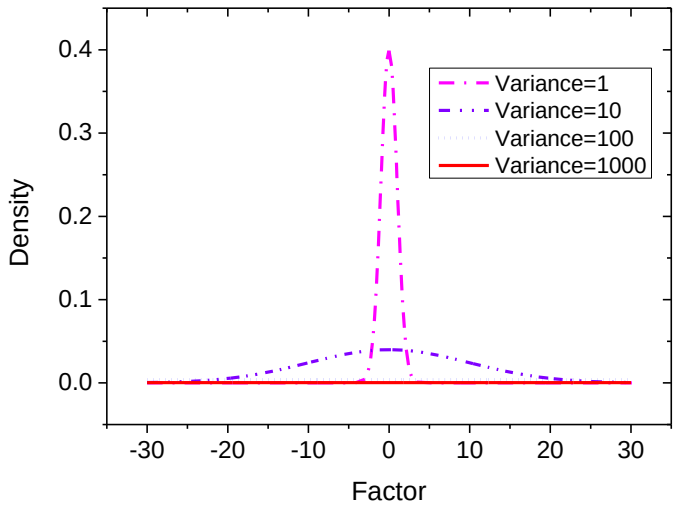

Figure 3.7 Prior distribution illustrating different levels of informativeness (Normal)

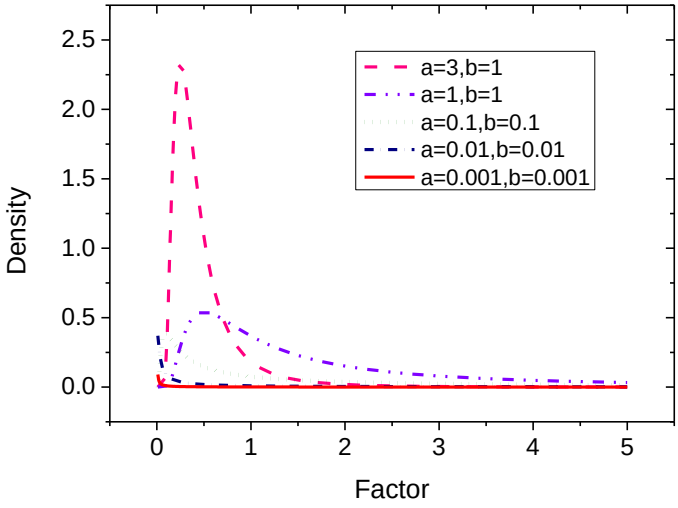

Figure 3.8 Prior distribution illustrating different levels of informativeness (Inverse-Gamma)

3.4.3.3 Parameter estimation

The Gibbs sampler method described in the previous section is used for estimating the posterior distribution of β_0, β_1 and σ^2. Here the total Markov chain iterations is chosen to be 25,000, of which the first 20,000 ($L_0 = 20{,}000$) iterations are discarded as burn-in replications. Thus, there remain 5,000 ($L_1 = 5{,}000$, $L_A = 0.1L_1, L_B = 0.5L_1, L_C = 0.4L_1$) posterior samples generated from the Gibbs sampler. As highlighted above, it is necessary to check if the generated posterior samples form a stationary distribution for making sure the accuracy of the results. Trace plots and CD test statistic are used together for checking the convergence of the posterior samples.

The left-hand panels of Figure 3.9 show the sample paths of retained 5,000 draws for

Model 1 (Ting Kau side). As shown in the figure, there is no evidence of lack of convergence based on the examination of the trace plots. The right hand panels of Figure 3.9 are the plots of the posterior distributions for β_1, β_2, σ^2 and the corresponding 95% confidence intervals (the blue area). Similarly, the sample paths and posterior densities of parameters for Model 2 (Tsing Yi side) are presented in Figure 3.10.

Table 3.1 summarizes the detailed information of the estimated parameters, including posterior mean, standard deviation (SD), 95% posterior confidence interval, skewness, kurtosis and convergence diagnostic CD. It is seen that the values of CD for the parameters are all close to 0, demonstrating that the posterior samples meet the requirement of convergence for parameter estimation. Since the analytical solutions for mean and SD are available as shown in section 3.2.3 and 3.2.4, the analytical values are also obtained for comparison with the results estimated by using the Gibbs sampler approach. It is apparent that the simulation values are pretty much the same as the analytical values, verifying the accuracy of the Gibbs sampler in the present study. The 95% posterior interval of each parameter covers the analytical values. The SD is a measure that can quantify the uncertainty of each parameter. From the table, it is seen that β_2 has the lowest SD value (0.03), β_1 comes second (0.75), and model error σ^2 owns the largest SD value (2.26). But their relative errors are 0.4%, 0.38% and 2.41% for β_1, β_2, σ^2, respectively, which implies the model error σ^2 has a higher uncertainty

than β_1, and β_2. As shown in the table, the values of skewness are nearly zero and kurtosis are close to 3, which indicate the estimated posterior densities are approximately normal distribution. The mean slopes of the linear regression functions are 7.93 and 6.88 mm/℃ for the expansion joints at the Ting Kau abutment and Tsing Yi abutment, respectively. The expansion lengths for spans on the left and right sides of the central tower are 575 m and 602 m, so the thermal expansion coefficients can be estimated as 13.7×10^{-6} per ℃ and 11.4×10^{-6} per ℃, which are close to the design value of 12.0×10^{-6} per ℃.

Compared with traditional model, the biggest advantage of Bayesian model is that the model error is quantitatively obtained simultaneously, making the model more reasonable. From Table 3.1 it is seen that Model 2 has a smaller model error that indicates Model 2 is relatively more accurate.

Using the mean values of the parameters β_1 and β_2, the linear relationship between the displacement of the expansion joints and the effective temperature of the deck can be determined as shown by red solid lines in Figure 3.11. It is seen that the results estimated by the Bayesian method agree well with the measurement.

Table 3.1 Summary of the evaluated parameters

Expansion joint		Ting Kau side (Model 1)			Tsing Yi side (Model 2)		
Parameters		β_1	β_2	σ^2	β_1	β_2	σ^2
Mean	Gibbs	-186.94	7.93	93.7	-152.65	6.88	84.18
	Analytical	-186.88	7.92	93.69	-152.83	6.88	84.03
SD	Gibbs	0.75	0.03	2.26	0.73	0.03	2.03
	Analytical	0.75	0.03	2.24	0.72	0.03	2.03
95% confidence interval		[-188.40, -185.43]	[7.87, 8.00]	[89.46, 98.33]	[-154.05, -151.23]	[6.82, 6.93]	[80.30, 88.36]
Skewness		-0.01	-0.005	0.15	0.04	-0.03	0.13
Kurtosis		2.98	2.97	2.97	2.92	2.93	3.06
CD		-0.024	0.025	-0.029	-0.001	0.003	0.012

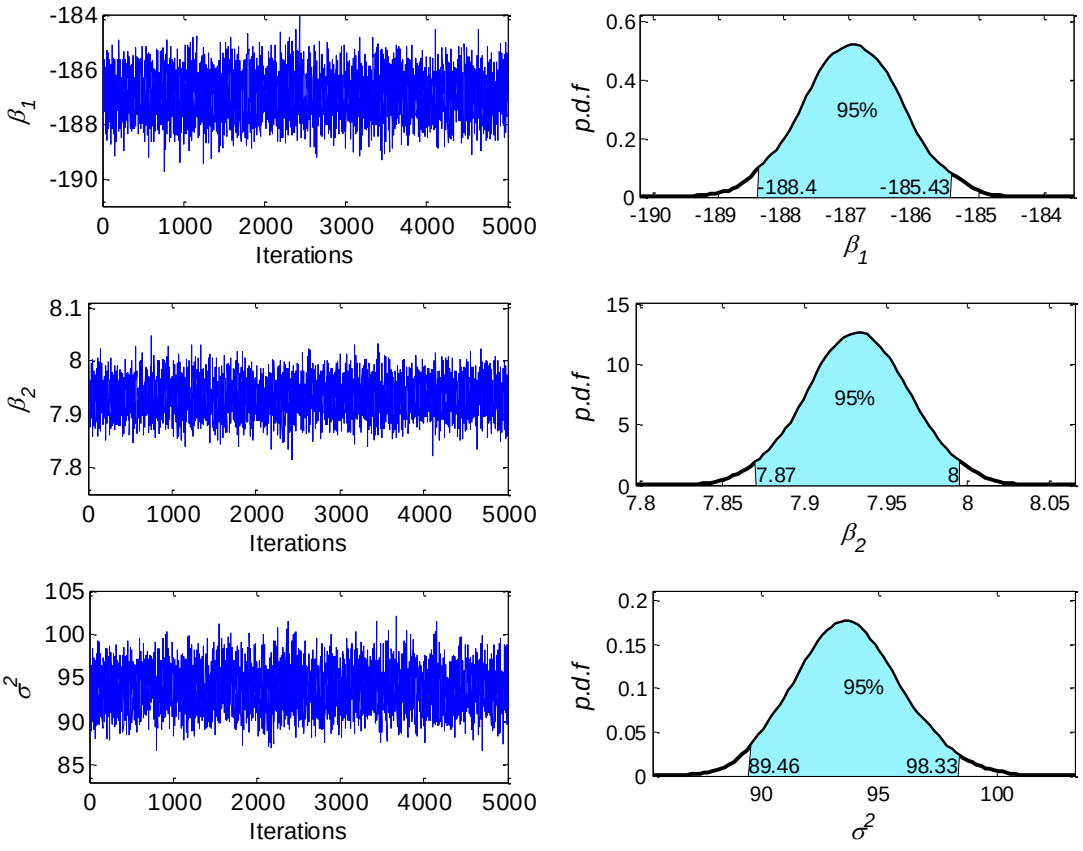

Figure 3.9 Sample paths and estimated posterior densities for parameters (Ting Kau side)

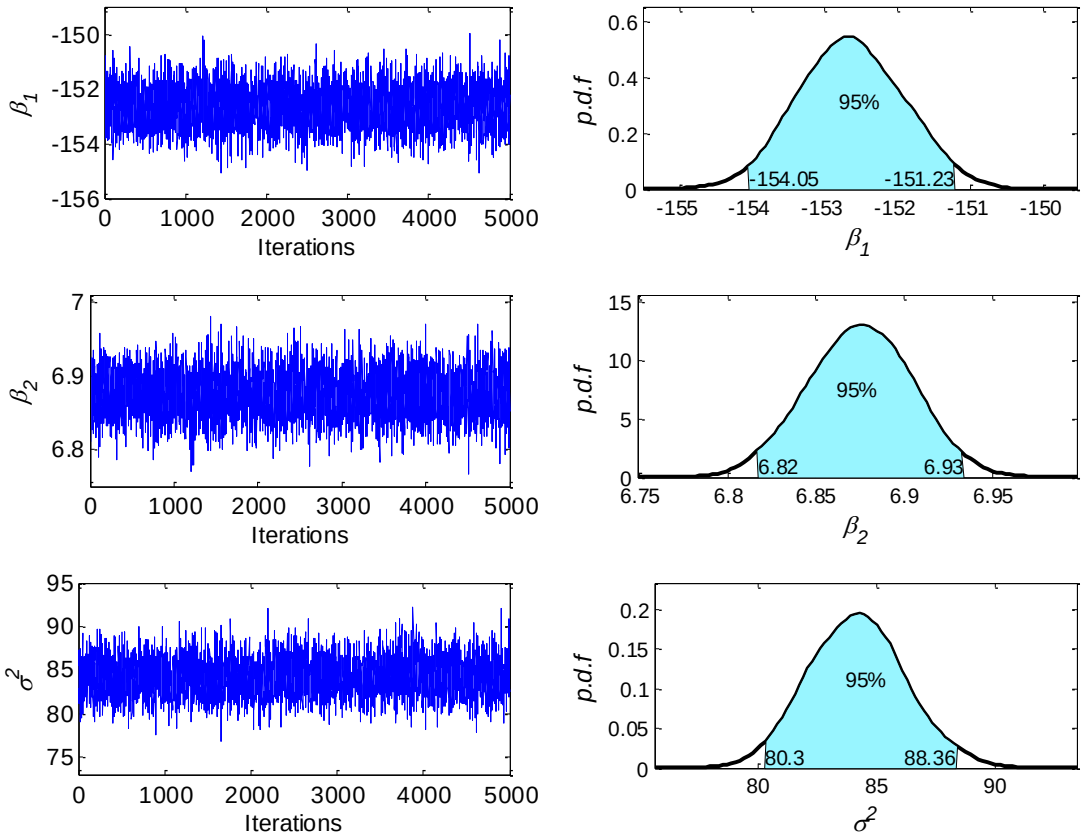

Figure 3.10 Sample paths and estimated posterior densities for parameters (Tsing Yi side)

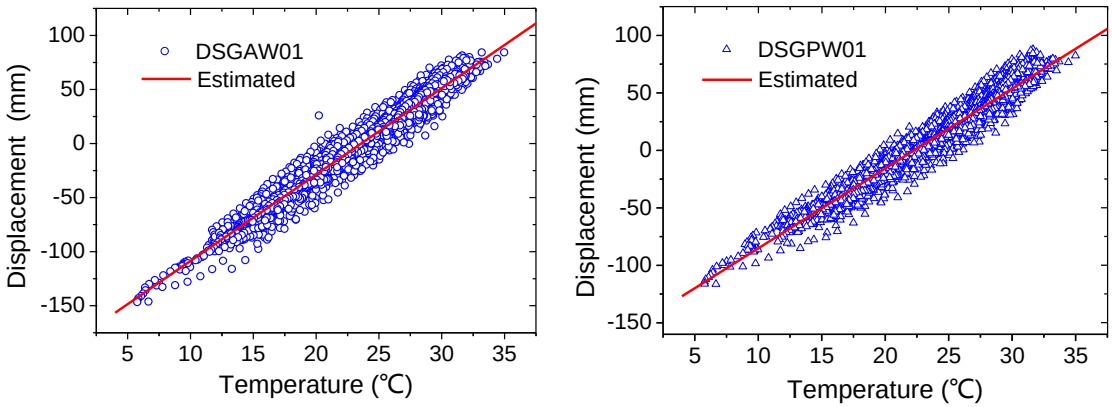

Figure 3.11 Measured and Bayesian linear relations between displacement and effective temperature

3.4.3.4 Anomaly index

With the uncertain parameters being identified, the probabilistic regression models are specified. As shown in Figure 3.12 and Figure 3.13, the predicted displacement of the expansion joint at any given temperature is not a definite value but a probability distribution. In practice, we mainly concern the probability of failure when a new measurement of displacement is obtained. Here a common performance indicator, named anomaly index, is introduced to evaluate the failure probability of the expansion joints based on new measurement data.

The probability of failure of a system is defined as the probability of violating any of its limit states (Frangopol 2011; Frangopol and Soliman 2013). A limit-state function is defined as

$$g = R - S \tag{3.17}$$

where R is the capacity of displacement of the expansion joints under a certainty temperature, S is the measured displacement response at the same temperature.

Based on this limit-state function, the failure probability can be expressed as

$$P_f = P(g < 0) = P(R - S < 0) = \int_{-\infty}^{0} F_R(x) f_S(x) dx \tag{3.18}$$

where $F_R(x)$ is the cumulative probability distribution function (CPDF) of the capacity and $f_S(x)$ is the probability density function (PDF) of the measured displacement.

Suppose the displacement capacity R and the displacement response S are

independent normal variates, with means and variances μ_R, μ_S and σ_R^2, σ_S^2, respectively. In this case, $g = R - S$ is also a normal variate with

$$\mu_g = \mu_R - \mu_S,\ \sigma_g^2 = \sigma_R^2 + \sigma_S^2.$$

The failure probability is

$$P_f = F_g(0) = \Phi\left(\frac{0 - \mu_g}{\sigma_g}\right) = \Phi\left(-\frac{\mu_R - \mu_S}{\sqrt{\sigma_R^2 + \sigma_S^2}}\right) \tag{3.19}$$

The corresponding anomaly index is

$$\lambda = \Phi^{-1}(P_f) \tag{3.20}$$

where $\Phi^{-1}(\cdot)$ is the inverse of the standard normal cumulative distribution function. The anomaly index can be computed as

$$\lambda = \frac{|\mu_R - \mu_S|}{\sqrt{\sigma_R^2 + \sigma_S^2}} \tag{3.21}$$

For instance, consider the distribution of the displacement of the expansion joint at Ting Kau side under the temperature of 20℃ whose mean and variance are 50.92 mm and 93.29 respectively. Assuming the measured displacement is 90, 80, 70, 60, 50, 40, 30, 20 mm under the same temperature, the corresponding abnormal index can be calculated by Equation (3.21), as shown in Figure 3.14. Note that the more the measured displacement deviating from the center of the distribution (blue dotted line), the bigger the anomaly index, which indicates a higher probability of failure about the expansion joint. Therefore, the degree of failure can be graded in term of the value of the anomaly index λ. Meanwhile, the 95% confidence level (red line in Figure 3.14) is shown as a

threshold for easily indicating anomaly values. It is figured out that there exists a risk of failure for the expansion joint when the anomaly index exceeds the threshold.

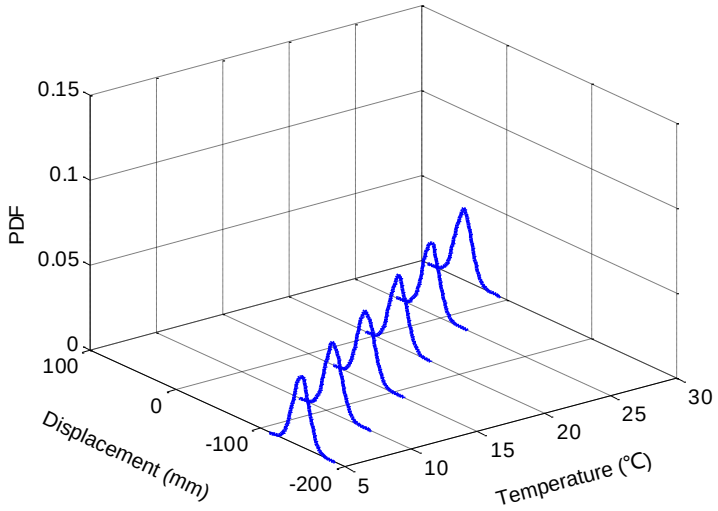

Figure 3.12 Distribution of expansion joint displacement under different temperatures (Ting Kau side)

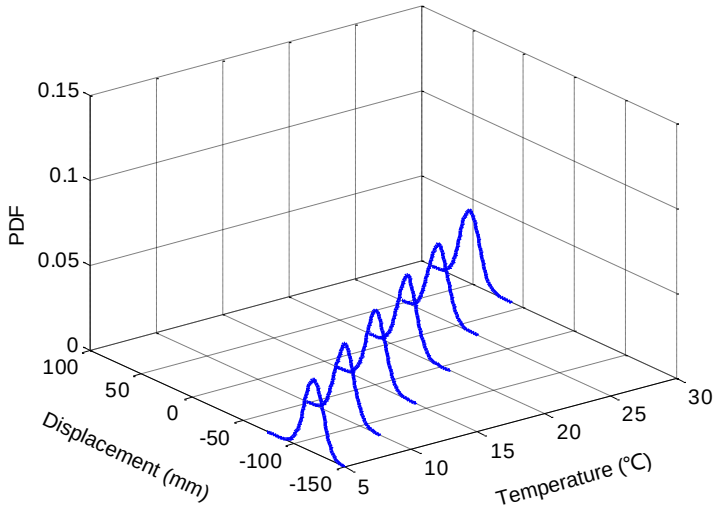

Figure 3.13 Distribution of expansion joint displacement under different temperatures (Tsing Yi side)

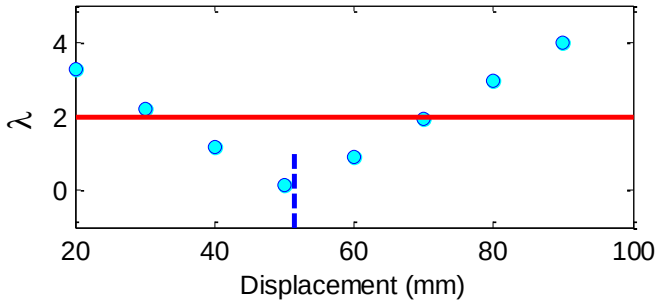

Figure 3.14 Anomaly index

3.4.3.5 Displacement prognosis

According to the design document, the maximum and minimum effective temperatures are 40℃ and -2℃ respectively (Wong *et al.* 2002). Substituting the design values in the formulated regression model, the distributions of the predicted maximum and minimum displacements are obtained, as shown in Figure 3.15 and Figure 3.16. The detailed information about the mean, SD, 95% confidence interval is summarized in Table 3.2. Since the analytical solutions of the predictive mean and variance are also available, the analytical values are also obtained for comparison with the numerical solutions. It is noted that the numerical values (means and SD) are very close to the analytical results, proving the accuracy of the Gibbs sampler approach. According to the predicted mean displacements at the maximum and minimum temperatures, the maximum mean displacements are 333.02 mm at the Ting Kau side and 288.88 mm at the Tsing Yi side, respectively, which are very close to the design values of 339 mm and 297 mm (Ni *et al.* 2007). The gaps between the prediction and design values are smaller than the SD.

However, the displacement ranges with 95% confidence interval are [298.52, 371.37] at the Ting Kau side and [252.99, 325.26] at the Tsing Yi side, whose upper bounds exceed the design criterion. It is better to increase the design values for the safety of the expansion joints.

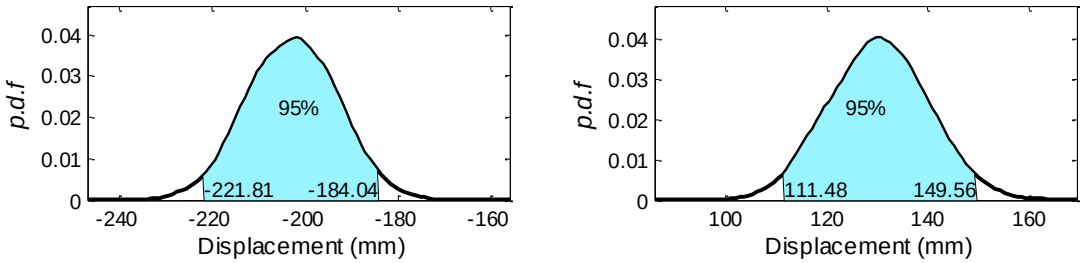

(a) Temperature = -2℃ (b) Temperature = 40℃

Figure 3.15 Distribution of predicted displacement at Ting Kau side

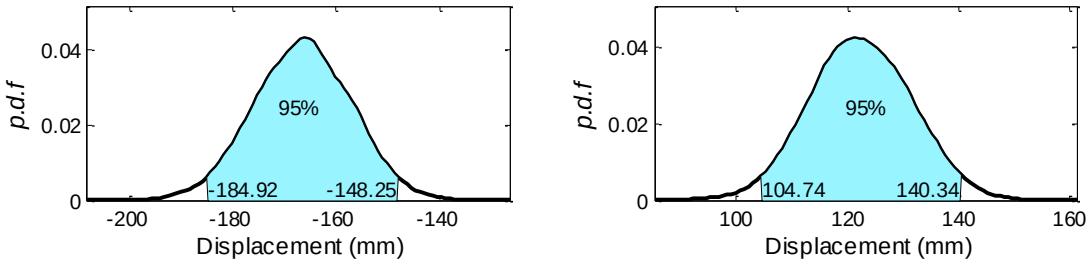

(a) Temperature = -2℃ (b) Temperature = 40℃

Figure 3.16 Distribution of predicted displacement at Tsing Yi side

Table 3.2 Predicted displacements corresponding to minimum and maximum temperatures

Expansion joint	T (℃)	Mean (mm)		SD		95 % confidence interval (mm)
		Gibbs	Analytical	Gibbs	Analytical	
Ting Kau side	-2	-202.78	-202.66	9.76	9.84	[-221.81, -184.04]
	40	130.24	130.01	9.81	9.82	[114.48, 149.56]
Tsing Yi side	-2	-166.50	-167.42	9.31	9.08	[-184.92, -148.25]
	40	122.38	122.77	9.12	9.06	[104.74, 140.34]

3.5 Summary

This chapter presents an efficient approach using Bayesian inference for condition assessment of bridge expansion joints. Making use of the long-term SHM data, Bayesian linear model (BLM) is formulated to characterize the relationship between the displacement of expansion joints and the effective temperature of bridge deck. The model parameters associated with their uncertainties are estimated by using Gibbs sampler, and then compared with the analytical results for validation. Based on the formulated BLM, the anomaly index is defined for evaluating the probability of failure of expansion joints when new measurement is available. The predicted mean displacements at the maximum and minimum temperatures are close to the design values, but the upper bounds of the predicted displacement ranges with 95% confidence interval exceed the design criterion. It is therefore suggested to appropriately increase the design values for the sake of the expansion joint safety.

Chapter 4

SHM-based Condition Assessment of Bridges Using BGLM

4.1 Introduction

Although the linear regression model is an easy and convenient technique for a variety of problems, in some practical situations, the response variables do not depend linearly on the explanatory variables. The purpose of the generalized linear model is to extend the idea of linear model to cases where an assumption of linear relationship between the explanatory variables and response variables is not appropriate, by introducing a suitable transformation. For example, if $y_i = x_{i1}^{b1} x_{i2}^{b2} \cdots x_{ik}^{bk} \times variation$, then $\log y_i = b_1 \log x_{i1} + \cdots + b_k \log x_{ik} + variation$, and a linear model relating $\log y_i$ to $\log x_{ij}$ is applicative.

A generalized linear model consists of three elements (Gelman *et al.* 1995): (i) a linear predictor, $\eta = X\beta$; (ii) a link function $g(\cdot)$ which provides the relationship between the linear predictor and the mean of the outcome variable $E(y) = \mu = g^{-1}(\eta) = g^{-1}(X\beta)$; (iii) a probability distribution for y from the exponential family. The most common exponential-family distributions along with link functions are shown in Table 4.1.

Table 4.1 Common distributions and link functions

Distribution	Support of distribution	Type of data	Link function	Mean function
Normal	Real: $(-\infty, +\infty)$	Linear-response data	$X\beta = \mu$	$\mu = X\beta$
Exponential	Real: $(0, +\infty)$	Exponential-response data	$X\beta = \mu^{-1}$	$\mu = (X\beta)^{-1}$
Poisson	Integer: 0,1,2,…	Count of occurrences in fixed amount of time/space	$X\beta = \ln(\mu)$	$\mu = \exp(X\beta)$
Binomial	Integar: 0,1,2,…,*N*	Count of 'yes' occurrences out of *N*	$X\beta = ln\left(\frac{\mu}{1-\mu}\right)$	$\mu = \frac{\exp(X\beta)}{1+\exp(X\beta)}$

In this study, the Bayesian generalized linear model (BGLM) aims to tackle the modeling and prediction of wind-induced displacement responses of bridges. The displacement response of a long-span bridge caused by aerostatic and fluctuating wind actions, is one of important parameters characterizing the safety of the bridge under strong winds. The lateral response of cable-supported bridges is in general susceptible to wind. The large-amplitude displacement under strong winds would threaten the safety of the whole bridge (Wang and Ding 2014). As an example, the first Tacoma Narrows Bridge in Washington State collapsed under winds of approximately 18m/s due to violent torsional flutter (Green and Unruh 2004). The lateral displacement response of bridges under winds has been evaluated by theoretical exploration, numerical simulation, and wind tunnel test (Cheng and Xiao 2006; Chan 2009; Soon *et al.* 2013). However, the actual displacement response of an in-service bridge is difficult to be accurately evaluated by the above approaches due to inappropriate ignorance of some subordinate factors, imprecise assignment of initial values, and uncertain boundary condition (Wang and Ding 2014).

During the past decades, structural health monitoring (SHM) has been emerging as a powerful technique for collecting reliable and objective data about structural responses, such as displacement response, under various operational conditions, and performing real-time diagnosis of structural status. Global Positioning System (GPS), among other types of sensory systems, is a powerful tool for measuring the static and dynamic

displacement response of civil structures and has been widely applied to long-span bridges (Ashkenazi and Roberts 1997; Fujino *et al.* 2000; Miyata *et al.* 2002; Ni *et al.* 2004; Guo *et al.* 2005). In Hong Kong, as a supplement to the Wind and Structural Health Monitoring System (WASHMS) instrumented on the Tsing Ma Bridge, Kap Shui Mun Bridge and Ting Kau Bridge, a GPS system has been deployed to monitor the displacement response of the bridge towers, cables and deck (Wong *et al.* 2001; Wong 2004).

With the monitoring data, investigations on correlation between the displacement response and wind speed have been conducted (Nakamura 2000; Xu and Chan 2009; Wang and Ding 2014). However, the formulated relations only involve the wind speed but ignore another important factor - the wind direction. From these models, the same displacement response would be produced under identical wind speeds but with different wind directions. It is obviously unreasonable. In addition, these relation models were formulated by estimating the deterministic model parameters based on statistical analysis of a large amount of monitoring data. Different from the classical estimation method, the Bayesian approach treats the unknown parameters as distributions rather than deterministic values and more importantly, it provides room for incorporating prior information with the obtained SHM data through Bayes' theorem to achieve a feasible estimation (Zhu and Frangopol 2013). Although the Bayesian approach has been widely

used in different engineering fields (Sohn and Law 1997; Enright and Frangopol 1999; Vanik 2000; Ching and Leu 2009; Yuen 2010; Au 2011; Au *et al.* 2012), no reported studies have been available on assessing wind-induced displacement responses of bridges by the Bayesian approach.

In this chapter, BGLM is formulated for modeling the wind-induced displacement responses of bridges with the use of monitoring data acquired during typhoons. In particular, the most suitable model is determined by the Bayesian model class selection technique. The formulated BGLM is then applied for response prediction.

4.2 Bayesian Generalized Linear Model (BGLM)

4.2.1 Theoretical formulation

Suppose we have *n* independent observations $\{(y_i, x_i), i = 1, \cdots, n\}$, where y_i's are the response variables and x_i's are the explanatory variables, and the relationship between them is expressed as the following non-linear function

$$\begin{aligned} y_i = \beta_0 &+ \beta_{11}x_{1i} + \beta_{12}x_{1i}^2 + \cdots + \beta_{1k_1}x_{1i}^{k_1} \\ &+ \beta_{21}x_{2i} + \beta_{22}x_{2i}^2 + \cdots + \beta_{2k_2}x_{2i}^{k_2} + \cdots \\ &+ \beta_{p1}x_{pi} + \beta_{p2}x_{pi}^2 + \cdots + \beta_{pk_p}x_{pi}^{k_p} + \varepsilon_i, \qquad i = 1, \cdots, n \end{aligned} \tag{4.1}$$

When the error ε_i is a normal distribution with mean 0 and variance σ^2,

$\varepsilon_i \sim N(0,\ \sigma^2)$, this model can be expressed as density form

$$f(Y|X,\beta,\sigma^2) = \frac{1}{(2\pi\sigma^2)^{n/2}} \exp\left[-\frac{(Y-X\beta)^T(Y-X\beta)}{2\sigma^2}\right] \tag{4.2}$$

with

$$Y = \begin{bmatrix} y_1 \\ y_2 \\ \vdots \\ y_n \end{bmatrix},\ \varepsilon = \begin{bmatrix} \varepsilon_1 \\ \varepsilon_2 \\ \vdots \\ \varepsilon_n \end{bmatrix}$$

$$\beta = \left[\beta_0, \beta_{11}, \cdots, \beta_{1k_1}, \beta_{21}, \cdots, \beta_{2k_2}, \cdots, \beta_{p1}, \cdots, \beta_{pk_p}\right]^T$$

$$X = \begin{bmatrix} 1 & x_{11} & \cdots & x_{11}^{k_1} & x_{21} & \cdots & x_{21}^{k_2} & \cdots & x_{p1} & \cdots & x_{p1}^{k_p} \\ 1 & x_{12} & \cdots & x_{12}^{k_1} & x_{22} & \cdots & x_{22}^{k_2} & \cdots & x_{p2} & \cdots & x_{p2}^{k_p} \\ \vdots & \vdots & \ddots & \vdots & \vdots & \ddots & \vdots & \ddots & \vdots & \ddots & \vdots \\ 1 & x_{1n} & \cdots & x_{1n}^{k_1} & x_{2n} & \cdots & x_{2n}^{k_2} & \cdots & x_{pn} & \cdots & x_{pn}^{k_p} \end{bmatrix}$$

The posterior inference for the model parameters $(\beta,\ \sigma^2)$ can be obtained by applying the computational methods for Bayesian linear models described in Chapter 3. However, the most plausible/suitable class of models among numerous candidate models will be identified by the Bayesian model class selection techique.

4.2.2 Optimal model class selection

One commonly encountered problem in regression modeling is to find the best/optical model to explore the relationship between the explanatory and response variables. Although a more complicated model can fit the data better than a less complicated one which has fewer adjustable parameters, it is likely to lead to over-fitting. When the over-fitted model is used for future prediction, it could lead to poor results because of the

identified model depending too much on the training data and the measurement noise in the data (Yuen 2010). Thus, the selected model should balance the accuracy and complexity. In other words, it is necessary to agree well with the observed data but others to be as simple as possible.

The Bayesian approach for selecting a model is to choose the model with the largest posterior probability among a set of candidate models. So the posterior probability is the fundamental objective of interest for model selection. The posterior distribution of model parameters (θ) is defined via Bayes' theorem

$$p(\theta|y) = \frac{p(y|\theta)p(\theta)}{p(y)} \tag{4.3}$$

where $p(y|\theta)$, $p(\theta)$ are the likelihood function and joint prior distribution, respectively; $p(y)$ is the marginal likelihood that we want to compute. The marginal likelihood in logs is

$$ln\, p(y) = ln\, p(y|\theta) + ln\, p(\theta) - ln\, p(\theta|y) \tag{4.4}$$

When the three terms in the right hand-side of Equation (4.4) are analytically available, the marginal likelihood, $ln\, p(y)$, can be computed easily. The value of θ is usually chosen as a point with high posterior density to maximize the accuracy of this approximation. However, the third term $p(\theta|y)$ is often difficult to calculate due to the unknown exact form of posterior distribution. In this situation, Chib (1995) proposed to divide the parameter vector θ into several blocks so that the full conditional distribution

for each block is available in closed form. To illustrate the idea, we consider the case of two blocks, as our example, $\theta = (\beta, \sigma^2)$ where $p(\beta|\sigma^2, y)$ and $p(\sigma^2|y)$ are available in closed form. The joint posterior distribution of θ can be estimated as

$$p(\theta|y) = p(\beta, \sigma^2|y) = p(\beta|\sigma^2, y)p(\sigma^2|y) \tag{4.5}$$

where an appropriate Monte Carlo estimate for $p(\sigma^2|y)$ is

$$\hat{p}(\sigma^2|y) \approx \frac{1}{L_1}\sum_{k=1}^{L_1} f\left(\sigma^2|y, \beta^{(k)}\right) \tag{4.6}$$

in which $\left\{\beta^{(k)}; k = 1, \cdots, L_1\right\}$ is a set of posterior samples from Gibbs sampler. The $\hat{p}(\sigma^2|y) \to p(\sigma^2|y)$ as L_1 becomes large. Therefore, the marginal likelihood can be estimated as

$$\begin{aligned} \ln p(y) \approx \ln p\left(y|\beta^\star, \sigma^{2^\star}\right) \\ + \ln p\left(\beta^\star, \sigma^{2^\star}\right) - \ln p\left(\beta^\star|\sigma^{2^\star}, y\right) - \ln \hat{p}\left(\sigma^{2^\star}|y\right) \end{aligned} \tag{4.7}$$

where the first three terms on the right-hand side are available in closed form. The value of $\beta^\star$, $\sigma^{2^\star}$ may be chosen as the posterior mean, posterior mode, posterior median or other point which can maximize the accuracy of this approximation.

4.3 Application: Wind-Induced Displacement of a Suspension Bridge

4.3.1 Tsing Ma Bridge and SHM system

A long-term SHM system has been implemented on the Tsing Ma Bridge (TMB) in

Hong Kong. The TMB is a suspension bridge with a main span of 1,377 m and a total length of 2,132 m, carrying both highway and railway (Figure 4.1). The height of the two bridge towers is 206 m from the base level to the tower saddle. Two online monitoring systems called Wind and Structural Health Monitoring System (WASHMS) and GPS On-Structure Instrumentation System (GPS-OSIS) were installed on the bridge in 1997 and 2000, respectively (Wong *et al.* 2001; Wong 2004, 2007; Ni *et al.* 2011).

The GPS-OSIS has a total of 14 GPS receivers deployed over several key components of the bridge, including the towers, main cables and four different sections of the bridge deck, to monitor the displacement responses of the TMB in longitudinal, lateral and vertical directions (see Figure 4.1). To avoid the obstruction of signal receiving caused by vehicles, the antennae of all the GPS receivers on the bridge deck were mounted at a height of 4 m above the deck level and with a view angle of above 15° (see Figure 4.2). The sampling rate of GPS is 10 Hz.

The WASHMS for the TMB includes a total of 6 anemometers, of which 2 ultrasonic anemometers are located at the mid-main span, 2 mechanical propeller-type anemometers at the middle of the Ma Wan side span, and 2 mechanical propeller-type anemometers on the top of the Tsing Yi tower and on the top of the Ma Wan tower, as shown in Figure 4.1. To eliminate the disturbance from the bridge deck, the anemometers at the deck level were installed on the south and north sides of the bridge deck respectively via a boom of

9 m long extended from the outmost of the deck. The sampling rate of anemometers is 2.56 Hz.

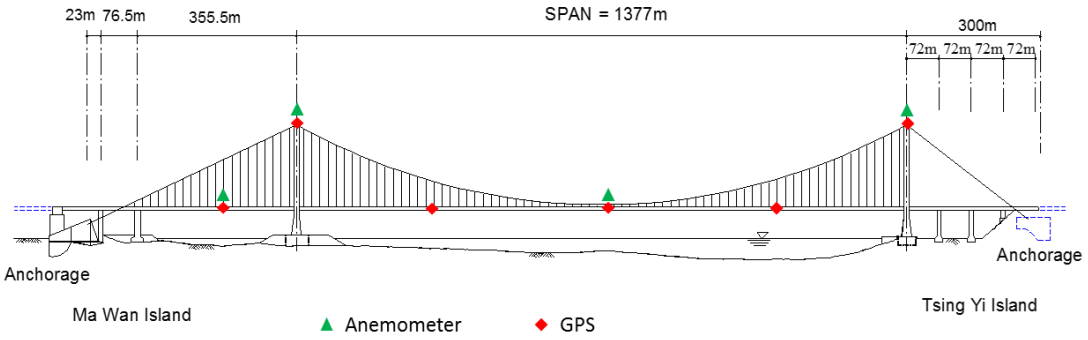

Figure 4.1 Location of GPS receivers and anemometers on Tsing Ma Bridge (TMB)

(a) Tower top (b) Main cable (c) Deck

Figure 4.2 Deployment of GPS receivers at different portions of TMB

4.3.2 SHM data

The wind-induced displacement responses of the bridge vary depending on the intensity of wind speed. Displacement responses resulting from strong wind are most interesting for design and assessment purpose. Although advances in computational

technologies or wind tunnel test allow the estimation of these critical displacement responses of bridge structure, the predicted results might still deviate from the real values, and lead to risky conservative design or performance assessment. Since the SHM system can provide real responses of a bridge structure under in-service conditions, integration of the SHM data will yield a more accurate assessment of displacement responses. Available for this study is continuously measured data during typhoons hitting Hong Kong in 2011. According to the Hong Kong Observation (HKO), there were 3 typhoons (Haima, Nesat, and Nockten) of signal No.3 and above during 2011 (HKO 2013). The first step of data processing is to ascertain wind data acquired from which anemometer, on the north or south side, at the deck in each typhoon to represent the actual wind load acting on the deck girder and cables. That is because only those coming from windward side are actual wind. Instead, the wind data collected from the anemometer at the leeward sider are interfered by the bridge deck and not the real wind load acting on the bridge. The 10-min wind speed and wind direction measured during the three typhoons are plotted in Figure 4.3.

The popular approaches for estimating wind-induced buffeting response of structures are largely based on the assumption of stationary wind excitations, which means the wind speed in a given time duration, e.g. 10 minutes, is regarded to be steady and the wind fluctuation around its mean is a stationary random process. However, the stationarity

assumption might be inappropriate in the case of typhoon or hurricane winds, where the magnitude and direction of mean wind speed may fluctuate violently with time and the random wind turbulence may show nonstationary characteristics (Chen and Kareem 2001; Chen 2012). Thus, we introduce the peak dynamic displacement (D_{max}) during typhoon periods, which is estimated from the standard deviation (σ_D) of displacement response multiplied by a statistical peak factor (m)

$$D_{max} = m\sigma_D \tag{4.8}$$

The value of m in Equation (4.8) is estimated based on a great deal of measurement data during typhoon events. Figure 4.4 shows the variation of the peak factor against the mean wind speed at different positions. It is found that the peak factor tends to stay fairly flat at high wind speeds. The mean values of peak factor at the mid-main cable, mid-main span and 1/4 main span, are approximately 2.5. Unfortunately, the measurement data at the 3/4 span are abnormal and therefore not considered in the following analysis. The detailed information of the peak factor is illustrated in Table 4.2.

The total displacement response of the bridge in lateral direction is then given by

$$\widehat{D} = D + m\sigma_D \tag{4.9}$$

where $\widehat{D}$ is the wind-induced total displacement of the bridge deck and cable; D represents the wind-induced mean displacement; σ_D denotes the standard deviation of wind-induced displacement; m is the statistical peak factor. Figure 4.5 shows the

relationship between mean wind speed and wind-induced total displacement at different positions in lateral direction. It is seen that there exists a nonlinear relationship between the displacement and wind speed.

Table 4.2 Peak factor at different positions

Location	Mid-main cable	Mid-main span	1/4 main span
Peak factor	2.37	2.42	2.54

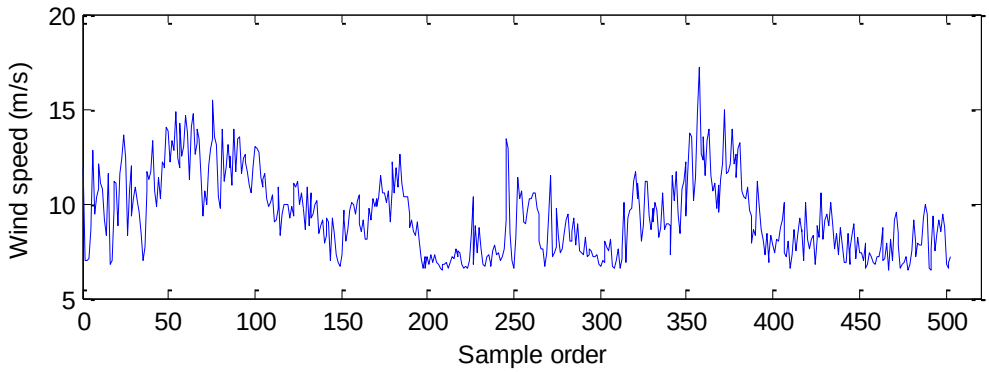

(a) Wind speed

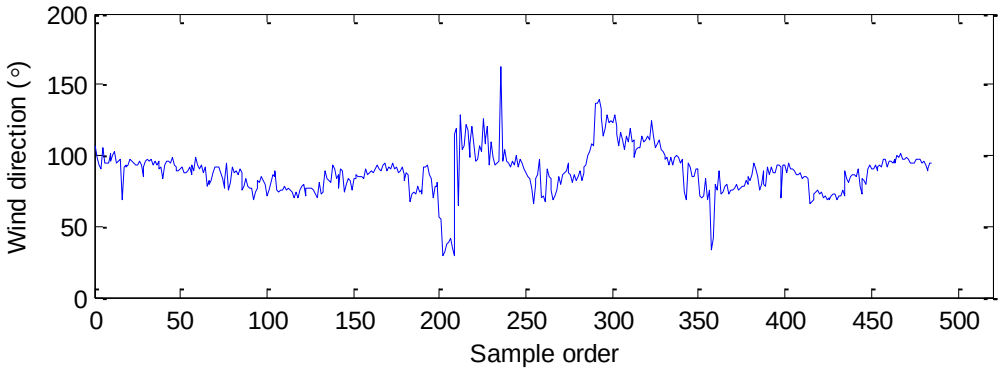

(b) Wind direction

Figure 4.3 Sequence of measured wind speed and wind direction

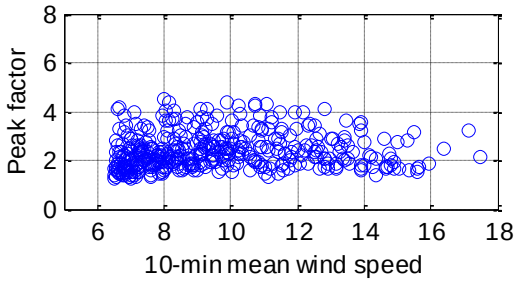

(a) Mid-main cable

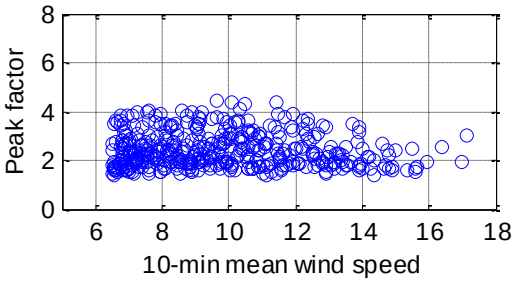

(b) Mid-main span

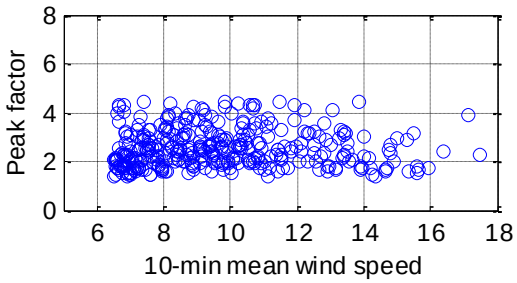

(c) 1/4 main span

Figure 4.4 Peak factor at different positions

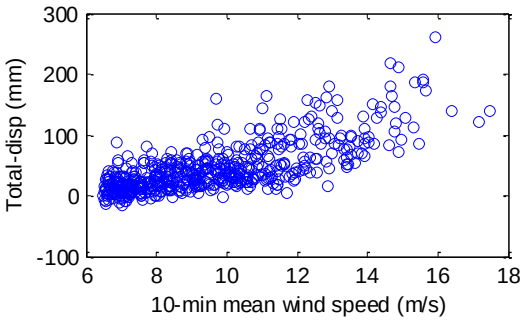

(a) Mid-main cable

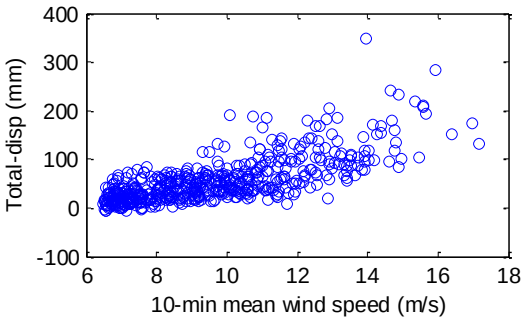

(b) Mid-main span

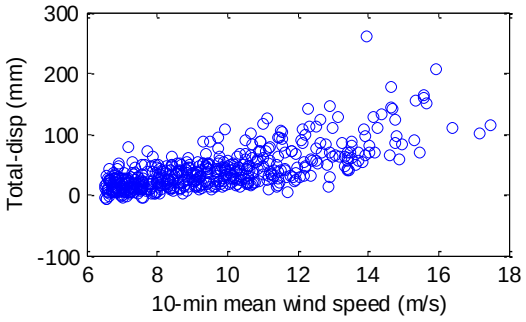

(c) 1/4 main span

Figure 4.5 Correlation between wind speed and total displacement in lateral direction

4.3.3 Model comparison

To determine an appropriate regression model between the displacement response and wind speed/wind direction, different explanatory variables and degrees of polynomial are considered and compared. The following five models are considered:

$$M_1 \quad : \quad y_i = \beta_0 + \beta_1 x_{1i} + \varepsilon_i$$

$$M_2 \quad : \quad y_i = \beta_0 + \beta_1 x_{1i} + \beta_2 x_{1i}^2 + \varepsilon_i$$

$$M_3 \quad : \quad y_i = \beta_0 + \beta_1 x_{1i} + \beta_2 x_{1i}^2 + \beta_3 x_{1i}^3 + \varepsilon_i$$

$$M_4 \quad : \quad y_i = \beta_0 + \beta_1 x_{1i} + \beta_2 x_{2i} + \varepsilon_i$$

$$M_5 \quad : \quad y_i = \beta_0 + \beta_1 x_{1i} + \beta_2 x_{1i}^2 + \beta_3 x_{2i} + \varepsilon_i$$

where y_i is the 10-min total displacement response, x_{1i} and x_{2i} are 10-min mean wind speed and wind direction. It is seen that only wind speed is treated as an explanatory variable in models M1, M2 and M3; whereas, both wind speed and wind direction are included in M4 and M5. Among the five candidate models, Bayesian model class selection is applied to select the optimal one for exploring the relationship between the wind-induced displacement and wind speed/direction. Meanwhile, root mean squared error (RMSE) is used for model performance assessment

$$RMSE = \sqrt{\frac{1}{n}\sum_{i=1}^{n}(y_i - \hat{y}_i)^2} \tag{4.10}$$

where y_i is the measurement value and $\hat{y}_i$ is the estimated mean value.

The measured data are decomposed into two sets training data set (data obtained from typhoons Haima and Nesat) and testing data set (data obtained from typhoon Nockten). The Bayesian regression model is formulated by using the training data, while the unseen testing data are only used to evaluate the performance of the formulated model. Figure 4.6 and Figure 4.7 compare the Log-ML and RMSE values for models M1 to M5 for the training data set. Both the Log-ML and RMSE show that M4 is the most suitable model for all three locations (mid-main cable, mid-main span, 1/4 main span), which implies that wind direction plays an important role in explaining the wind-induced displacement. Comparing the results among M1 to M3, RMSE is slightly better for M3 while Log-ML is maximized for M2. Although M5 has extra quadratic term of wind speed, it does not perform better than M4 in terms of either Log-ML or RMSE. Figure 4.8 shows the RMSE of each model for the testing data set. similar to the results in the training data set, M4 has the best RMSE score, M5 comes second and M1 does worst. In general, the predictive performance for the testing data set is poorer than for the training data set according to RMSE, but insignificant.

As shown in Figure 4.5, there exists a nonlinear relationship between the wind-induced displacement and wind speed, especially in the range of high wind speed. However, the optimal model M4 is a linear relationship model between the displacement and wind speed and direction. The reason may be that the number of measured data under

not very high wind speeds (< 10m/s) accounts for a large proportion, affecting the final results of model selection. Once the wind speed is strong enough, such as 50m/s or above, quadratic term plays a heavier role in assessing wind-induced displacement, which is useful for predicting the displacement response under strong winds. So in the next section, both M2 and M4 will be compared and discussed.

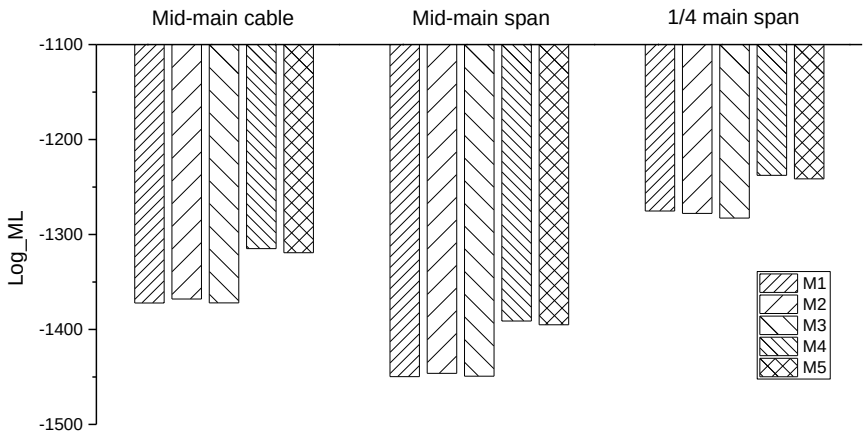

Figure 4.6 Log-ML values for training data

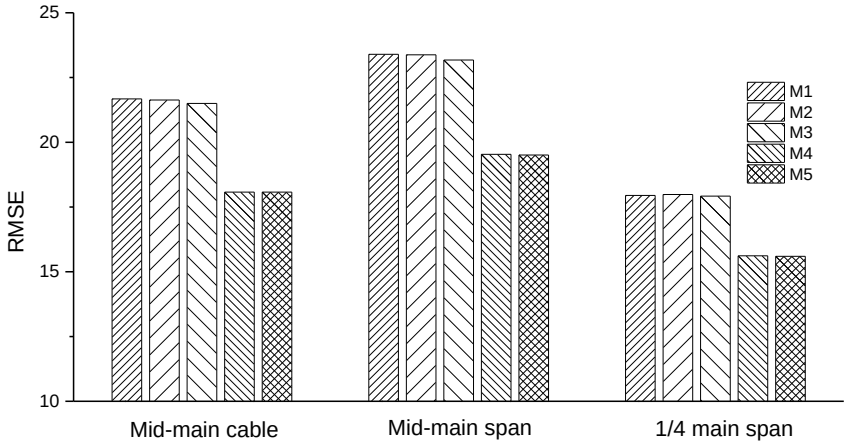

Figure 4.7 RMSE values for training data

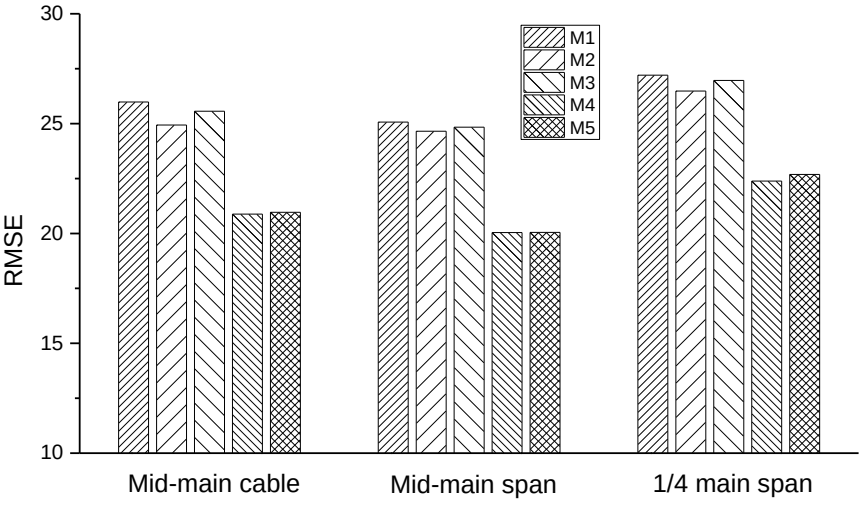

Figure 4.8 RMSE values for testing data

4.3.4 Parameter estimation

4.3.4.1 Parameters of M2

In M2, there are four parameters $\beta_0,\ \beta_1,\ \beta_2\ and\ \sigma^2$. Here, the total number of Markov chain iterations is chosen to be 100,000, of which the first 50,000 ($L_0 = 50{,}000$) iterations are discarded as burn-in replications. Thus, there remain 50,000 ($L_1 = 50{,}000$, $L_A = 0.1L_1,\ L_B = 0.5L_1,\ L_C = 0.4L_1$) posterior samples generated from Gibbs sampler for parameter estimation. As indicated previously, it is important to examine the convergence of Gibbs sequences before making Bayesian inference. Both trace plots and CD test statistic are used to check the convergence of the posterior samples.

With respect to the various locations (mid-main cable, mid-main span and 1/4 main span), three different regression models on wind-displacement are constructed. Thus, three sets of parameters for three models should be determined. Figure 4.9 to Figure 4.11 show the results of the model parameters of M2 for the three models. In the left panels of the figures are plots of sample paths of 50,000 draws and the right panels are the corresponding posterior densities. It is seen that the Markov chain is stationary by examining the trace plots. With the complete set of draws, the posterior density of each parameter is determined and the corresponding 95% confidence interval (the blue area) is also specified. The values of CD are all close to 0, indicating the posterior samples meet the requirement of convergence in parameter estimation. By using the posterior samples,

the posterior mean, standard deviation and 95 confidence interval are calculated, as shown in Table 4.3. The 95% confidence interval is estimated using the 2.5^{th} and 97.5^{th} percentiles of the posterior samples, which is regarded covering the true parameter values. To facilitate visual comparison, the results of model coefficients for different models are presented in terms of box plots, as shown in Figure 4.12. It clearly shows the variation range of each model coefficient and provides indications of symmetry of the data.

Figure 4.13 shows the relationships of mean wind speed and displacement, together with 95% confidence intervals. The red curve denotes the mean values of the model parameters, which agrees well with the measurement. The majority of measurement lie between the upper and lower bounds of the 95% confidence interval. The most striking feature of Bayesian approach is that the parameters of a Bayesian model are treated as distributions rather than deterministic values; as a result, the predicted displacement response also conforms to a distribution when a wind speed is given. It makes sense for civil engineering application because there are various types of modeling and parametric uncertainty in civil engineering problems. In Figure 4.13, the distribution of displacement response at the wind speed 12m/s is presented as an example. Based on the distribution, the displacement response with greatest probability or its probability for any given displacement response can be calculated. This function benefits the bridge manager to prepare for the arrival of a strong typhoon, such as making a decision as to whether or

when to shut down the traffic for safety according to the wind speed forecast issued by observatory. Another important point is that such model can be updated through updating the distributions of the model parameters when more monitoring data are available, so as to yield an evolutionary wind-resistant performance assessment of the bridge. The more valid monitoring data (especially those recorded under strong wind conditions), the narrower the variation range of model parameters (in terms of SD) and the higher the reliability of prediction. Meanwhile the model error σ^2 will be smaller too.

Table 4.3 Summary of estimated parameters for M2

Location	Parameter	Mean	Standard deviation	95% confidence interval		CD
Mid-main cable	β_0	3.89	8.77	-13.14	21.26	-0.001
	β_1	-3.97	1.78	-7.50	-0.63	-0.002
	β_2	0.81	0.09	0.63	0.99	0.006
	σ^2	721.11	44.17	640.01	812.67	-0.004
Mid-main span	β_0	2.48	9.06	-15.35	20.22	0.001
	β_1	-3.34	1.87	-7.02	0.35	0.001
	β_2	0.87	0.10	0.68	1.07	-0.003
	σ^2	962.30	59.23	853.23	1084.51	0.002
1/4 main span	β_0	4.99	8.57	-11.81	21.69	0.007
	β_1	-2.74	1.73	-6.13	0.66	-0.010
	β_2	0.63	0.09	0.46	0.80	0.012
	σ^2	548.94	35.13	484.24	622.73	0.001

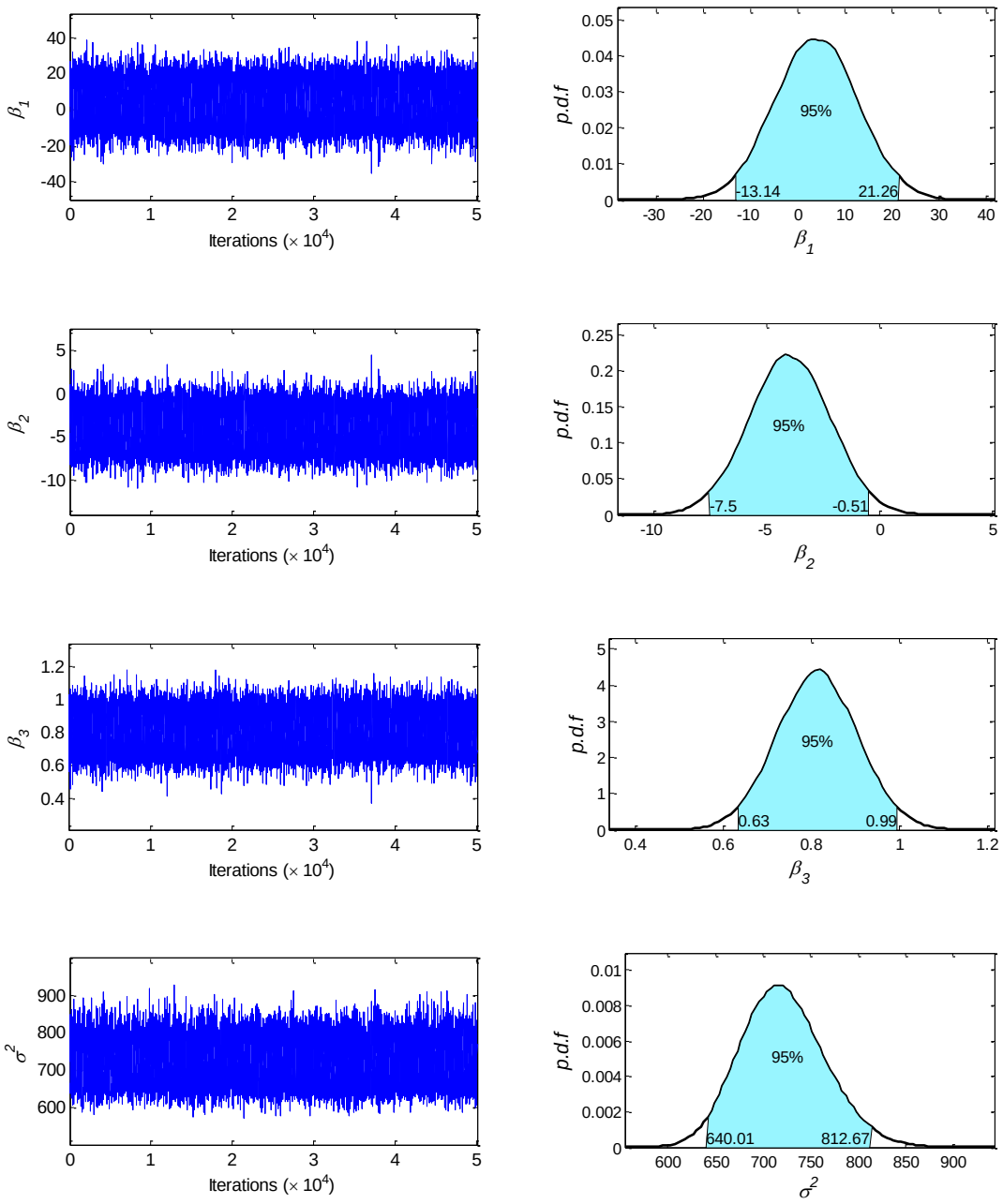

Figure 4.9 Sample paths and posterior distributions for M2 (mid-main cable)

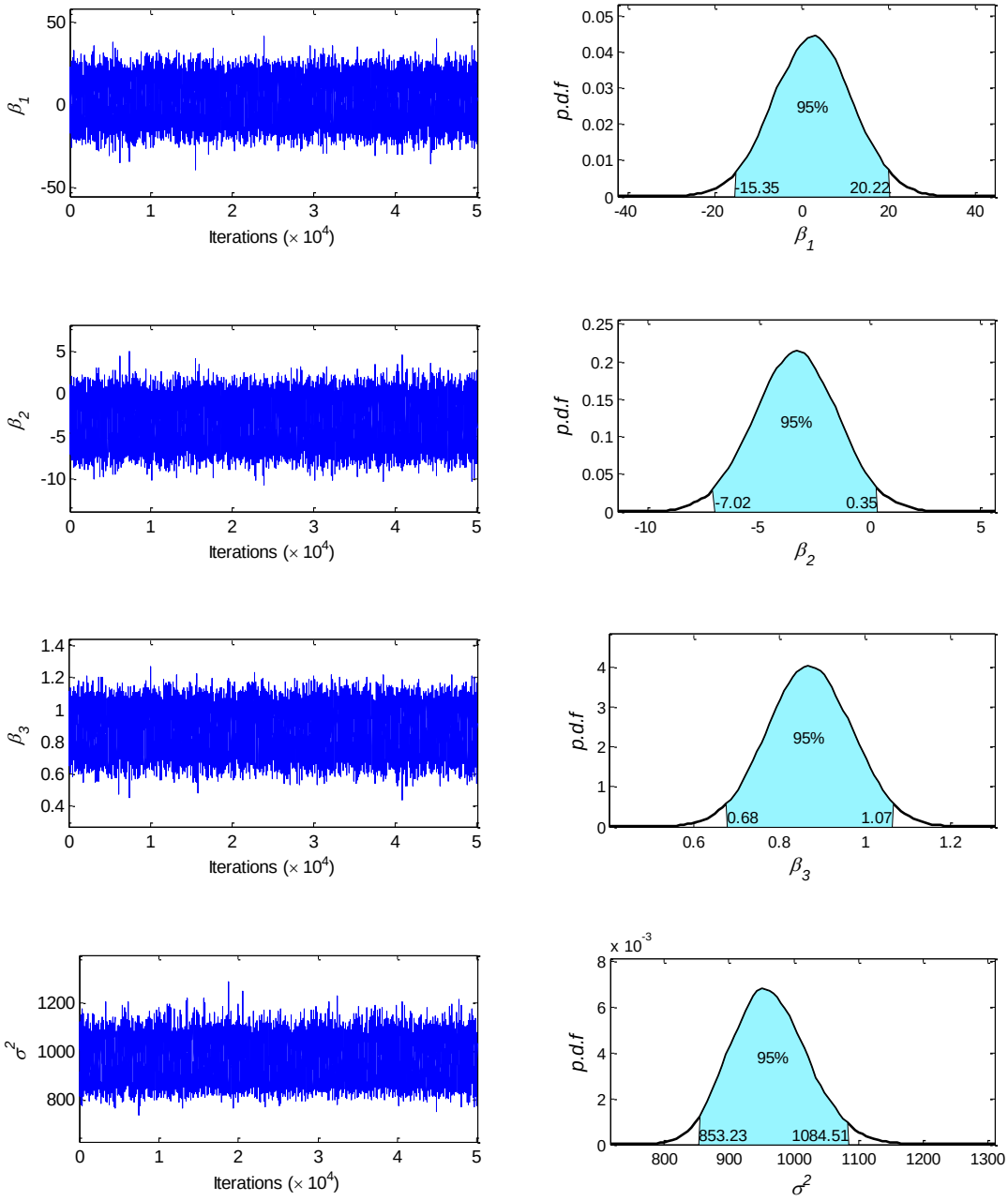

Figure 4.10 Sample paths and posterior distributions for M2 (mid-main span)

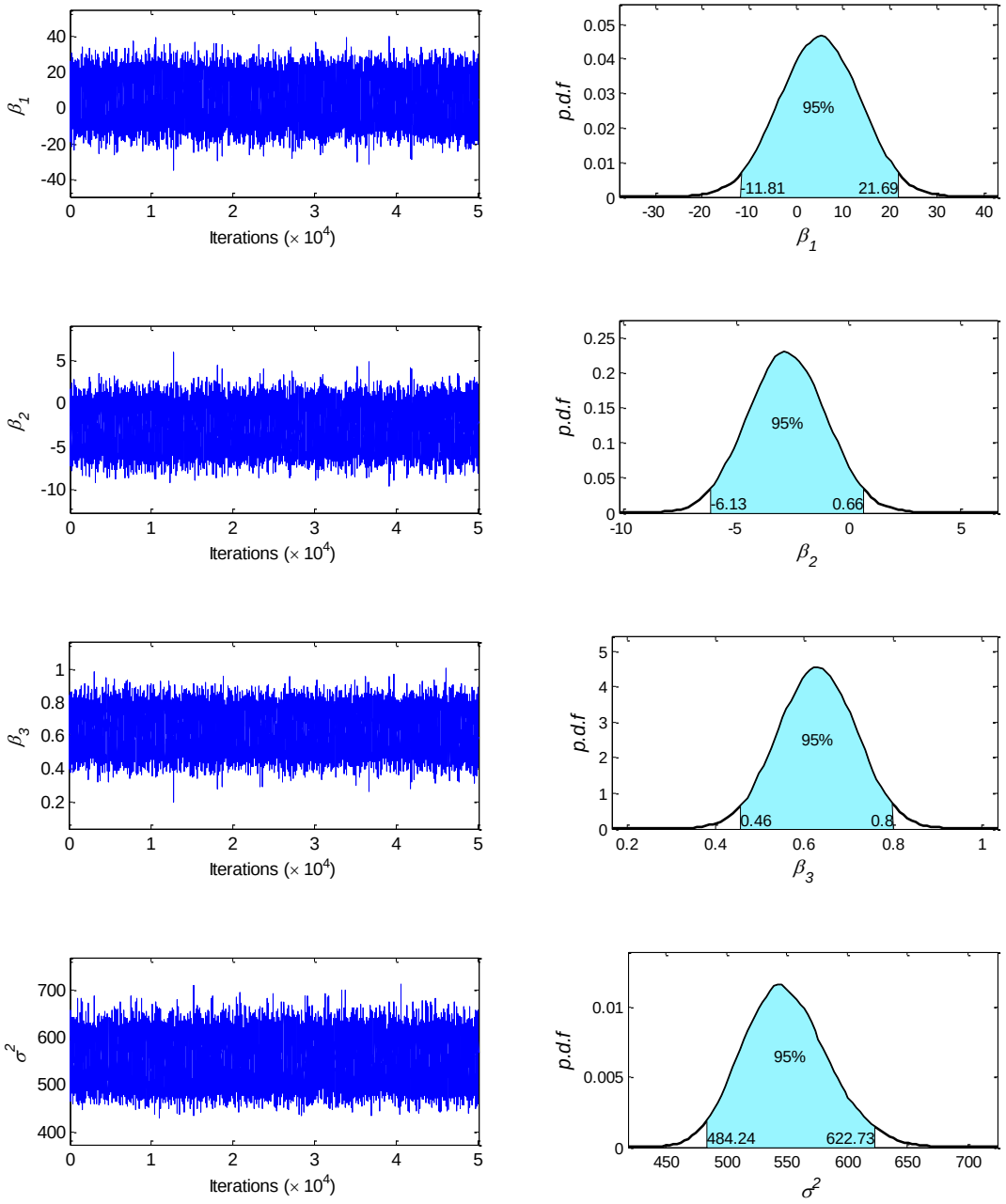

Figure 4.11 Sample paths and posterior distributions for M2 (1/4 main span)

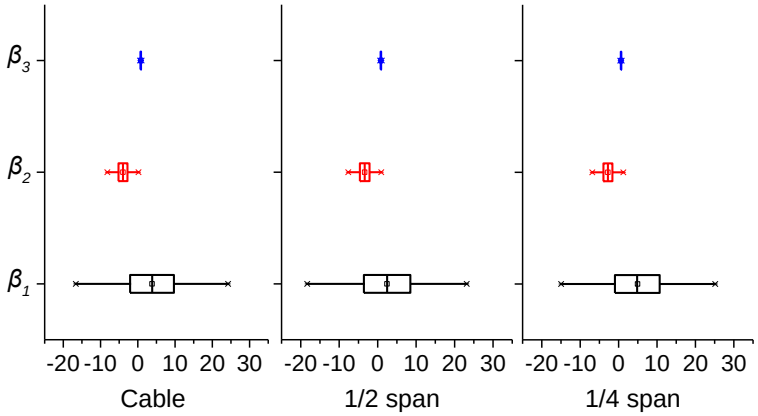

Figure 4.12 Estimated model coefficients for M2

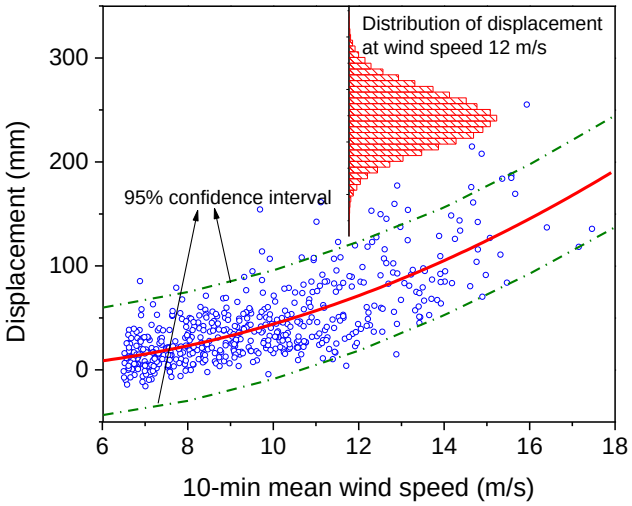

(a) Mid-main cable

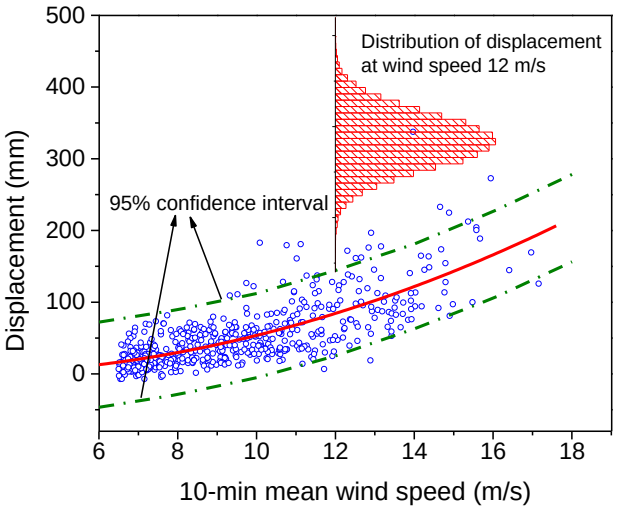

(b) Mid-main span

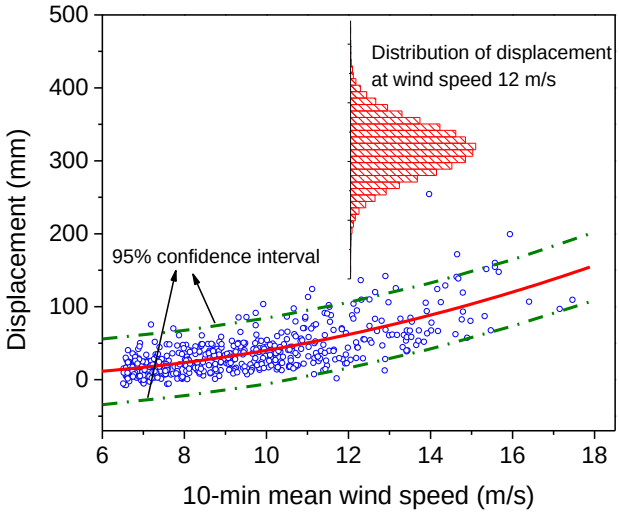

(c) 1/4 main span

Figure 4.13 Measured and fitted relationship between wind-induced displacement and wind speed (M2)

4.3.4.2 Parameters of M4

In M4, both wind speed and wind direction are taken as explanatory variables. Same as M2, the total number of Markov chain iterations is also chosen to be 100,000, of which the first 50,000 ($L_0 = 50{,}000$) iterations are discarded as burn-in replications, and there remain 50,000 ($L_1 = 50{,}000,\ L_A = 0.1L_1,\ L_B = 0.5L_1, L_C = 0.4L_1$) posterior samples generated from Gibbs sampler. Trace plots and CD test statistic are employed to examine convergence of the posterior samples. For three different locations (mid-main cable, mid-main span and 1/4 main span), the relationship models are formulated separately. Figure 4.14 shows the sample paths of the remaining 50,000 draws and corresponding posterior distributions for mid-main cable. As shown in the figure, there is no evidence of lack of

convergence by examining the trace plots. The posterior mean, standard deviation, 95% confidence interval and CD are summarized in Table 4.4. The values of CD are almost 0, again proving the convergence of posterior samples. The 95% confidence interval is estimated using the 2.5^{th} and 97.5^{th} percentiles of the posterior samples, which is regarded covering the true parameter values. Akin to the mid-main cable, the summary of the model parameters for the mid-main span and 1/4 main span is also presented in Table 4.4. Note that the model errors σ^2 for all three locations using M4 is reduced by 30% in comparison with M2. This further proves that M4 is more suitable than M2 explaining the wind-induced displacement response when the wind speed is not very high (< 20m/s). Taking into account both wind speed and wind direction, a three dimensional wind-induced displacement is plotted in Figure 4.17. The circle dots are the measured displacement and the two planes represent the 95% confidence surfaces. It is seen that most of the monitoring data lie within the two confidence surfaces. Although M4 can well explain the wind-induced displacement here, it has its limitations. M4 can merely express the linear relationship between the wind-induced displacement and wind speed and wind direction. From Figure 4.5 it is clearly seen that there exists a nonlinear relationship between the wind-induced displacement and wind speed with the increase of wind speed. The above model can well describe the wind-induced displacement at relatively low wind speeds, but may not be appropriate for high wind speeds, such as for predicting the

displacement at the design wind speed. The detailed information will be discussed in the next sub-section.

Table 4.4 Summary of estimated parameters for M4

Location	Parameter	Mean	Standard deviation	95% confidence interval		CD
Mid-main cable	β_0	11.98	5.15	3.43	20.50	-0.004
	β_1	10.99	0.36	10.41	11.58	-0.002
	β_2	-0.85	0.05	-0.93	-0.76	0.007
	σ^2	352.12	21.88	317.60	389.49	0.005
Mid-main span	β_0	14.67	5.35	5.94	23.52	-0.003
	β_1	11.64	0.39	10.99	12.29	-0.003
	β_2	-0.86	0.05	-0.94	-0.77	0.003
	σ^2	380.05	24.11	342.33	420.99	0.004
1/4 main span	β_0	12.88	4.97	4.77	21.10	0.009
	β_1	9.31	0.35	8.74	9.88	-0.005
	β_2	-0.72	0.05	-0.80	-0.64	-0.006
	σ^2	313.87	20.20	282.17	348.82	0.001

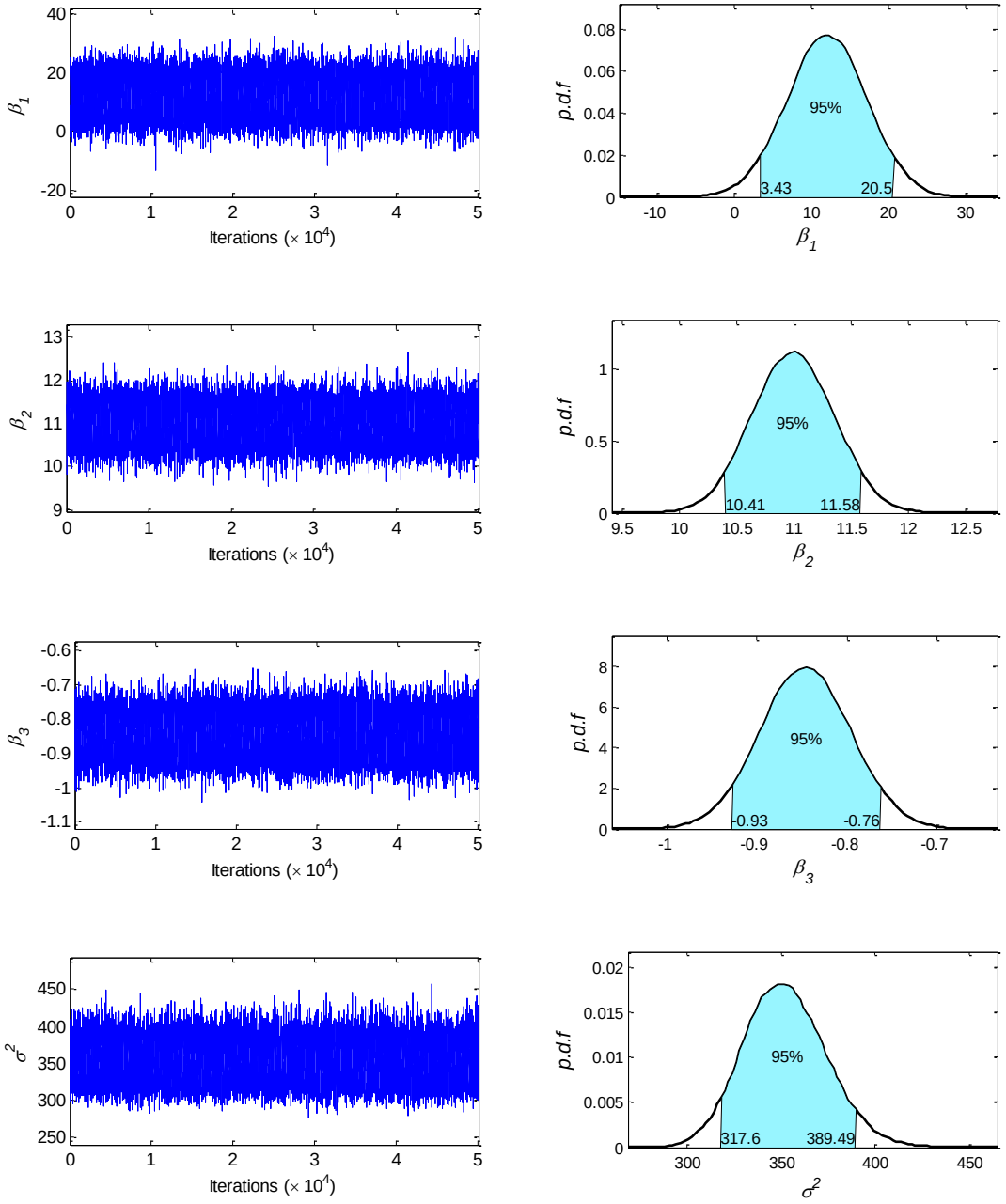

Figure 4.14 Sample paths and posterior distributions for M4 (mid-main cable)

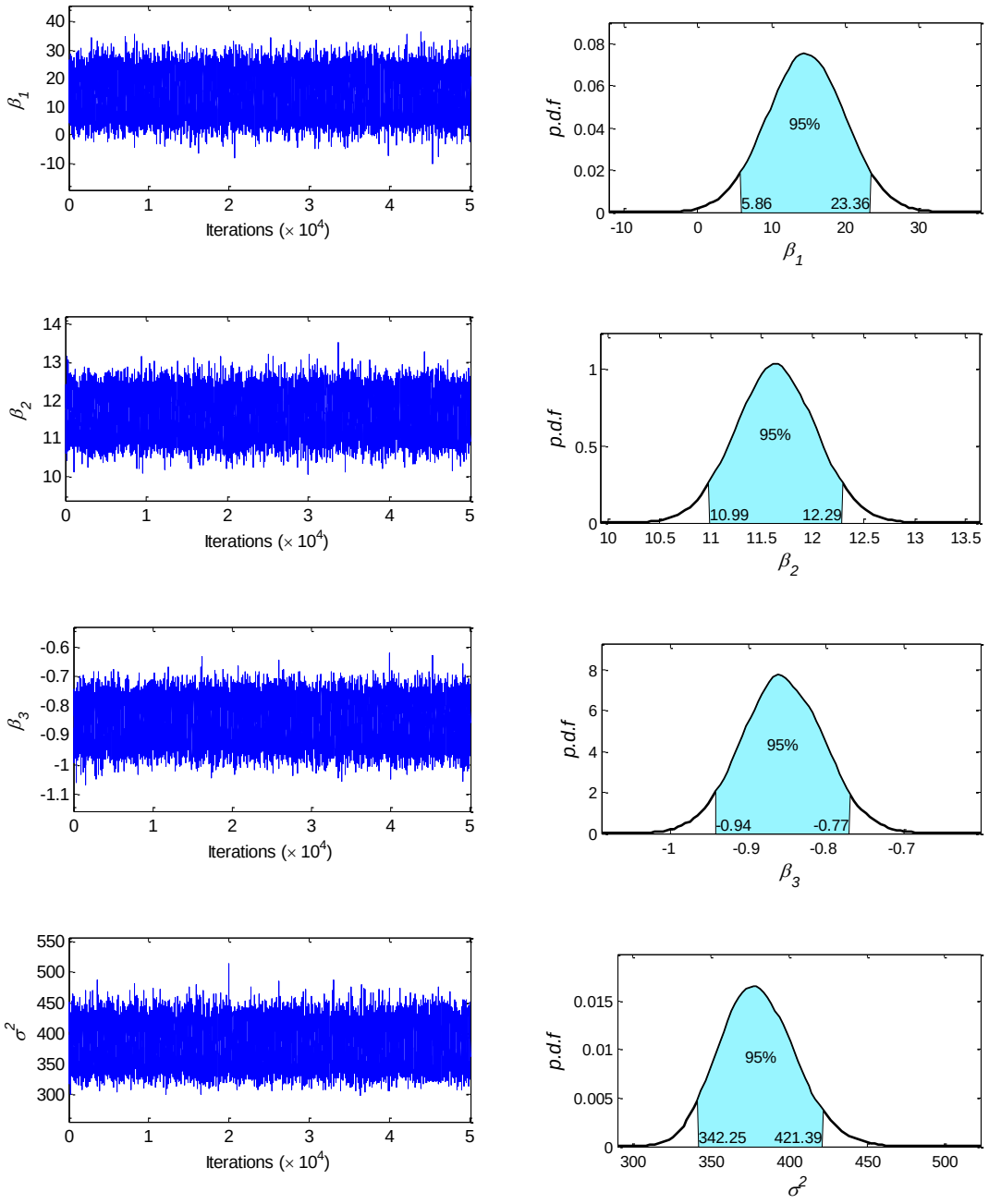

Figure 4.15 Sample paths and posterior distributions for M4 (mid-main span)

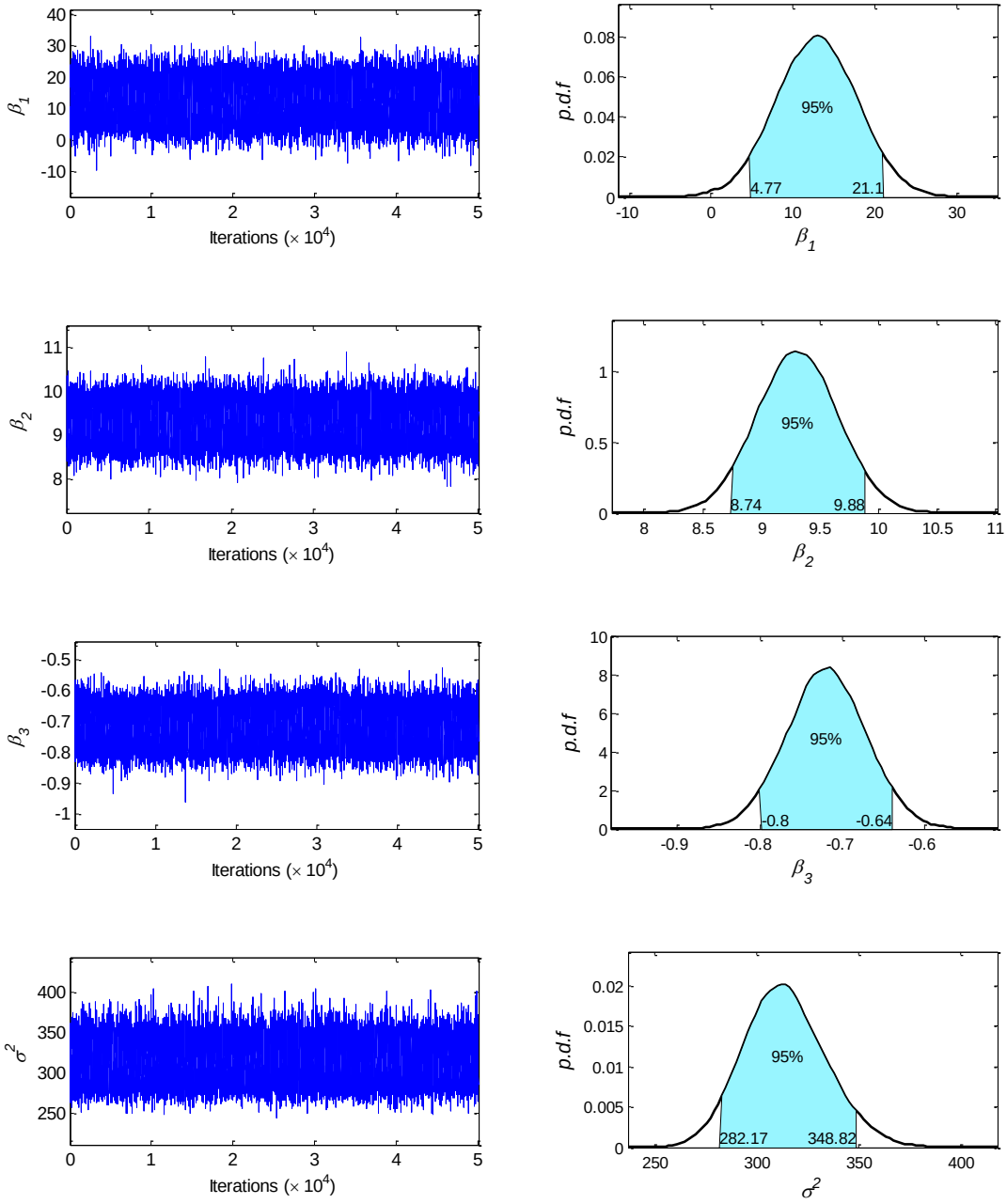

Figure 4.16 Sample paths and posterior distributions for M4 (1/4 main span)

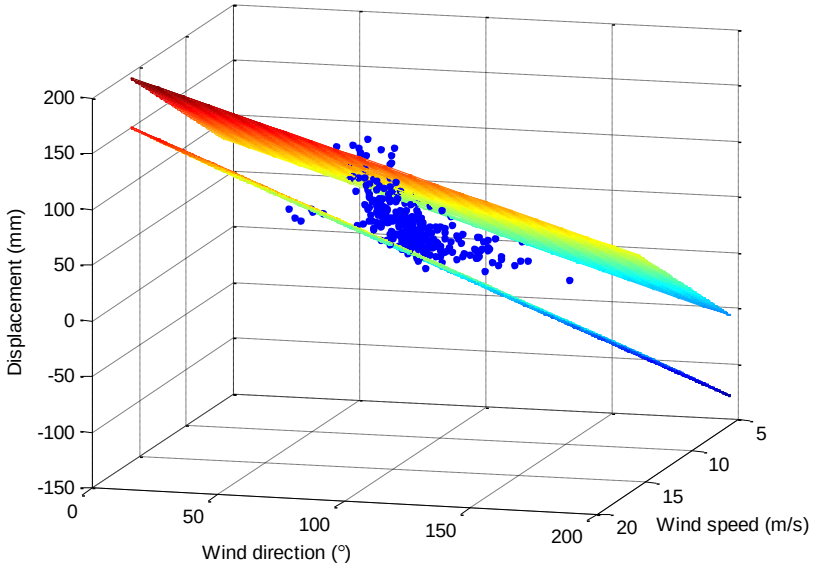

(a) Mid-main cable

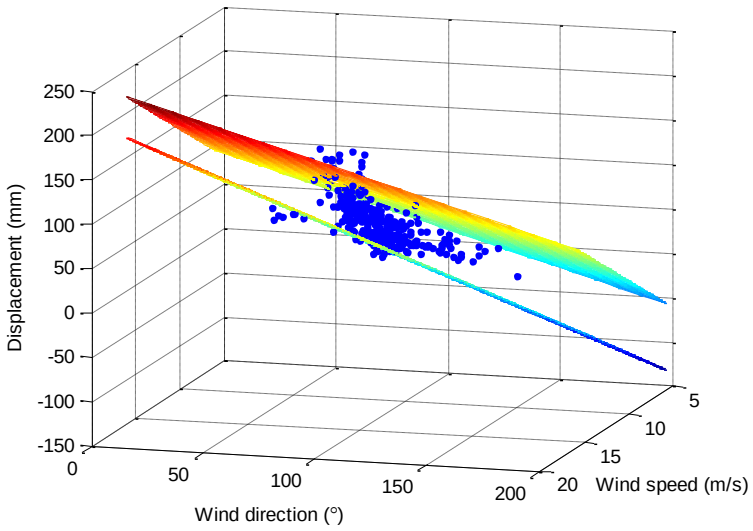

(b) Mid-main span

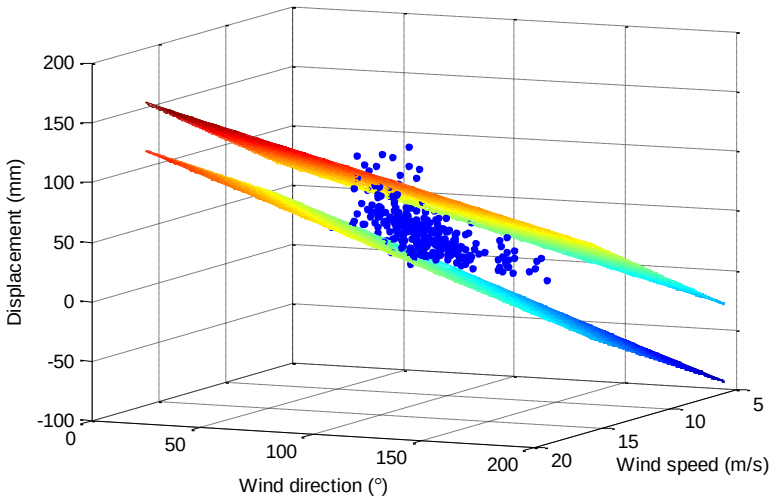

(c) 1/4 main span

Figure 4.17 Measured and fitted relationship between wind-induced displacement and wind speed/direction (M4)

4.3.5 Displacement prediction

In practice, we often concern the wind-induced displacement response at extreme scenarios, such as strong typhoons or hurricanes. For the TMB, the design 10-min wind speed for serviceability limit state (SLS) is 53.3m/s for a 120 year return period and the maximum allowable total displacement of the bridge in lateral direction is 2.9 m under the serviceability design wind speed (Xu and Chan 2009). So the design wind speed can be fed into the formulated regression model for wind-resistant performance assessment. The predicted total displacement responses at different locations of the bridge (mid-main cable, mid-main span and 1/4 main span) using models M2 and M4 are presented in Table 4.5. The total displacement at mid-main cable is close to that at the mid-main span, but

both of them are larger than that at 1/4 main span. The main reason is that the main span has greater span than the side spans and is more sensitive to wind effects. Comparing the predicted displacement responses from M2 and M4, it is found that the predicted displacement from M2 are much larger than from M4. The possible cause is the quadratic term in M2 which plays a significant role for high wind speed. M4 is not suitable for predicting the displacement under high wind speed. According to M2, the maximum predicted displacement occurs at the mid-main span of the bridge deck, whose mean value and 95% confidence interval are 2.32 m and 1.93-2.71 m, respectively. Compared with the maximum allowable total displacement given in the design stage, the predicted total displacement of the mid-main span, even the upper bound, is less than the design value in SLS. It can be concluded that the design is reasonable with appropriate safety reserve. One important point is that this model can be updated when more monitoring data are available, especially under high wind speed conditions, so as to yield an evolutionary wind-resistant performance assessment of the bridge. The confidence interval of forecast displacement will be narrower and more accurate with the increase of valid monitoring data obtained under strong winds.

Table 4.5 Predicted displacement responses under design wind speed

Model	Location	Mean (m)	Standard deviation	95% confidence interval (m)	
M2	Mid-main cable	2.11	0.18	1.76	2.47
	Mid-main span	2.32	0.19	1.93	2.71
	1/4 main span	1.66	0.17	1.32	1.99
M4	Mid-main cable	0.70	0.03	0.64	0.76
	Mid-main span	0.80	0.03	0.73	0.87
	1/4 main span	0.57	0.03	0.52	0.62

4.4 Summary

An extended BLM termed as Bayesian generalized linear model (BGLM) is proposed for assessing wind-induced displacement responses of an instrumented bridge. Among a set of candidate models considering different explanatory variables and degrees of polynomial, Bayesian model class selection is applied to choose the optimal model for exploring the relationship between the wind-induced displacement and wind speed/direction. According to Log-ML and RMSE values, the model M4 taking into account both wind speed and wind direction as explanatory variables, is the optimal one to fit the wind-induced displacement response under low wind speed. However, for predicting the displacement response under strong winds, the model M2 with quadratic term of wind speed performs better. This is because the quadratic term plays an important role in assessing wind-induced displacement when the wind speed is very large (such as 50m/s). The predicted maximum wind-induced displacement responses in lateral direction are less than the design value in serviceability limit state (SLS).

Chapter 5

BDLM for Real-time Condition Prediction

5.1 Introduction

Civil structures and infrastructure systems in service are always aging, deteriorating and eventually approaching their service life limit (Yao and Glisic 2015). A promising solution for mitigating the risk caused by ageing structures is to deploy appropriate sensors at the critical locations to monitor the condition of the structures in real-time. Despite that SHM systems have capacity to collect huge amounts of data, interpreting these data to obtain useful information on structural condition remains a challenge. One of the difficulties is to identify the baseline response of structures without the effect of external actions such as temperature and make a rational prediction of structural response in real-time. To succeed at this task, a Bayesian dynamic linear model (BDLM) is formulated to express the time-dependent responses of structures by assembling combinations of generic components. Then the formulated model is applied to forecast the structural responses at several steps ahead beyond the current time.

BDLMs (also called state space models in the field of machine learning) treat the time series as the output of a dynamic system perturbed by random disturbances. They are suitable for modeling univariate and, multivariate time series, also for representing the

structural changes, non-stationarity and irregular patterns (Perris *et al.* 2009). Unlike the classical time series method assuming a fixed relationship between the dependent variables (response variables) and the independent variables (regressors), dynamic linear model considers that the relationship changes over time. It is able to directly capture features of time series data, such as trend, seasonality, and regression effects. More importantly, the dynamic linear model allows for the description of temporary or permanent shifts in time series parameters that occur abruptly, which is necessary for outlier and damage detection in structural health monitoring paradigm. Although BDLM has gained application in engineering field in 1960s after the emergence of well-known Kalman filter (Kalman 1960, 1961), it appeared and became well known in handing the time series during 1970s (Akaile 1974) and 1980s (Aoki 1987; Harvey 1990), and became a center of interest in recent decades (Pole *et al.* 1994; Harrison and West 1999). BDLMs have recently obtained wide applications in a vast range of fields, from applied statistics to economics, from biology to genetics, from geophysical to engineering, and so on. It is partially attributed to the development of efficient computational methods, such as Markov Chain Monte Carlo algorithms that can deal with complex nonlinear and non-Gaussian cases, and sequential Monte Carlo methods that are suitable for online analysis (Petris *et al.* 2009).

This study develops a framework employing BDLM for modeling the time-dependent

structural responses, and then apply it to make online short-term prediction. The model is constructed by superposing generic components, such as locally linear trend, seasonal effect, and regression component. One advantage of Bayesian forecasting is that the forecast result is a posterior response distribution, in contrast to most non-Bayesian methods that only produce deterministic response and cannot quantify the reliability of forecast result. Bayesian forecasting is a continuous learning process that the state of prior knowledge is revised sequentially by incorporating new data. As a result, the proposed model can promptly respond to changes in time series of structural response and provide a posterior distribution of predictive structural response reflecting both the prior information and real-time data. The posterior structural response distribution can be used to generate a single-value (typically but not necessarily the mean) response as well as confidence level which represents the uncertainty of structural response prediction. The proposed method is then applied and validated with the use of monitoring data of strain response from an in-service cable-stayed bridge.

5.2 Bayesian Dynamic Linear Model

5.2.1 Model form and notation

In general, the dynamic linear model consists of the following two equations (West

and Harrison 1999):

$$\text{Observation Equation:} \quad y_t = F_t'\theta_t + v_t \qquad v_t \sim N[0, V_t] \tag{5.1}$$

$$\text{System Equation:} \quad \theta_t = G_t\theta_{t-1} + \omega_t \qquad \omega_t \sim N[0, W_t] \tag{5.2}$$

The observation equation describes the relationship between the observed data y_t and the unknown state parameters θ_t, and the system equation represents the state parameters θ_t vary through the passage of time, illustrating the dynamic changes of the state variables. The notations in the Equation (5.1) and (5.2) are:

- Observations: y_t is the observation series at time t;
- Regression vector: F_t is a $p \times 1$ vector of known constants (the regression vector);
- State parameters: θ_t is the $p \times 1$ vector of unknown parameters;
- Evolution matrix: G_t is an $p \times p$ matrix of known coefficients, determining the evolution of the state parameters;
- Observational and evolution errors: v_t and ω_t, are assumed to be mutually independent, and obey Gaussian distribution with mean zero and covariance matrices V_t and W_t, respectively. The error v_t is a random perturbation in the measurement process that affects the observation y_t but has no further influence on the series. By contrast, the error ω_t affects the development of the system into the future.

5.2.2 Sequential updating

Based on the observed data $\{y_1, y_2, \cdots, y_t\}$ and other relative information, it is assumed that the posterior distribution of state parameter at time t is $P(\theta_t|D_t) \sim N(m_t, C_t)$. The prior distribution of the state parameters for time $t+1$, $P(\theta_{t+1}|D_t)$, can be obtained by exploring the system equation

$$\begin{aligned} E[\theta_{t+1}|D_t] &= G_{t+1}E[\theta_t|D_t] + E[\omega_{t+1}] = G_{t+1}m_t = a_{t+1} \\ Var[\theta_{t+1}|D_t] &= G_{t+1}Var[\theta_t|D_t]G'_{t+1} + Var[\omega_{t+1}] = G_{t+1}C_tG'_{t+1} + W_{t+1} \\ &= R_{t+1} \end{aligned} \tag{5.3}$$

where D_t denotes the state of information at time t. Its normal form is $P(\theta_{t+1}|D_t) \sim N(a_{t+1}, R_{t+1})$.

The 1-step forecast distribution $P(y_{t+1}|D_t)$ for observation series can be derived by exploring the observation equation

$$\begin{aligned} E[y_{t+1}|D_t] &= F'_{t+1}E[\theta_{t+1}|D_t] + E[v_{t+1}] = F'_{t+1}a_{t+1} = f_{t+1} \\ Var[y_{t+1}|D_t] &= F'_{t+1}Var[\theta_{t+1}|D_t]F_{t+1} + Var[v_{t+1}] = F'_{t+1}R_{t+1}F_{t+1} + V_{t+1} \\ &= Q_{t+1} \end{aligned} \tag{5.4}$$

Its normal form is $P(y_{t+1}|D_t) \sim N(f_{t+1}, Q_{t+1})$.

When the observation y_{t+1} is available, the distribution of state parameter at time $t+1$ is updated to $P(\theta_{t+1}|D_{t+1}) \sim N(m_{t+1}, C_{t+1})$, where the means and variances are given by

$$m_{t+1} = a_{t+1} + A_{t+1}e_{t+1},$$

$$\begin{aligned} C_{t+1} &= R_{t+1} - A_{t+1}A_{t+1}^T Q_{t+1} \\ e_{t+1} &= y_{t+1} - f_{t+1}, \\ A_{t+1} &= R_{t+1}F_{t+1}/Q_{t+1} \end{aligned} \tag{5.5}$$

where $D_{t+1} = \{D_t, y_{t+1}\}$. The flowchart of updating of the Bayesian DLM is illustrated in Figure 5.1.

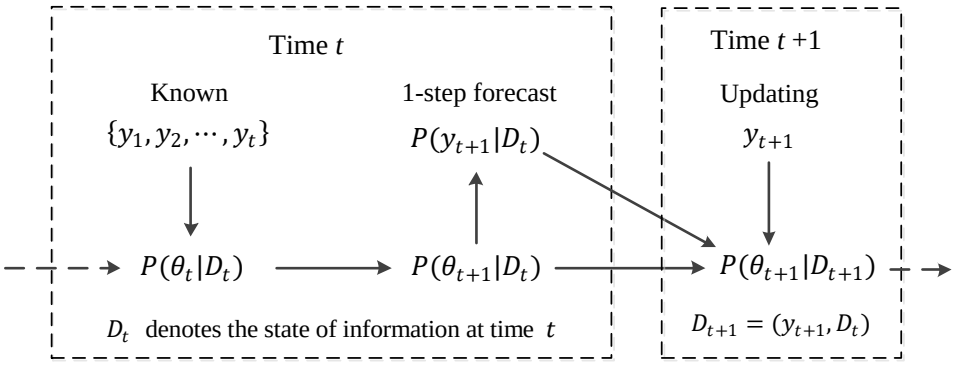

Figure 5.1 Flowchart of updating of Bayesian DLM

5.2.3 *k*-steps ahead predictions

Forecasting several steps ahead requires the prior information to be projected into the future through repeated application of the system equation. Given the posterior distribution of state parameter at time *t*, $P(\theta_t|D_t) \sim N(m_t, C_t)$, the mean and variance of state parameter for 1-steps ahead forecast are

$$\begin{aligned} E[\theta_{t+1}|D_t] &= G_{t+1}E[\theta_t|D_t] + E[\omega_{t+1}] = G_{t+1}m_t = a_t(1) \\ Var[\theta_{t+1}|D_t] &= G_{t+1}Var[\theta_t|D_t]G'_{t+1} + Var[\omega_{t+1}] = G_{t+1}C_tG'_{t+1} + W_{t+1} \\ &= R_t(1) \end{aligned} \tag{5.6}$$

Similarly, the mean and variance of state parameter at 2-step ahead forecast are

$$\begin{aligned} E[\theta_{t+2}|D_t] &= G_{t+2}E[\theta_{t+1}|D_t] + E[\omega_{t+2}] = G_{t+2}a_t(1) = a_t(2) \\ Var[\theta_{t+2}|D_t] &= G_{t+2}Var[\theta_{t+1}|D_t]G'_{t+2} + Var[\omega_{t+2}] = G_{t+2}R_t(1)G'_{t+2} \\ &\quad + W_{t+2} = R_t(2) \end{aligned} \tag{5.7}$$

Extending this procedure to *k*-steps ahead forecast, its mean and variance are

$$\begin{aligned} E[\theta_{t+k}|D_t] &= G_{t+k}E[\theta_{t+k-1}|D_t] + E[\omega_{t+k}] = G_{t+k}a_t(k-1) = a_t(k) \\ Var[\theta_{t+k}|D_t] &= G_{t+k}Var[\theta_{t+k-1}|D_t]G'_{t+k} + Var[\omega_{t+k}] \\ &= G_{t+k}R_t(k-1)G'_{t+k} + W_{t+k} = R_t(k) \end{aligned} \tag{5.8}$$

Its normal form is $P(\theta_{t+k}|D_t) \sim N(a_t(k), R_t(k))$.

Once the forecast of the state parameters is known, the associated forecast for the observation series can be calculated by the observation equation as

$$\begin{aligned} E[y_{t+k}|D_t] &= F'_{t+k}E[\theta_{t+k}|D_t] + E[v_{t+k}] = F'_{t+k}a_t(k) = f_t(k) \\ Var[y_{t+k}|D_t] &= F'_{t+k}Var[\theta_{t+k}|D_t]F_{t+k} + Var[v_{t+k}] \\ &= F'_{t+k}R_t(k)F_{t+k} + V_{t+k} = Q_t(k) \end{aligned} \tag{5.9}$$

Its normal form is $P(y_{t+k}|D_t) \sim N(f_t(k), Q_t(k))$.

5.2.4 Variance analysis

In most applications, the observation variance, V_t, and the system evolution covariance, W_t, are rarely completely known. Thus, several approaches are specified to estimate V_t and W_t: (i) both V_t and W_t are constant unknown, i.e., $V_t = V$ and $W_t = W$; (ii) $V_t = \alpha\bar{V}_t$ and $W_t = \beta\bar{W}_t$ where $\bar{V}_t$ and $\bar{W}_t$ are assumed to be known

while α and β are unknown constants; (iii) $V_t = V$ while W_t is explicitly related to G_t via a discount factor.

A commonly used model for the first case is to consider the observation and evolution variance matrices are time-invariant, for instance, $V_t = \sigma_y^2$ and $W_t = diag(\sigma_{\theta,1}^2, \sigma_{\theta,2}^2, \cdots, \sigma_{\theta,p}^2)$. Here the unknown parameters $(\sigma_y^2, \sigma_{\theta,1}^2, \sigma_{\theta,2}^2, \cdots, \sigma_{\theta,p}^2)$ need to be evaluated. Often the prior distributions of the unknown parameters are assumed to conform to Inverse-Gamma distribution with

$$\begin{aligned} \sigma_y^2 &\sim IG(\alpha_y, \beta_y) \\ \sigma_{\theta,i}^2 &\sim IG(\alpha_{\theta,i}, \beta_{\theta,i}),\ i = 1, \ldots., p \end{aligned} \tag{5.10}$$

Given the observations $y^{1:T}$, the joint posterior of the states $\theta^{1:T}$ and the unknown parameters $\psi = (\sigma_y^2, \sigma_{\theta,1}^2, \sigma_{\theta,2}^2, \cdots, \sigma_{\theta,p}^2)$ is (Petris *et al.* 2009)

$$\begin{aligned} \pi(y^{1:T}, \theta^{1:T}, \psi) &= \pi(y^{1:T}|\theta^{1:T}, \psi) \cdot \pi(\theta^{1:T}|\psi) \cdot \pi(\psi) \\ &= \prod_{t=1}^{T} \pi(y_t|\theta_t, \sigma_y^2) \cdot \prod_{t=1}^{T} \pi(\theta_t|\theta_{t-1}, \sigma_{\theta,1}^2, \sigma_{\theta,2}^2, \cdots, \sigma_{\theta,p}^2) \cdot \\ &\quad \pi(\theta_0) \cdot \pi(\sigma_y^2) \cdot \prod_{i=1}^{p} \pi(\sigma_{\theta,i}^2) \end{aligned} \tag{5.11}$$

What we are interested in is making inference about the unobservable states $\theta^{1:T}$ and the unknown parameters ψ. Obviously, it is analytically intractable and has to resort to a simulation method, such as MCMC approach. The Gibbs sampler is suitable for simulating draws from the full conditional distribution of states and from the full

conditional distributions of unknown parameters in turn. The detail of the simulation-based Bayesian inference will be given in Section 5.4.

The full conditional distribution of σ_y^2 is

$$\begin{aligned}\pi\left(\sigma_y^2|y^{1:T},\theta^{1:T},\sigma_{\theta,1}^2,\sigma_{\theta,2}^2,\cdots,\sigma_{\theta,p}^2\right) &\propto \prod_{t=1}^{T}\pi\left(y_t|\theta_t,\sigma_y^2\right)\cdot\ \pi\left(\sigma_y^2\right)\\ &\propto {\sigma_y^2}^{\frac{T}{2}+\alpha_y-1}exp\left\{-\sigma_y^2\cdot\left[\frac{1}{2}\sum_{t=1}^{T}(y_t-F_t'\theta_t)^2+\beta_y\right]\right\}\end{aligned} \tag{5.12}$$

which is again an Inverse-Gamma distribution

$$\sigma_y^2|y^{1:T},\theta^{1:T},\sigma_{\theta,1}^2,\sigma_{\theta,2}^2,\cdots,\sigma_{\theta,p}^2\sim \mathrm{I}G\left(\frac{T}{2}+\alpha_y,\frac{1}{2}SS_y+\beta_y\right) \tag{5.13}$$

with $SS_y=\sum_{t=1}^{T}(y_t-F_t'\theta_t)^2$. Similarly, the full conditional distribution of $\sigma_{\theta,i}^2$ is

$$\begin{gathered}\sigma_{\theta,i}^2|y^{1:T},\theta^{1:T}\sigma_{\theta,1}^2,\ldots,\sigma_{\theta,i-1}^2,\sigma_{\theta,i+1}^2,\sigma_{\theta,p}^2\sim G\left(\frac{T}{2}+\alpha_{\theta,i},\frac{1}{2}SS_{\theta,i}+\beta_{\theta,i}\right),\\ i=1,\ldots.,p\end{gathered} \tag{5.14}$$

with $SS_{\theta,i}=\sum_{t=1}^{T}\left(\theta_{t,i}-(G_t\theta_{t-1})_i\right)^2$.

5.3 Component Forms

The key issue in applying the BDLM to characterize the time-dependent responses of structures due to various external effects is the superposition of generic components such as trend component, seasonal component, and regression component. For this purpose, the observe data y_t can be expressed as

$$y_t=y_{Tt}+y_{St}+y_{Rt}+v_t \tag{5.15}$$

where y_{Tt}, y_{St}, y_{Rt} and v_t denote the trend component, seasonal component, regression component and error, respectively. In terms of the state space Equations (5.1) and (5.2), these terms can be expressed as

$$\theta_t = \begin{pmatrix} \theta_{Tt} \\ \theta_{St} \\ \theta_{Rt} \end{pmatrix},\ F_t = \begin{pmatrix} F_{Tt} \\ F_{St} \\ F_{Rt} \end{pmatrix},\ G_t = \begin{pmatrix} G_{Tt} & & \\ & G_{St} & \\ & & G_{Rt} \end{pmatrix}$$

$$W_t = \begin{pmatrix} W_{Tt} & & \\ & W_{St} & \\ & & W_{Rt} \end{pmatrix},\ V_t = \sigma_{obs}^2$$

5.3.1 Trend component

In time series, polynomial models can be used to describe trends that are viewed as smooth developments over time. Especially, the first- and second-order polynomial models are often found in application. The simplest trend model is the first-order polynomial trend. The observed time series data can be written as

$$\begin{aligned} y_t &= \mu_t + v_t,\ v_t \sim N(0, \sigma_{obs}^2) \\ \mu_t &= \mu_{t-1} + \omega_t,\ \omega_t \sim N(0, \sigma_{level}^2) \end{aligned} \tag{5.16}$$

which can be expressed in the form of state space model by setting

$$\theta_{Tt} = \mu_t,\ F_{Tt} = 1,\ G_{Tt} = 1,\ W_{Tt} = \sigma_{level}^2,\ V_t = \sigma_{obs}^2$$

A second-order polynomial trend model allows for systematic decline or growth in level and has the form

$$y_t = \mu_t + v_t,\ v_t \sim N(0, \sigma_{obs}^2)$$
$$\mu_t = \mu_{t-1} + \alpha_{t-1} + \omega_{1t},\ \omega_{1t} \sim N(0, \sigma_{level}^2) \tag{5.17}$$
$$\alpha_t = \alpha_{t-1} + \omega_{2t},\ \omega_{2t} \sim N(0, \sigma_{trend}^2)$$

The state vector has two elements, μ_t and α_t, the first denoting the current level and the second denoting the current rate of change in level. In the form of state model, it can be written as

$$\theta_{Tt} = \begin{pmatrix}\mu_t \\ \alpha_t\end{pmatrix},\ F_{Tt} = \begin{pmatrix}1 \\ 0\end{pmatrix},\ G_{Tt} = \begin{pmatrix}1 & 1 \\ 0 & 1\end{pmatrix},\ W_{Tt} = \begin{pmatrix}\sigma_{level}^2 & 0 \\ 0 & \sigma_{trend}^2\end{pmatrix},\ V_t = \sigma_{obs}^2$$

Higher order polynomial trend can be introduced by extending the first and second order models, but practically such higher orders are rarely used.

5.3.2 Seasonal component

Cyclical or periodic behavior is evident in many time series associated with structural systems. For example, the displacement of bridge expansion joints changes periodically every day. It is important to recognize and include cyclical patterns in forecasting models. The cyclical behavior of time series can be well modelled using mathematical functions, such as sines and cosines (Laine *et al.* 2014). Consider the time series y_t that are represented by a series of harmonics as

$$y_t = \sum_{k=1}^{n} (a_k \cos(k\omega t) + b_k \sin(k\omega t)) + v_t \tag{5.18}$$

where $\omega = 2\pi/s$. If the number of cyclic components is s, the full seasonal model has $s/2$ harmonics and $n \leq s/2$. The kth harmonic of y_t is defined as

$$u_{kt} = a_k \cos(k\omega t) + b_k \sin(k\omega t)$$

In order to realize the kth harmonic evolution from time $(t-1)$ to time t, the conjugate harmonic of u_{kt} is introduced

$$u_{kt}^* = -a_k \sin(k\omega t) + b_k \cos(k\omega t)$$

Thus the corresponding state vector has two variables

$$\theta_{seas(k)} = (u_{kt}, u_{kt}^*)'$$

By defining the evolution matrix

$$G_{seas(k)} = \begin{pmatrix} \cos k\omega & \sin k\omega \\ -\sin k\omega & \cos k\omega \end{pmatrix}$$

we have

$$\begin{pmatrix} u_{kt} \\ u_{kt}^* \end{pmatrix} = G_{seas(k)} \begin{pmatrix} u_{k(t-1)} \\ u_{k(t-1)}^* \end{pmatrix} + \begin{pmatrix} \omega_{kt} \\ \omega_{kt}^* \end{pmatrix}, \omega_{kt}, \omega_{kt}^* \sim N(0, \sigma_{seas(k)}^2).$$

The regression vector and error matrix are

$$F_{seas(k)} = \begin{pmatrix} 1 \\ 0 \end{pmatrix}$$

$$W_{seas(k)} = \begin{pmatrix} \sigma_{seas(k)}^2 & 0 \\ 0 & \sigma_{seas(k)}^2 \end{pmatrix}$$

when seasonality can be well explained by n $(n \leq s/2)$ harmonics, the seasonal effect model in the form of state space model becomes

$$\theta_{St} = \left(\theta'_{seas(1)}, \cdots, \theta'_{seas(n)}\right)'$$

$$F_{St} = \left(F'_{seas(1)}, \cdots, F'_{seas(n)}\right)'$$

$$G_{St} = diag(G_{seas(1)}, \cdots, G_{seas(n)})$$

$$W_{St} = diag(W_{seas(1)}, \cdots, W_{seas(n)})$$

5.3.3 Regression component

In the context of SHM, regression components are employed to describe the dependence between the response of a structure and the hidden state variables associated with other observations, such as temperature and wind. Now consider the modeling of the time series y_t by regressing on q independent variables labelled $\{x_1, x_2, \cdots, x_q\}$. For each *t*, the model equations are

$$\begin{aligned} y_t &= \beta_{1t}x_{1t} + \cdots + \beta_{qt}x_{qt} + v_t \\ \beta_{it} &= \beta_{it-1} + \omega_{it},\ \omega_{it} \sim N(0, \sigma_i^2)\ \ i = 1, \cdots, q \end{aligned} \tag{5.19}$$

In terms of state space model, the regression model can be expressed as

$$\theta_{Rt} = (\beta_{1t}, \cdots, \beta_{qt})'$$

$$F_{Rt} = (x_{1t},, \cdots, x_{qt})'$$

$$G_t = I_q$$

$$W_{Rt} = diag(\sigma_1^2, \cdots \sigma_q^2)$$

5.4 Simulation-Based Bayesian Inference

For convenience, some symbols are defined firstly. We use the vectors

$$y^{1:T} = [y_1, y_2, \dots, y_T]$$

$$\theta^{1:T} = [\theta_1, \theta_2, \cdots, \theta_T]$$

to represent the history of observed data and state parameters until time T, and

$$y^{T+1:T+H} = [y_{T+1}, y_{T+2}, \dots, y_{T+H}]$$

$$\theta^{T+1:T+H} = [\theta_{T+1}, \theta_{T+2}, \cdots, \theta_{T+H}]$$

to represent potential future observation and state parameters from time T onward to $(T + H)$. Let the unknown observation variance $V_t = \sigma_y^2$ and evolution covariance $W_t = diag(\sigma_{\theta,1}^2, \sigma_{\theta,2}^2, \cdots, \sigma_{\theta,p}^2)$. Thus the unknown parameters can be expressed collectively as $\psi = (\sigma_y^2, \sigma_{\theta,1}^2, \sigma_{\theta,2}^2, \cdots, \sigma_{\theta,p}^2)$, which is also called hyperparameters.

5.4.1 Posterior predictive density

From a Bayesian perspective, we are going to obtain the posterior distribution for the objects of interest. If we are interested in a forward prediction, the posterior predictive distribution is what we want. Conditional on prior information and available data through time T, beliefs about the future can be expressed by the joint posterior distribution

$$p(y^{T+1:T+H}, \theta^{T+1:T+H}, \theta^{1:T}, \psi | y^{1:T})$$

While it is complicated in manipulation, the above expression can be decomposed into tractable components

$$p(y^{T+1:T+H}, \theta^{T+1:T+H}, \theta^{1:T}, \psi | y^{1:T}) \\ = p(\theta^{1:T}, \psi | y^{1:T}) \times p(y^{T+1:T+H}, \theta^{T+1:T+H} | \theta^{1:T}, \psi) \tag{5.20}$$

This expression decomposes the joint distribution into two parts: the first part, $p(\theta^{1:T}, \psi | y^{1:T})$, is the joint posterior density for history of states and hyperparameters; the second part, $p(y^{T+1:T+H}, \theta^{T+1:T+H} | \theta^{1:T}, \psi)$, is the joint distribution for future data and states based on the current states and hyperparameters. Analytical solution for each part is impossible, even for simple cases. Therefore, we employ MCMC methods to explore the posterior distribution. According to the components in Equation (5.20), the algorithm is split into two steps: (i) draw a pair of $(\theta^{1:T}, \psi)$ from $p(\theta^{1:T}, \psi | y^{1:T})$, and (ii) plug the draw into $p(y^{T+1:T+H}, \theta^{T+1:T+H} | \theta^{1:T}, \psi)$ to generate the future states $\theta^{T+1:T+H}$ and data $y^{T+1:T+H}$.

5.4.2 BDLM parameter estimation: Gibbs sampler

The posterior distribution for states $\theta^{1:T}$ and hyperparameters ψ can be expressed as

$$p(\theta^{1:T}, \psi | y^{1:T}) = p(y^{1:T} | \theta^{1:T}, \psi) p(\theta^{1:T}, \psi) \propto p(\theta^{1:T} | \psi, y^{1:T}) p(\psi | y^{1:T}) \tag{5.21}$$

where $p(\theta^{1:T}, \psi)$ represents a joint prior for states and hyperparameters; $p(y^{1:T} | \theta^{1:T}, \psi)$ is a conditional likelihood. Following Kim and Nelson (1999), Gibbs sampler is suitable for simulating draws from $p(\theta^{1:T}, \psi | y^{1:T})$, which iterates on two

operations. First, we draw states from $p(\theta^{1:T}|\psi, y^{1:T})$ conditional on the data and hyperparameters. Second, we draw hyperparameters from $p(\psi|\theta^{1:T}, y^{1:T})$ conditional on the data and states. Subject to regularity conditions (Roberts and Smith 1994), the sequence of draws converges to a draw from the joint distribution $p(\theta^{1:T}, \psi|y^{1:T})$.

For convenience in being natural conjugates, the prior for (θ_0, ψ_0) is taken as a conjugate normal inverse gamma, that is

$$P(\theta_0|\psi_0) \propto N(\bar{\theta}, \bar{P})$$

$$P(\psi_0) \propto IG(T_0, \bar{\psi}^{-1}).$$

5.4.2.1 Gibbs step 1: drawing states given hyperparameters

The conditional density $p(\theta^{1:T}|\psi, y^{1:T})$ in the first part of Equation (5.21) can be factored as (Kim and Nelson 1999; Cogley and Sargent 2001)

$$p(\theta^{1:T}|\psi, y^{1:T}) = p(\theta_T|\psi, y^{1:T}) \prod_{t=1}^{T-1} p(\theta_t|\theta_{t+1}, \psi, y^{1:T}) \tag{5.22}$$

The first term $p(\theta_T|\psi, y^{1:T})$ is the marginal posterior for the terminal state, and the other terms are conditional densities for the preceding time periods. Since the densities on the right-hand side of the expression conform to Gaussian, the samples can be separately drawn from Equations (5.23) and (5.24)

$$p(\theta_T|\psi, y^{1:T}) \sim N(\theta_{T|T}, P_{T|T}) \tag{5.23}$$

$$p(\theta_t|\theta_{t+1}, \psi, y^{1:T}) \sim N(\theta_{t|t+1}, P_{t|t+1}) \tag{5.24}$$

1. Mean and variance of $p(\theta_T|\psi, y^{1:T})$

The mean $\theta_{T|T}$ and variance $P_{T|T}$ can be obtained via the Kalman filter, which is a recursive algorithm via estimating the state variable at each time period given information up to that time period. It consists the following equations which are evaluated recursively over time. Starting from an initial value $\theta_{0|0}$ and $P_{0|0}$, the conditional means and variances can be obtained by iteration (Kim and Nelson 1999)

$$\begin{aligned}
\theta_{t|t-1} &= G_t \theta_{t-1|t-1} \\
P_{t|t-1} &= P_{t-1|t-1} + W \\
\eta_{t|t-1} &= y_t - F_t' \theta_{t|t-1} \\
f_{t|t-1} &= F_t' P_{t|t-1} F_t + V \\
\theta_{t|t} &= \theta_{t|t-1} + K_t \eta_{t|t-1} \\
P_{t|t} &= P_{t|t-1} - K_t F_t' P_{t|t-1}
\end{aligned} \tag{5.25}$$

where $K_t = P_{t|t-1} F_t f_{t|t-1}^{-1}$. The first equation $\theta_{t|t-1} = G_t \theta_{t-1|t-1}$ predicts state variable one step ahead using the transition equation and the second equation estimates the variance of state parameter at time t based on the information at time $t-1$. The third and fourth equations calculate the mean and variance of prediction error, respectively. The final two equations are referred to updating state variable using the new observation y_t at time t. Running these equations for periods $t = 1,2 \ldots, T$, the final

recursion yields $\theta_{T|T}$ and $P_{T|T}$ for the terminal state.

2. Mean and variance of $p(\theta_t|\theta_{t+1}, \psi, y^{1:T})$

After the terminal state θ_T is drawn from $p(\theta_T|\psi, y^{1:T})$, the next task is to recursively draw θ_t (for $t = T-1, T-2, \ldots, 0$) from $p(\theta_t|\theta_{t+1}, \psi, y^{1:T})$ by the forward filtering backward sampling (FFBS) algorithm. Assuming that we already have $(\theta_T, \ldots, \theta_{t+1})$, the next step is to draw θ_t from $N(\theta_{t|t+1}, P_{t|t+1})$, where $\theta_{t|t+1}$ and $P_{t|t+1}$ can be computed by iteration

$$\begin{aligned} \theta_{t|t+1} &= \theta_{t|t} + P_{t|t}P_{t+1|t}^{-1}(\theta_{t+1} - \theta_{t|t}) \\ P_{t|t+1} &= P_{t|t} - P_{t|t}P_{t+1|t}^{-1}P_{t|t} \end{aligned} \tag{5.26}$$

Note that $\theta_{t|t+1}$ explicitly depends on the value of θ_{t+1} already generated. The process of FFBS algorithm is summarized in Algorithm 5.1.

Algorithm 5.1 Forward filtering backward sampling (FFBS)

1. Run Kalman filter;
2. Draw $\theta_T \sim N(\theta_{T|T}, P_{T|T})$
3. For $t = T-1, T-2, \ldots, 0$, draw $\theta_t \sim N(\theta_{t|t+1}, P_{t|t+1})$

To summarize, the Gibbs sampling for drawing states has two steps. First, draw θ_T from Equation (5.23), by using Equation (5.25) to compute the mean and variance. Next draw θ_{T-1} from Equation (5.24), by using Equation (5.26) to compute the mean and variance conditional on θ_T. Then draw θ_{T-2} conditional on the realization of θ_{T-1}

until to the beginning of sample.

5.4.2.2 Gibbs step 2: drawing hyperparameters given states

Conditional on $\theta^{1:T}$ and $Y^{1:T}$, the hyperparameters are observable. Since the prior of ψ is an inverse Gamma distribution and the conditional likelihood is Gaussian, the posterior is also an inverse Gamma density

$$p(\psi|\theta^{1:T}, y^{1:T}) = IG(T_1, \psi_1^{-1}) \tag{5.27}$$

where

$$T_1 = T_0 + \frac{T}{2}$$

$$\psi_1 = \bar{\psi} + \frac{1}{2}\bar{V}_T$$

$$\bar{V}_T = diag(SS_{y,}SS_{\theta,1}, \cdots, SS_{\theta,p})$$

$$SS_y = \sum_{t=1}^{T}(y_t - F_t'\theta_t)^2$$

$$SS_{\theta,i} = \sum_{t=1}^{T}\left(\theta_{t,i} - (G_t\theta_{t-1})_i\right)^2,\ i = 1, \cdots, p$$

5.4.2.3 Summary of Gibbs sampling

As described above, the Gibbs sampler algorithm consists of two simulations, drawing the state parameters from their conditional distribution given the hyperparameters and observations, and drawing the hyperparameters from the conditional

distribution given the states and observations, as summarized in Algorithm 5.2. After a burn-in period, the sequence of draws approximates a sample from $p(\theta^{1:T}, \psi | y^{1:T})$.

Algorithm 5.2 Gibbs sampler

0. Initialize: set and $\psi^{(0)}$
1. For $i = 1, \cdots, N$
a) Draw $\theta^{1:T(i)}$ from $p(\theta^{1:T} \| \psi^{(i-1)}, y^{1:T})$ using FFBS
b) Draw $\psi^{(i)}$ from $p\left(\psi \| \theta^{1:T(i)}, y^{1:T}\right)$

5.4.3 Beliefs about the future

Having processed the known data, the next step is to simulate the future states and observations. Conditional on the current state and hyperparameters, the posterior density for future data and states is quite traceable and can be factored into

$$\begin{aligned} & p(y^{T+1:T+H}, \theta^{T+1:T+H} | \theta_T, \psi, y^{1:T}) \\ & \quad = p(\theta^{T+1:T+H} | \theta_T, \psi, y^{1:T}) \\ & \quad \times p(y^{T+1:T+H} | \theta^{T+1:T+H}, \theta_T, \psi, y^{1:T}) \end{aligned} \tag{5.28}$$

in which the first term on the right-hand side is a marginal distribution for future states, and the second term is a conditional distribution for future observations. Since the states are Markov, the first term continues to be factored into

$$p(\theta^{T+1:T+H} | \theta_T, \psi, y^{1:T}) = \prod_{i=1}^{H} p(\theta_{T+i} | \theta_{T+i-1}, \psi, y^{1:T}) \tag{5.29}$$

where $p(\theta_{T+i}|\theta_{T+i-1}, \psi, y^{1:T}) \sim N(\theta_{T+i-1}, W)$. Therefore, to sample future states from Equation (5.29), we take H random draws of ω_i from $N(0, W)$ and iterate on the system equation

$$\theta_{T+i} = \theta_{T+i-1} + \omega_i \tag{5.30}$$

Having obtained the future states, all that remains is to simulate future data. The second term in Equation (5.28) can be factored as

$$\begin{aligned} &p(y^{T+1:T+H}|\theta^{T+1:T+H}, \theta_T, \psi, y^{1:T}) \\ &= \prod_{i=1}^{H} p(y_{T+i}|y^{T+1:T+i-1}, \theta^{T+1:T+H}, \theta_T, \psi, y^{1:T}) \end{aligned} \tag{5.31}$$

where $p\left(y_{T+i}\middle|y^{T+1:T+i-1}, \theta^{T+1:T+H}, \theta_T, \psi, y^{1:T}\right) \sim N(F'_{T+i}\theta_{T+i}, V)$. To sample future observation from Equation (5.31), we take H random draws of v_i from $N(0, V)$ and iterate on the measurement equation

$$y_{T+i} = F'_{T+i}\theta_{T+i} + v_i. \tag{5.32}$$

5.5 Application: Strain Data from a Cable-Stayed Bridge

Integrating monitoring data from an on-line SHM system into structural condition assessment would enable engineers to evolutionally trace the health status of in-service structures (Ni *et al.* 2012). One of the most common measurands in structural monitoring is strain, which is aimed to derive information about stresses experienced by the monitored structure during its service/operation. Stress is probably the most important

response, as it can directly indicate the safety reserve of a structural component or provide information about the load-carrying capacity of the whole structure (Koshiba *et al.* 2001). Strain/stress is better suited to characterize local damage of a structure than vibration data such as acceleration. Here, the BDLM is applied to model the time-dependent strain responses of a bridge by use of the monitoring data acquired from the SHM system instrumented on the Ting Kau Bridge (TKB).

5.5.1 TKB and measurement data

As part of long-term SHM system installed on the TKB, a total of 88 strain gauges (66 single strain gauges and 22 rosette strain gauges) were deployed to monitor the strain response at four bridge deck cross sections denoted by CH113782.0, CH12082.5, CH12217.5 and CH12555.0 as illustrated in Figure 5.2 (Wong 2004). A total of 83 temperature sensors were installed to measure the temperature change of steel, concrete, asphalt and air. Figure 5.3 and 5.4 show the layout of strain gauges and temperature sensors on the deck cross section of CH12217.5. The sampling rates of the strain gauges and temperature sensors are 25.6 Hz and 0.07 Hz, respectively.

In this study, 27 days of continuous monitoring data from the SHM system are used. There are 12 values per a day, by averaging the monitoring data in every two hours, making up a total of 324 observations. Figure 5.5(a) shows the time history of strain data

from the strain gauge SS-GLW-06 (Figure 5.3). It is seen that the strain time series display periodical behavior, with a period of one day, which implies that it is suitable to incorporate a season component in modeling. Figure 5.5(b) shows the temperature of structural steel, atmosphere and asphalt for the same time period. Similar to the strain data, the temperature time series exhibit periodical behavior as well. It might be appropriate to include a regression component for representing the relationship between strain and temperature.

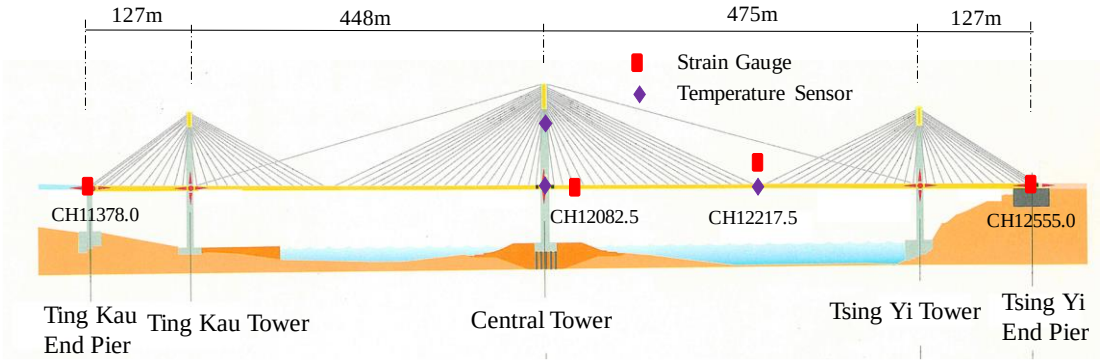

Figure 5.2 Location of strain gauges and temperature sensors along bridge deck

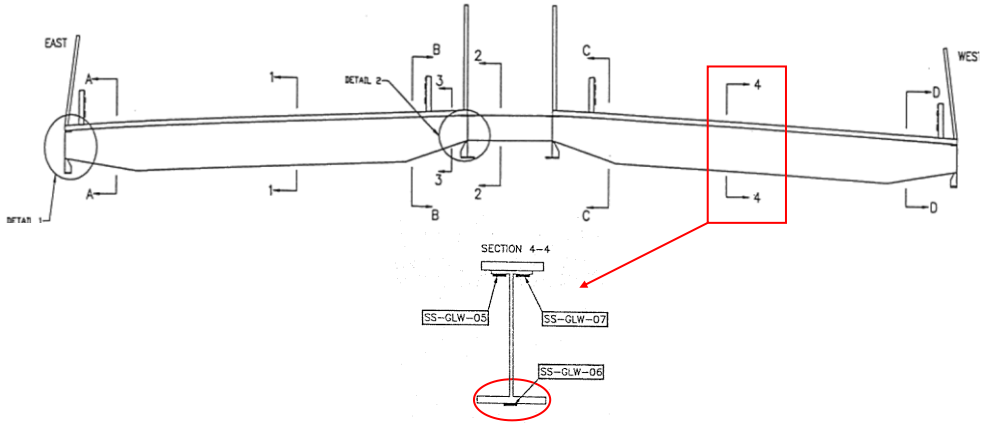

Figure 5.3 Location of strain gauges on deck cross section (CH12217.5)

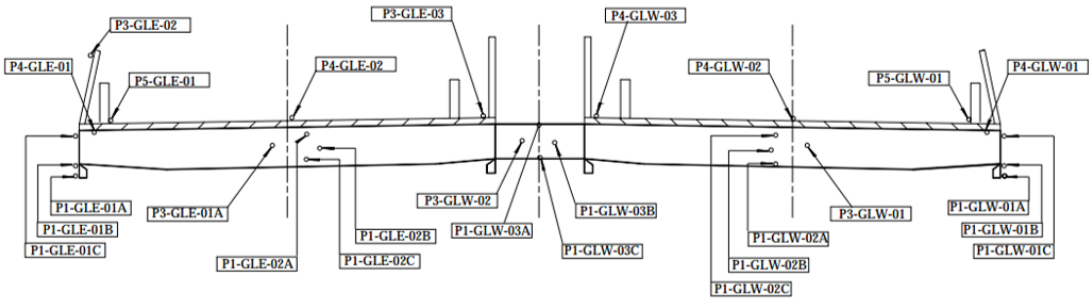

Figure 5.4 Location of temperature sensors on deck cross section (CH12217.5)

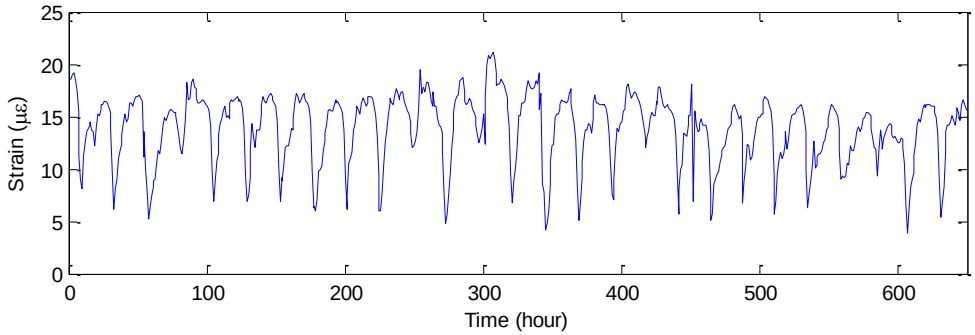

(a) Strain

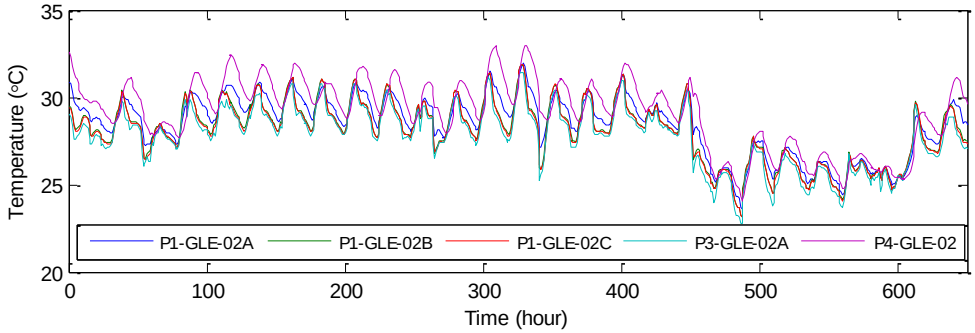

(b) Temperature

Figure 5.5 Time histories of strain and temperature data

5.5.2 Model selection

5.5.2.1 Model selection criteria

To validate the accuracy of prediction, two common statistics indicators are used, namely, root mean squared error (RMSE) and mean absolute percentage error (MAPE). They are defined as

$$RMSE = \sqrt{\frac{\sum_{t=1}^{n}(\hat{y}_t - y_t)^2}{n}} \tag{5.33}$$

$$MAPE = \frac{1}{n}\sum_{t=1}^{n}\left|\frac{\hat{y}_t - y_t}{y_t}\right| \tag{5.34}$$

where $\hat{y}_t$ and y represent the predicted and observed values at time t, respectively, and n is the number of observations.

In the context of Bayesian analysis, the Bayesian predictive information criterion (BPIC) proposed by Ando (2007) is a useful tool to evaluate the quality of Bayesian models from predictive point of view, which is an estimator for the posterior mean of expected log-likelihood of the Bayesian predictive distribution, defined as

$$LLH = \sum_{t=1}^{T}\log(p(y_t|D_{t-1})) \tag{5.35}$$

where y_t is the real observed data, and $p(y_t|D_{t-1})$ is the probability of y_t in accordance with the predictive distribution. The maximum of LLH is favored.

5.5.2.2 Model 1: trend and season

The first suggested model for strain data is a two components model which includes a linear trend component and seasonal component,

$$y_t = y_{Tt} + y_{St} + v_t$$

At first, it is unclear how many harmonics representing the seasonal component give the best fit for the data, so each alternative is explored. The following four models are considered

Model 1a: linear trend + one harmonic;

Model 1b: linear trend + two harmonics;

Model 1c: linear trend + three harmonics;

Model 1d: linear trend + four harmonics.

Assume that the initial prior is non-informative, thus the initializers of variance for all parameters are set adequately large. Table 5.1 shows the summary of forecast performance for different models. According to the results given in the table, Model 1c with three harmonics has the best forecast performance, with its scores in RMSE and MAPE being minimum, and LLH score being maximum.

The results from Model 1c are illustrated in Figure 5.6. Figure 5.6(a) shows the real observed data together with 1-step ahead prediction and the corresponding 90% prediction interval. Generally, most of the observations lie within the predictive interval in addition to some extrema. The forecast performance is satisfactory. In Figure 5.6(b), the results of trend analysis with 90% probability envelope are plotted. The level remains relatively stable and to an extent it reflects the trend of change. Figure 5.6 (c) shows the seasonal component of the DLM, with 90% credibility interval. It is varying with time, but very slowly. Compared with the temperature in Figure 5.5(b), the seasonal effect seems to have a relationship with temperature. This suggests that temperature might be considered as potential explanatory variables.

Next we take a closer look at the residuals of the model, as the inadequacies and flaws

in the model can be revealed and the prediction performance can be assessed by studying the residuals. Figure 5.6(d) shows the scaled prediction errors with 90% probability interval (red dashed line). It is seen that most of the prediction errors are within the probability region. Figure 5.6(e) plots the autocorrelation function of the prediction errors. It is found that the residuals are not perfectly uncorrelated, as some relative autocorrelations exist at some lags. Figure 5.6(f) gives the Q-Q plot of the prediction errors, which compares the empirical quantiles of the prediction errors with those obtained from the theoretical distribution. The result shows that the points (normalized error values) approximately lie on the line of expectation.

Table 5.1 Summary of forecast performance of Model 1

Model No.	RMSE	MAPE (%)	LLH
Model 1a	2.08	13.66	-448.58
Model 1b	1.82	11.81	-359.92
Model 1c	1.76	11.03	-331.53
Model 1d	1.84	11.39	-359.65

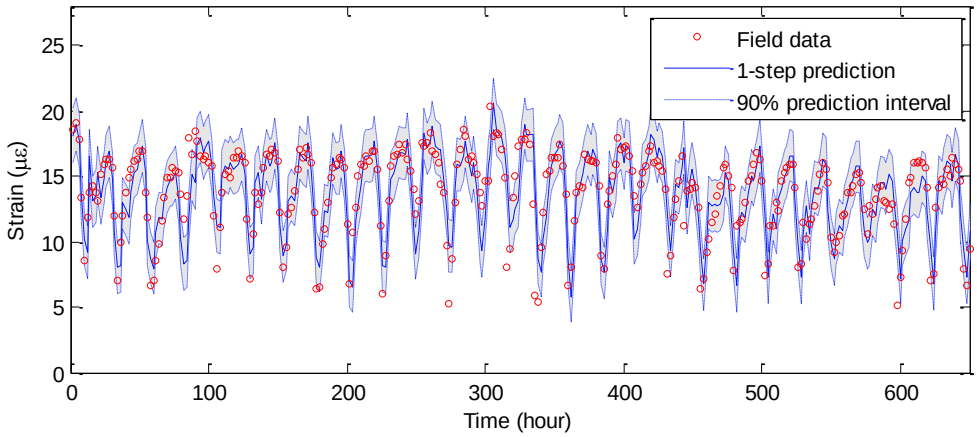

(a) 1-step ahead prediction

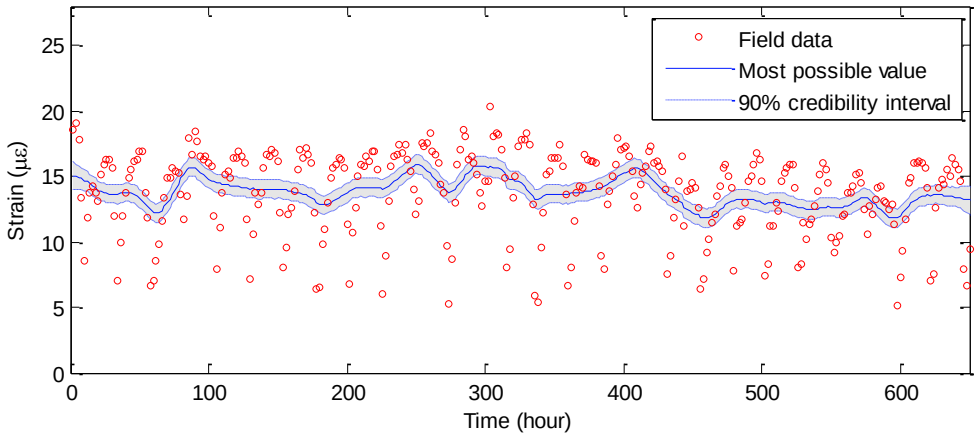

(b) Trend component

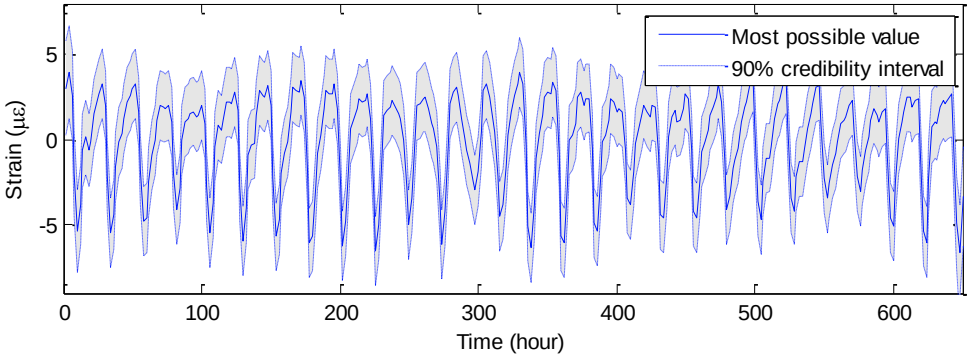

(c) Seasonal component

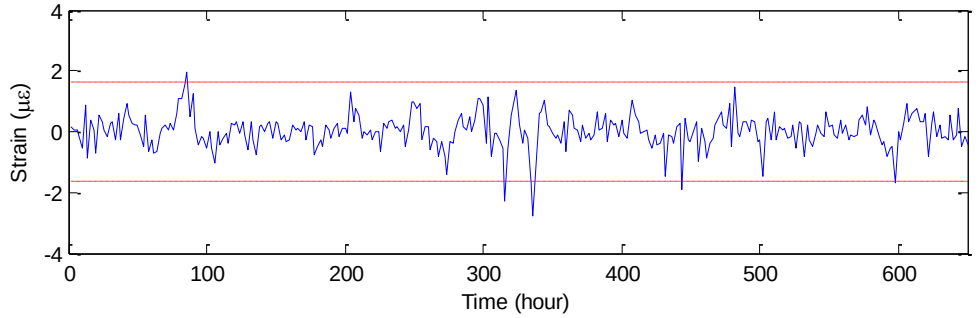

(d) Forecast residual

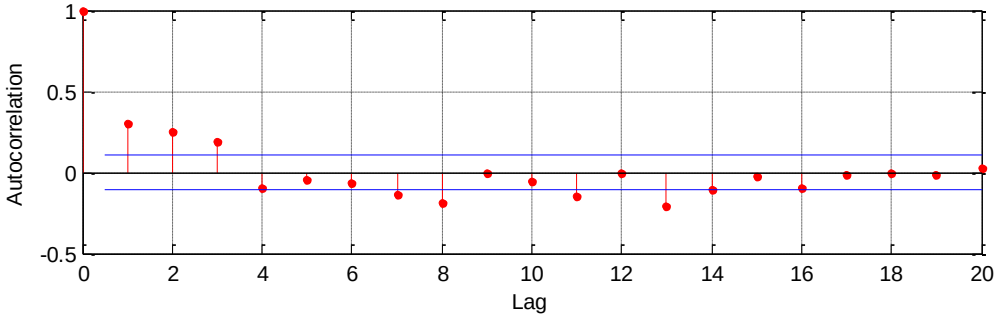

(e) Autocorrelation of forecast residuals

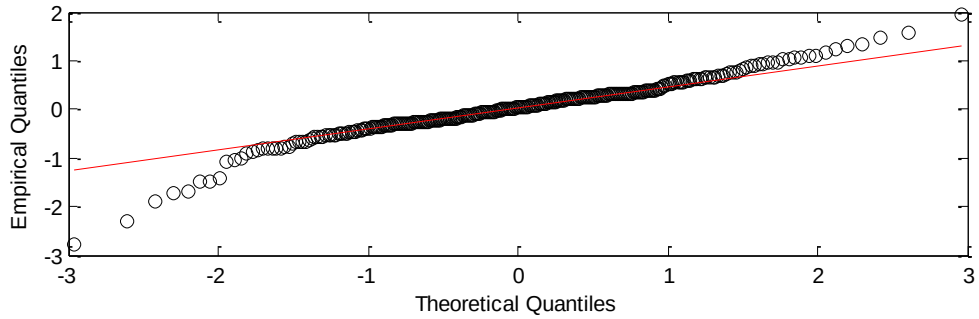

(f) Q-Q plot of forecast residuals

Figure 5.6 Model 1c: linear trend + 3 harmonics

5.5.2.3 Model 2: trend and regression

In the second model, we introduce a regression block, with temperature as an explanatory variable. Model 2 includes both a trend and a regression component

$$y_t = y_{Tt} + y_{Rt} + v_t$$

Temperature in bridge deck cross section can be decomposed into two portions: differential temperature and effective temperature. The differential temperature is temperature differences between the upper and lower surfaces of the bridge deck cross section, which causes the internal stresses and bending moments when section ends are restrained; while the effective temperature is an average temperature distributed along the section, which results in longitudinal movements of the bridge deck (Ni *et al.* 2007). Hence it is necessary to try two different model versions according to the temperature category. In Model 2a, the differential temperature is regarded as an explanatory, while Model 2b only uses the temperature data from the sensor (P1-GLE-02C) which is close to the strain gauge. Since the contribution from temperature effect, the level may lie above or below the underlying level of the data. To achieve a level independent of the regression effects, the temperature variable is shifted to reach a zero mean,

$$Temp_t^* = Temp_t - \sum_{t=1}^{T} \frac{Temp_t}{T} \tag{5.36}$$

where T is the number of the observation in dataset. When the dataset is static, this solution is reasonable. Problem arises when the dataset is dynamic, such as in the case of doing real-time analysis. An alternative approach is to carry out a dynamic shifting

$$Temp_t^{\#} = Temp_t - \sum_{i=t-k}^{t+k} \frac{Temp_i}{2k+1} \tag{5.37}$$

It should be noted that the dynamic shifting method requires information of future

temperature and to determine an appropriate window size k. Another convenient alternative is applying the value of mean temperature which is calculated by using the last year's temperature data at the same period, just as we do in this study. Figure 5.7 shows the shifted temperature that has zero mean.

The performance of the two models are summarized in Table 5.2. According to the three criteria, Model 2a has better performance than Model 2b. Figure 5.8 shows the results of Model 2a. The 1-step ahead predictions for Model 2a in Figure 5.8(a) do not perform better than for Model 1c in Figure 5.6(a), especially for the prediction of extreme observations. The RMSE and MAPE are 2.83 and 18.65% respectively, both higher than the results of Model 1c, while the value of LLH is -825.16, lower than that of Model 1c (-331.53). Compared with the level for Model 1c, the level for Model 2a in Figure 5.6(b) fluctuates greater and does not well represent the underlying level of the time series of strain data. Figure 5.8(c) displays the effect of temperature. It also exhibits periodicity like the temperature in Figure 5.7(a). Figure 5.8(d) shows the standardized prediction errors. The errors are visibly larger than those in Model 1c, and more errors lie beyond 90% probability interval. From the autocorrelation function and Q-Q plot for prediction errors presented in Figure 5.8(e)-(f), it is seen that there are still some correlations in the errors and the residuals are not well consistent with normal distribution.

Table 5.2 Summary of forecast performance of Model 2

Model No.	RMSE	MAPE (%)	LLH
Model 2a	2.83	18.65	-825.16
Model 2b	2.94	19.47	-926.42

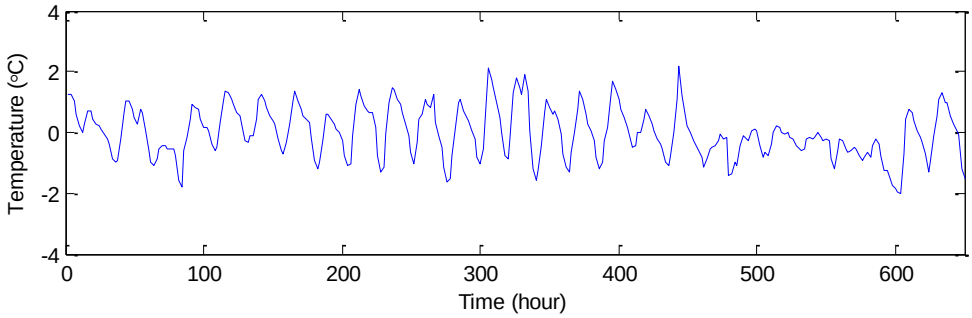

(a) Differential temperature

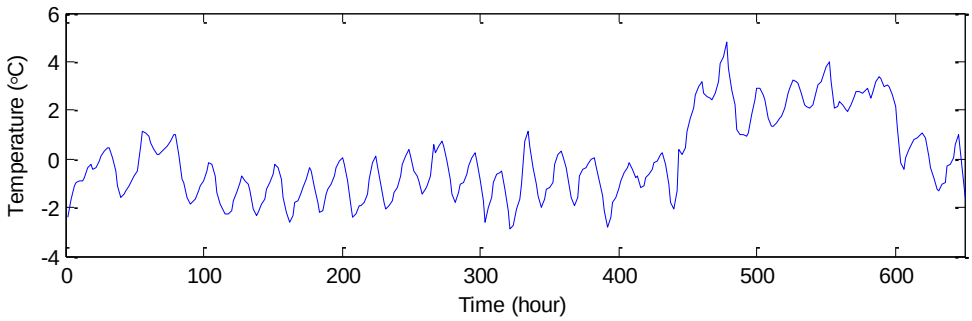

(b) Temperature measured from the sensor P1-GLE-02C

Figure 5.7 Shifted temperature

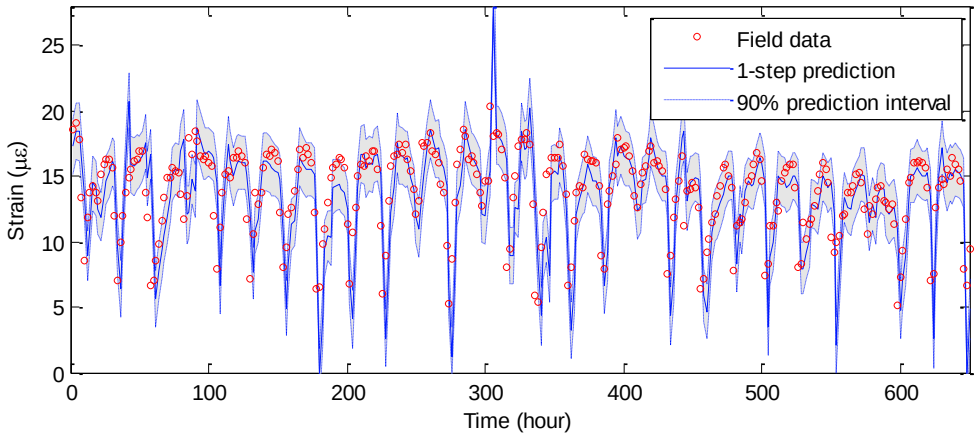

(a) 1-step ahead prediction

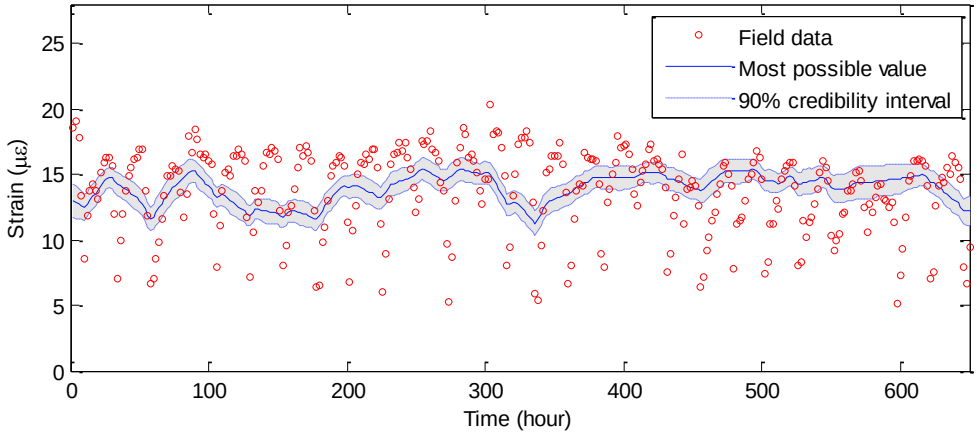

(b) Trend component

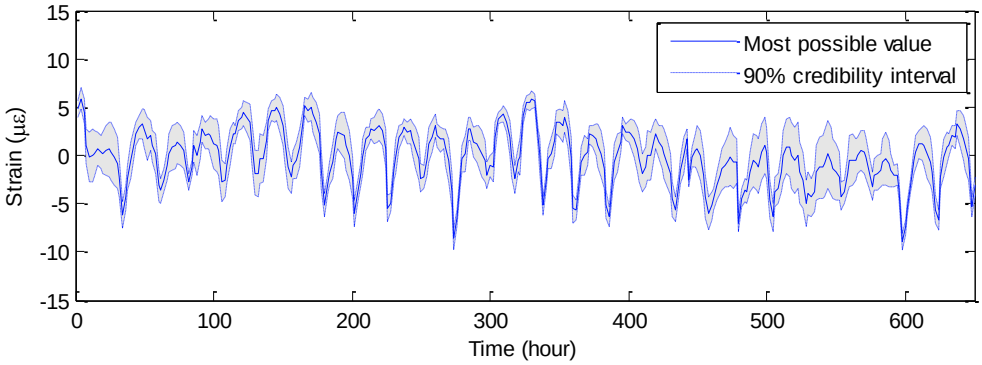

(c) Regression component

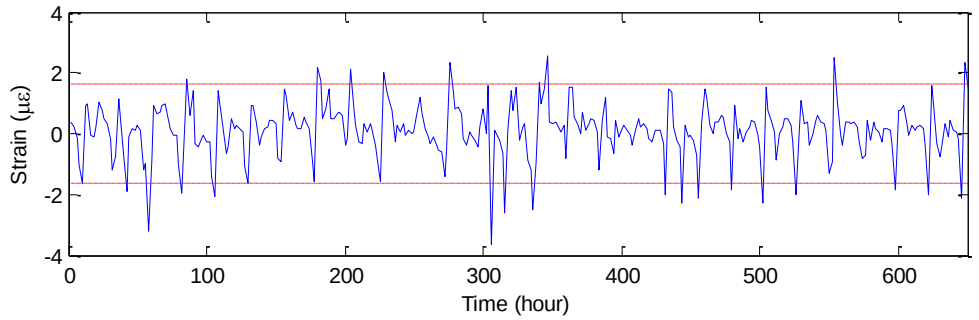

(d) Scaled forecast residuals

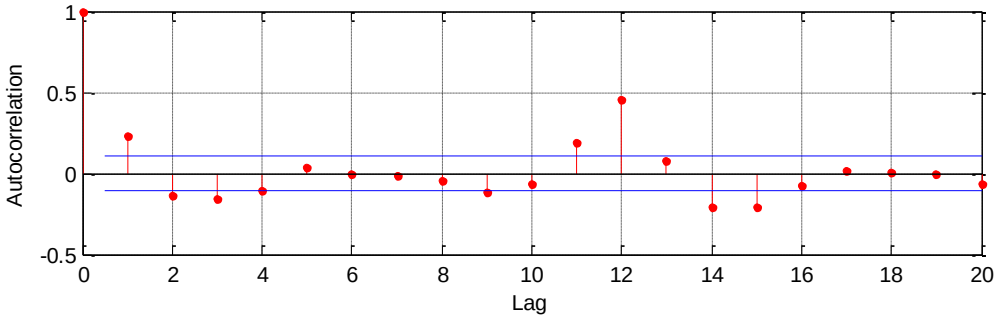

(e) Autocorrelation of forecast residuals

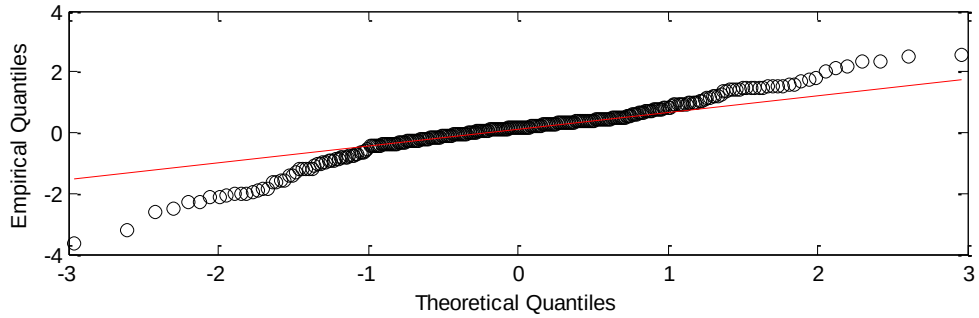

(f) Q-Q plot of forecast residuals

Figure 5.8 Model 2a: linear trend + regression

5.5.2.4 Model 3: trend, seasonal and regression

In Model 3, we take into account all three components to explain the strain response

$$y_t = y_{Tt} + y_{St} + y_{Rt} + v_t$$

where y_{Tt} is a linear trend, y_{St} is three harmonics, and y_{Rt} is a regression component with differential temperature as an explanatory variable.

The forecasting accuracy of Model 3 is presented in Table 5.3. Figure 5.9 compares the forecast performance of Model 1c, Model 2a, and Model 3. According to the scores of RMSE, MAPE and LLH, Model 3 has the best performance as expected among the three models.

In Figure 5.10, the result from Model 3 is plotted. Figure 5.10(a) shows the observed data with 1-step ahead prediction and 90% prediction interval. The prediction is satisfactory on the whole, except several extreme observations which are outside the prediction interval. Comparing the level parameters among the three models, it is seen that the levels for Model 3 (Figure 5.10(b)) and Model 1c are quite similar, and they are much more representative of the underlying level than that in Model 2a. The seasonal effect in Model 3 (Figure 5.10(c)) is less than that in Model 1c. This can be explained by the effect of differential temperature in Figure 5.10(d), which also has the seasonal properties that affect each other. Figure 5.10(e) shows the scaled prediction errors for Model 3, which are better than Model 2a and Model 1c. The autocorrelation of forecast errors in Figure 5.10(f) and normal test in Figure 5.10(g) have been improved in comparison with the earlier models.

Table 5.3 Summary of forecast performance of Model 3

Model No.	RMSE	MAPE (%)	LLH
Model 3	1.64	10.05	-291.39

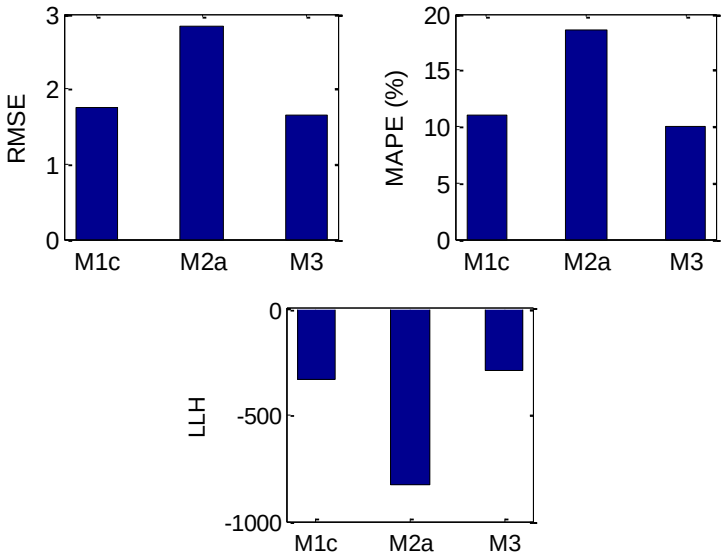

Figure 5.9 Forecast performance of Model 1c, Model 2a and Model 3

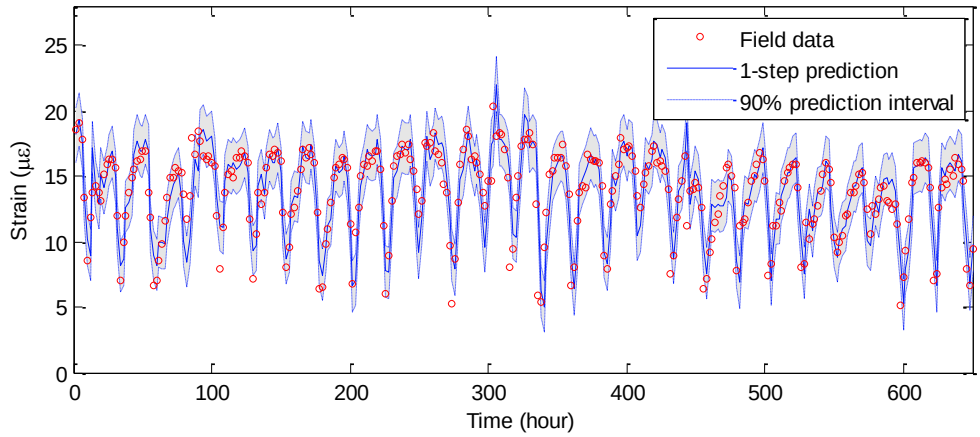

(a) 1-step ahead prediction

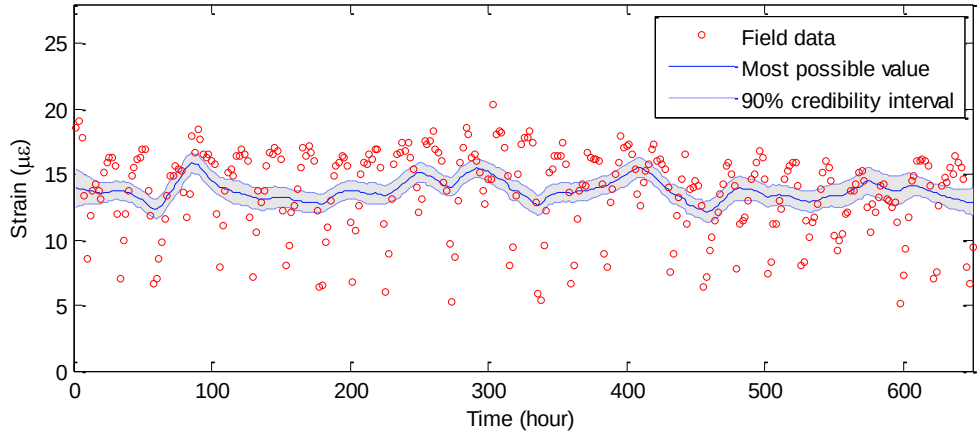

(b) Trend component

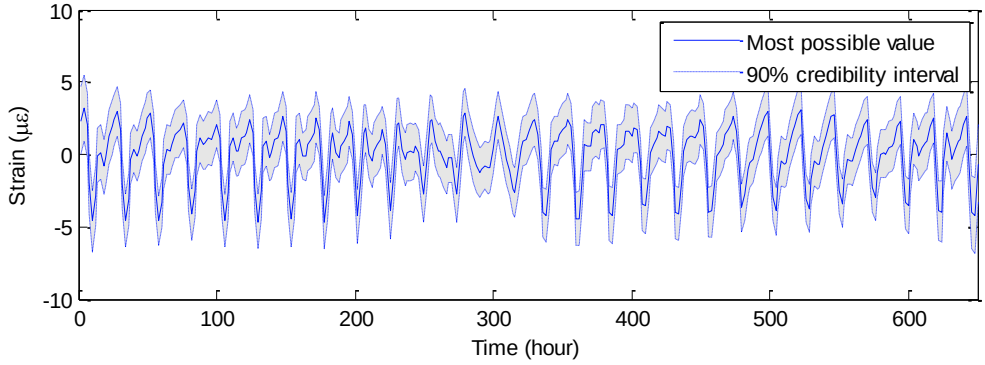

(c) Seasonal component

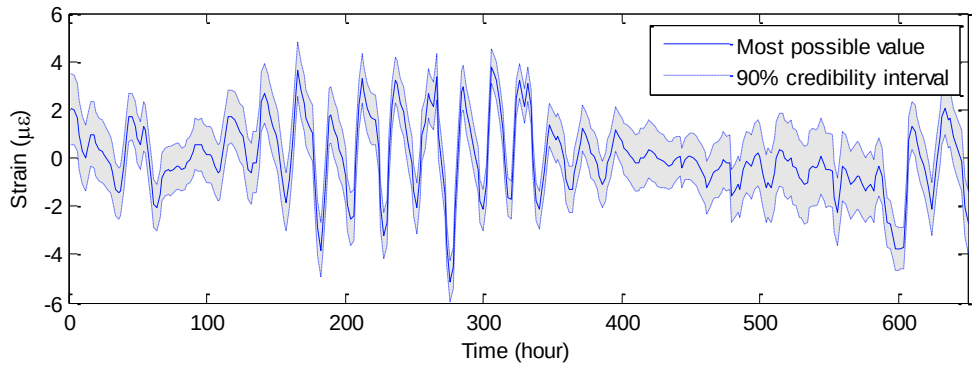

(d) Regression component

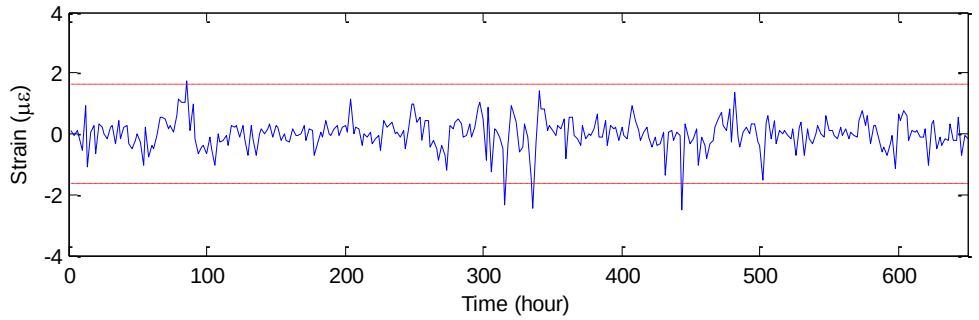

(e) Scaled forecast residuals

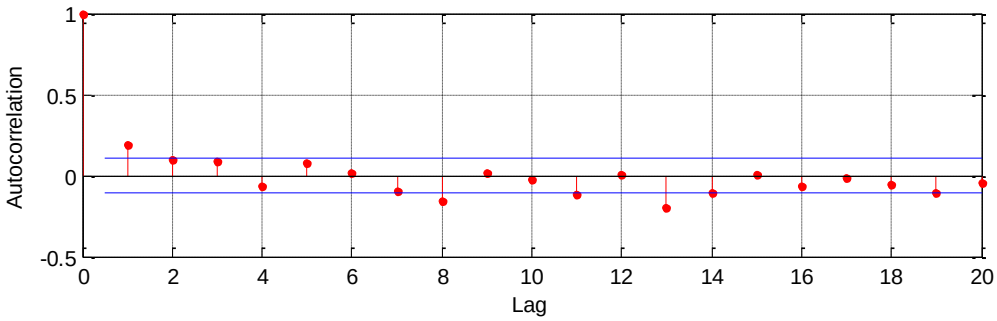

(f) Autocorrelation of forecast residuals

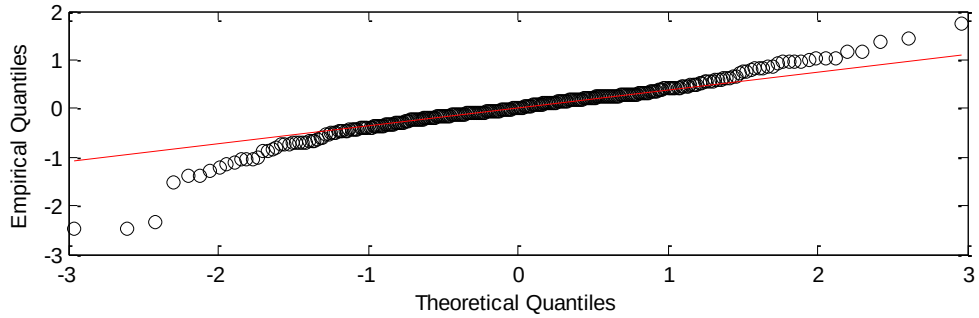

(g) Q-Q plot of forecast residuals

Figure 5.10 Model 3: linear trend + season + regression

5.5.3 *k*-steps ahead predictions

In sub-section 5.5.2, the 1-step ahead forecast performance of three different models has been investigated. Here we further examine the prediction performance on *k*-steps ahead based on Model 1c, Model 2a and Model 3. For each model we make *k*-steps ahead predictions with start point at two different times: the 240th hour and the 500th hour. Thus the *k*-steps ahead predictions are based on all known information at the start point. To compare the short- and long- term forecast performance, a range of different *k* values, 6, 12, 24, 36, are tested. As there are 12 observations per day, the above *k* values correspond to 0.5, 1, 2, 3 days respectively.

Figure 5.11 shows the *k*-steps ahead predictions with starting time at the 240th hour for the three models. It is clear that prediction performance of Model 3 is best, Model 1c comes second and Model 2 performs worst. This is because Model 1c only contains trend and seasonal components, which changes slowly and cannot make timely adjustments for larger *k* values, while Model 3 with additional regression component can quickly make compensation via the differential temperature. The bad prediction performance of Model 2a is due to the lack of seasonal component which is important to describe the periodic characteristics, albeit the regression component also has periodicity. For all three models, most of the observations lie within the 90% prediction interval. The prediction interval of the three models increases over time, which means that uncertainty of prediction grows

along with time. Especially the prediction interval of Model 2a is quite unstable and wider after $k = 6$

Figure 5.12 shows the performance scores for the three models with different *k* values. For the convenience to compare the LLH for datasets with different sizes, we uses the average log likelihood per step, LLH/k. It can be seen that Model 3 (with smallest scores of RMSE and MAPE, and largest scores of LLH/k) has the best prediction performance according to all three criteria, except for $k = 6$. When $k = 6$, Model 2a only with trend and regression component is the best model according to the three criteria. That happens to be where the prediction results meet well with the observations at the *k* ranging from 1 to 6, as shown in Figure 5.11(b). For all three models, the scores of RMSE and MAPE slightly decrease with k, while LLH/k are quite stable, except $k = 6$, since all three measures, RMSE, MAPE and LLH/k are sensitive to outliers for small k values.

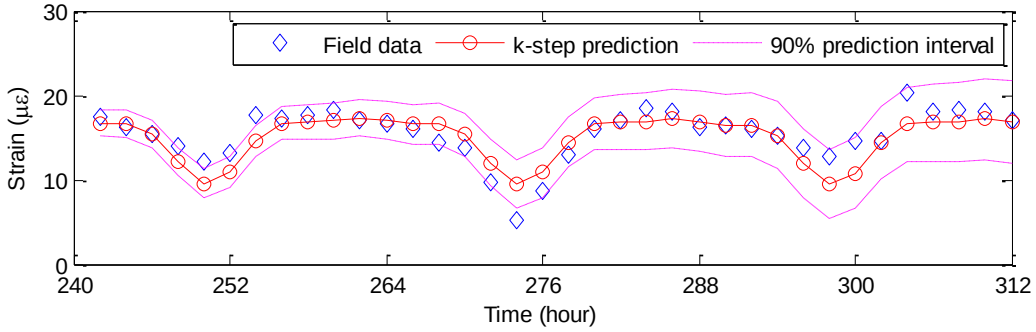

(a) Model 1c, *k* ranging from 1 to 36

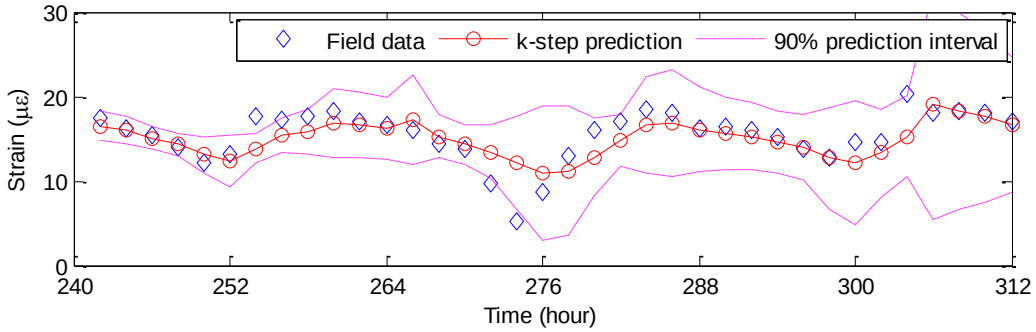

(b) Model 2a, *k* ranging from 1 to 36

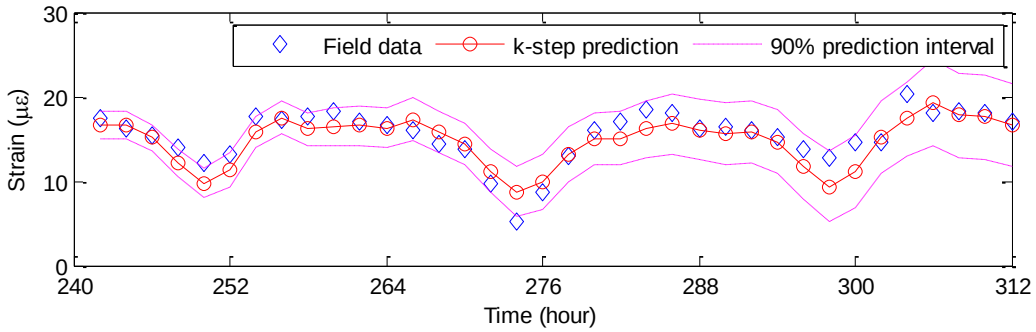

(c) Model 3, *k* ranging from 1 to 36

Figure 5.11 *k*-steps ahead prediction made at the 240th hour

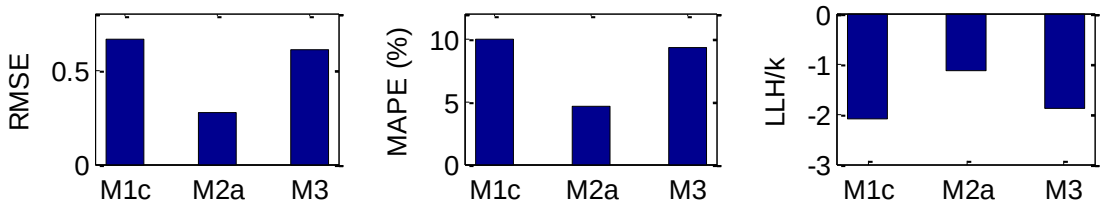

(a) k=6

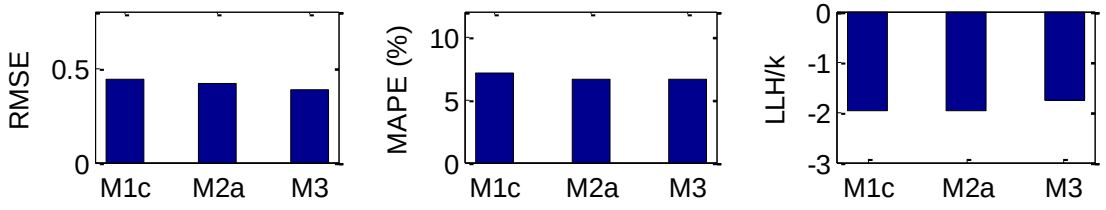

(b) k=12

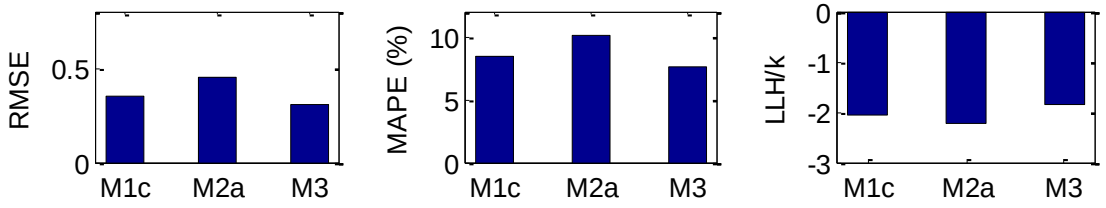

(c) k=24

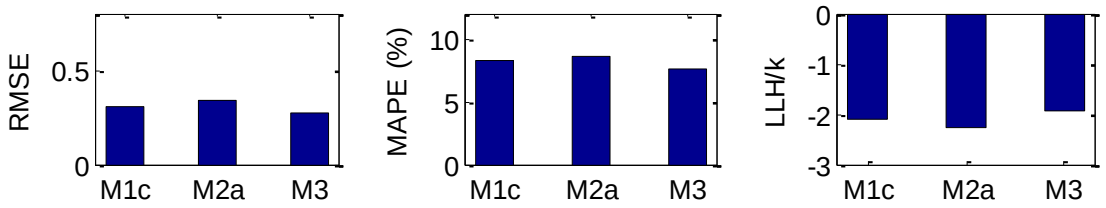

(d) k=36

Figure 5.12 Forecast performance for different k-steps ahead starting at the 240th hour

Figure 5.13 shows the k-steps ahead predictions with staring time at the 500th hour for three models. It is seen again that, Model 3 has the best prediction performance, Model 1c comes second, and Model 2a performs worst. In Model 3 and Mode 1c, most predictions agree well with the observed data, and lie within the 90% prediction interval.

In Model 2, the predictions are far from satisfactory, especially after $k = 24$, and the confidence interval is larger than that in other two models. The prediction intervals of the three models increase over time, implying prediction uncertainty increases with the number of prediction steps.

Figure 5.14 shows the performance scores for the three models with different prediction steps. Among the three models, Model 3 has the best RMSE, MAPE and LLH/k scores, Model 1c comes next, and Model 2s is worst. For all three models, the scores of RMSE and MAPE slightly decrease with increasing *k*, with exception from $k = 24$ to $k = 36$ in Model 2, while LLH/k is quite stable, since RMSE, MAPE and LLH/k are all sensitive to outliers for small *k* values.

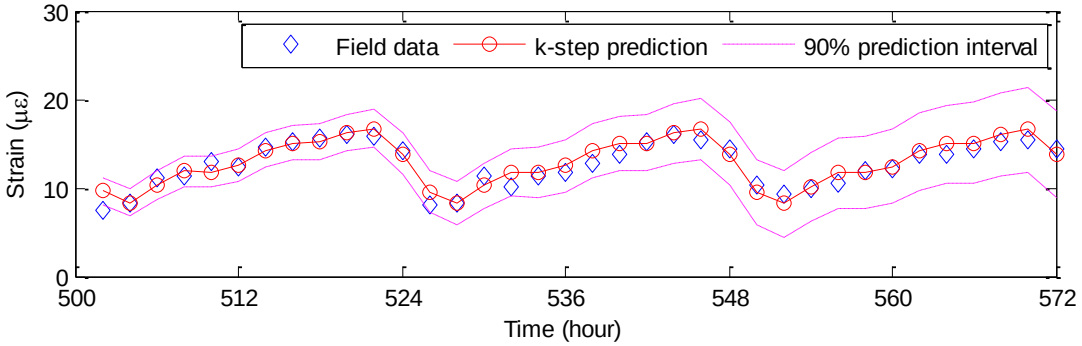

(a) Model 1c, *k* ranging from 1 to 36

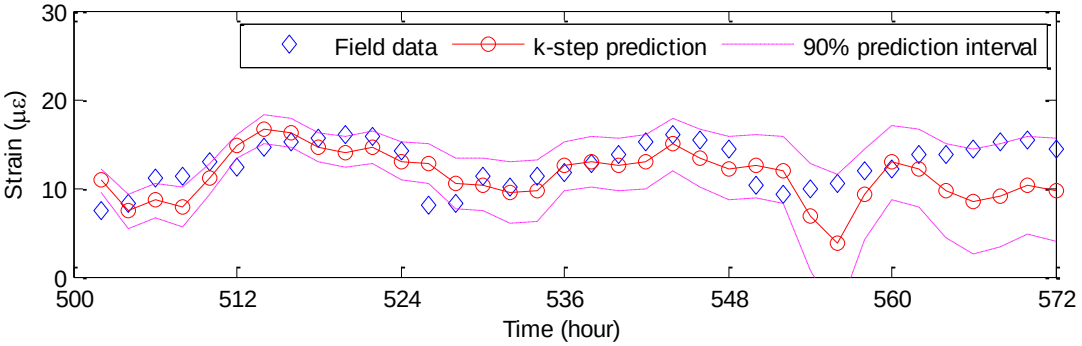

(b) Model 2a, *k* ranging from 1 to 36

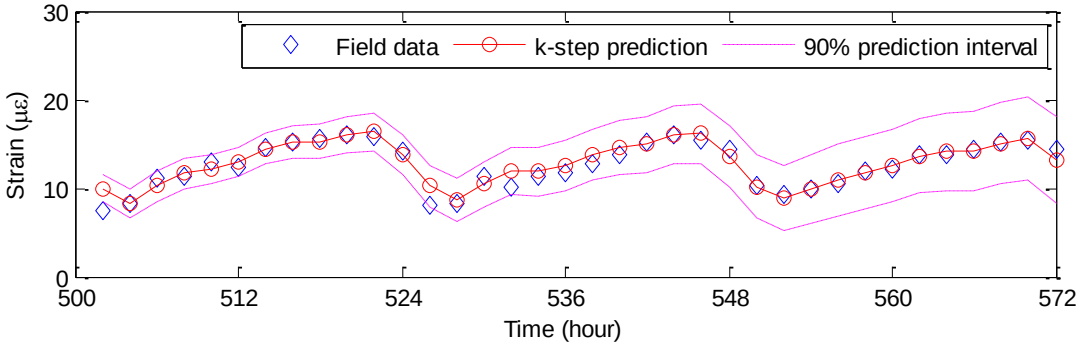

(c) Model 3, *k* ranging from 1 to 36

Figure 5.13 *k*-steps ahead prediction made at the 500th hour

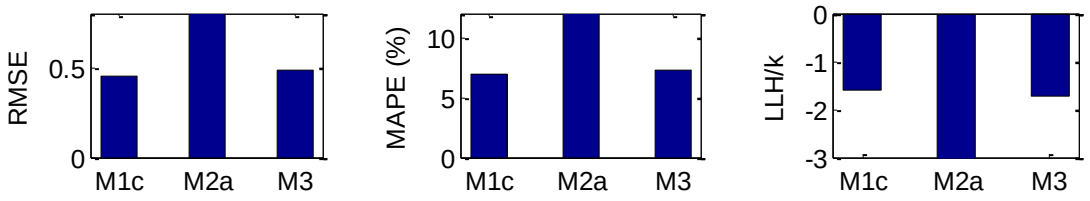

(a) k=6

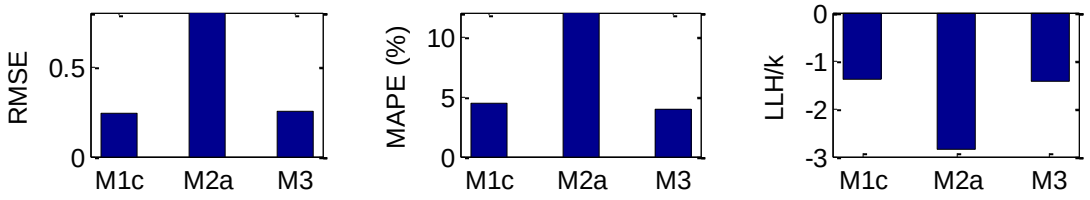

(b) k=12

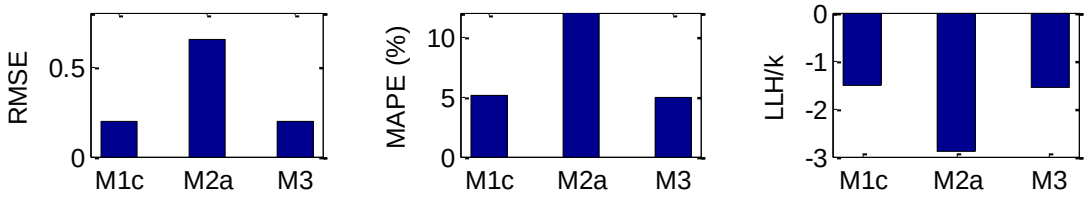

(c) k=24

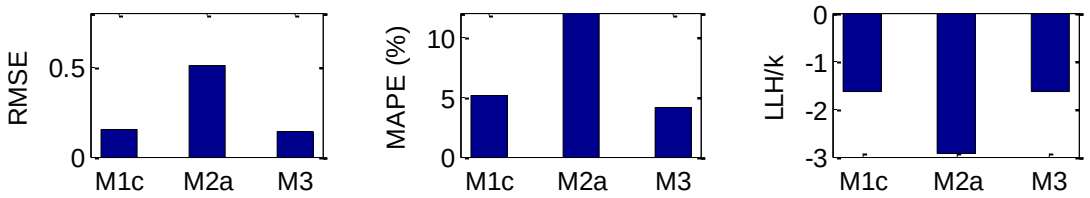

(d) k=36

Figure 5.14 Forecast performance for different k-steps ahead starting at the 500th hour

5.6 Summary

This chapter presents a framework for formulating Bayesian dynamic linear model (BDLM) for the purpose of providing accurate and reliable predictions of structural

response time series. The structural responses subjected to external effects are characterized by superposing generic components including baseline response, seasonal component, and regression component. In contrast to classical time series model, BDLM does not require the data series to be stationary and can provide structural response predictions along with their associated confidence interval to account for the response dynamics and uncertainty. Moreover, the state space method directly contains a model error term, which makes the analysis more robust to mis-specification of the model. By using MCMC simulation method, the unknown parameters and their corresponding uncertainties are estimated. The effectiveness and robustness of the proposed method are illustrated by applying it to strain responses measured from a cable-stayed bridge. According to three model criteria, various models with different components are compared to select the most suitable model for making one or several steps ahead predictions. The results show that the selected optimal model performs well in prediction.

Chapter 6

BDLM for Structural Damage Detection

6.1 Introduction

An ideal SHM system is expected to possess the ability of near real-time automated structural health diagnosis through a continuous monitoring process, and provide managers critical information to make cost-effective, risk-based decisions that maintain safety of the structure. Hence a real-time detection algorithm is desirable. In this chapter, a real-time damage detection technique based on Bayesian dynamic linear model (BDLM) and Bayesian forecasting will be proposed. The BDLM is a tool for time series analysis and Bayesian forecasting enables to calculate one-step ahead forecast distribution. The change detection will be carried out by checking the current observation against the routine model (forecast distribution generated by the BDLM for current instant) as well as against an alternative model (whose mean value is shifted by a prescribed offset). The detection rule is that if the alternative model better fits the actual observation, a potential change is alarmed. To further determine whether the current observation is an outlier or the beginning of a change, a specific logic will be developed by introducing the Bayes factor and maximum cumulative Bayes factor. While the potential change in time series of structural response is alarmed, Bayesian hypothesis testing will be conducted for

damage extent assessment and uncertainty quantification. In short, the real-time automated structural health diagnosis technique proposed in this chapter possess the following features: (i) potential outliers being detected; (ii) the beginning of change being identified; (iii) damage extent and uncertainty being quantified.

6.2 Bayesian Probabilistic Damage Detection

6.2.1 Bayes factor

Bayes factor, a quantity for comparing models or for testing hypothesis in a Bayesian framework, plays a significant role in assessing the goodness of fit of competing models (Ando 2010). Suppose we have two models, the routine model M_R and an alternative model M_A. The Bayes factor is defined as the ratio of the marginal likelihood of the data y_t

$$H = \frac{p(y_t|M_A)}{p(y_t|M_R)} \tag{6.1}$$

which measures the evidence for model M_A versus model M_R on the basis of data information. Bayes factor prefers the model with the larger value of marginal likelihood. For better quantitative comparison between two models, Jeffreys (1961) suggested interpreting the Bayes factor as a scale of evidence, as shown in Table 6.1. This table provides some descriptive statements although the partitions are somewhat arbitrary.

Table 6.1 Jeffreys' scale of evidence for Bayes factor

Bayes factor	Interpretation
$H < 1$	Negative support for M_A
$1 < H < 3$	Barely worth mention evidence for M_A
$3 < H < 10$	Substantial evidence for M_A
$10 < H < 30$	Strong evidence for M_A
$30 < H < 100$	Very strong evidence for M_A
$100 < H$	Decisive evidence for M_A

6.2.2 Outlier detection

Detection of potential outliers is the first step in the proposed algorithm, which is conducted based on the calculation of Bayes factor. The basic idea is to check the current observation against the routine model M_R (forecast distribution for current time), and against an alternative model M_A (its mean value is shifted by +h based on the forecasting distribution). For time t, the Bayes factor can be expressed as

$$H_t = \frac{p(y_t|D_{t-1}, M_A)}{p(y_t|D_{t-1}, M_R)} \tag{6.2}$$

where y_t is the measurement at time t and D_{t-1} refers to the history information up to time $t-1$. In the case of Gaussian distributions, the Bayes factor is (Lipowsky *et al.* 2010)

$$H_{1,t} = exp\left(\frac{2h \cdot (y_t - f_t) - h^2}{2\sigma_t^2}\right). \tag{6.3}$$

where h is the shift value, y_t is the observation value, f_t and σ_t are the mean and standard deviation of the forecasting distribution. A Bayes factor $H = 1$ indicates that

the probability of the observation derived from model M_R is identical to the probability of that derived from Model M_A. According to the suggestion by Jeffreys (1961), the threshold can be set as $H_{min} = 10$ for outlier detection. However, the shift value h should be determined according to the required confidence level. After H_{min} and h are confirmed, an uncertainty limit (*ucl*) can be obtained by the following equation

$$ucl = \frac{ln(H_{min})}{h}\sigma_t^2 + \frac{h}{2} \tag{6.4}$$

When the shift value is set to $h = 1.645\sigma_t$ at 90% confidence level, the uncertainty limit $ucl = 2.22\sigma_t$. It amounts to saying that, an observation will be diagnosed as outlier if its deviation from the mean value of Model M_R is larger than ucl.

According to the Bayes factor defined in Equation (6.4), only the outliers with positive deviation can be detected. To make the outliers with negative deviation detectable as well, a second Bayes factor is defined as

$$H_{2,t} = exp\left(\frac{-2h \cdot (y_t - f_t) - h^2}{2\sigma_t^2}\right) \tag{6.5}$$

In the process of automatic monitoring, both the Bayes factors $H_{1,t}$ and $H_{2,t}$ will be examined in parallel to detect positive and negative outliers.

6.2.3 Change detection

In the monitoring context, individual Bayes factor only focuses on the outlier

detection and cannot distinguish between outliers and the beginning of a change. To overcome this, cumulative Bayes factor is introduced, which is defined as the product of k consecutive Bayes factors,

$$H_t(k) = \prod_{t-k+1}^{t} H_t, k = 1,2, \dots, l_{max} \tag{6.6}$$

where l_{max} is the maximum number of Bayes factor taken into account. For each k, $H_t(k)$ measures the evidence provided by the most recent k consecutive observations. The maximal cumulative Bayes factor is obtained by

$$L_t = \max\big(H_t(k)\big) = H_t(l_t) \tag{6.7}$$

where l_t refers to the run length which counts the number of recent, consecutive observations that contribute to the maximum value of L_t. It can be calculated recursively by

$$l_t = \begin{cases} 1, & if \ \ L_{t-1} \leq 1 \\ 1 + l_{t-1}, & if \ \ L_{t-1} > 1 \end{cases}$$

The rational run length threshold of l_t is suggested as $l_{min} = 4$ by Pole *et al.* (1994). If $L_t > H_{min}$, then a notification of change is issued at time t (time of notification, TON), and the time of occurrence (TOC) is $(t - l_t + 1)$, which calls for feed-back interventions.

The sequence of L_t realizes the real-time tracing forecasting performance of model M_R relative to model M_A. If $L_t < H_{min}$, the routine model M_R operates as usual. On the other hand, breakdown in forecasting performance of M_R is indicated. The signal of

changes can be triggered by the following two reasons:

(1) The occurrence of two consecutive Bayes factors $H_t > H_{min}$, which is equivalent to $L_t > H_{min}^2$;

(2) The concurrence of $L_t > H_{min}$ and $l_t > l_{min}$.

Beginning at time t, the procedure of automated detection algorithm is summarized in the flowchart in Figure 6.1. Firstly calculate the single Bayes factor and judge whether y_t is an outlier. If not, calculate the maximum cumulative Bayes factor L_t and run length l_t for change detection. Once a change is detected, the intervention is carried out by resetting the time to the time of occurrence and by adjusting the mean value of M_R to the observation y_t, $f_t = y_t$, then proceed to analyze starting at TOC.

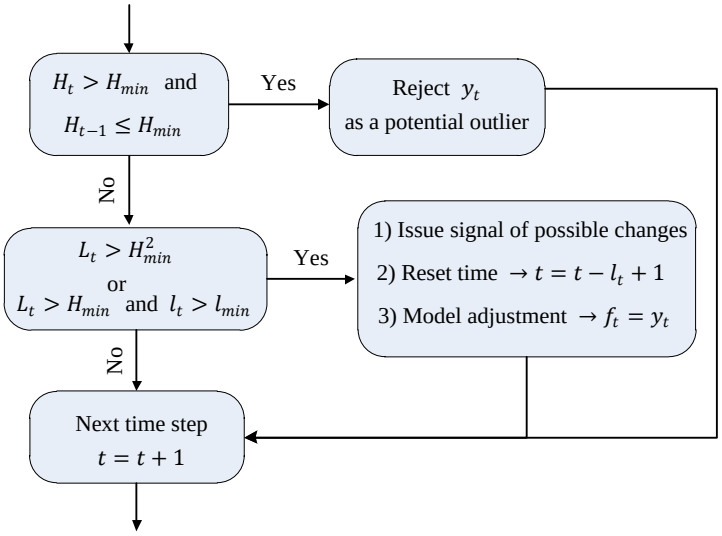

Figure 6.1 Flowchart of detection algorithm

6.2.4 Damage assessment

Suppose we have a set of time series response consisting of different sets, of which

dataset *j*-1, dataset *j* and dataset *j*+1 obtained under different structural health states are shown in Figure 6.2. The main purpose of this study is to automatically detect the changes in time series response by use of the detection logic proposed in Sub-section 6.2.3, for example, to find out TOC 1 and TOC 2 in this case, and then to assess the damage extent based on Bayesian hypothesis testing through comparing the time series response measured before and after the potential change point.

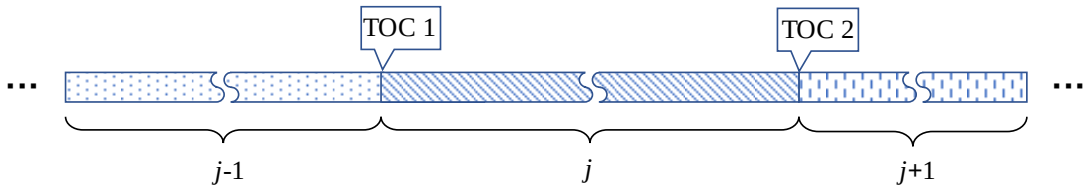

Figure 6.2 Time series datasets obtained under different conditions

The structural damage assessment involves comparing two sets of structural responses obtained under two different structural conditions. When the structural response measured from one status is compared with the response obtained from another status, the difference between them will be used to identify structural damage. For example, it is assumed that dataset *j*-1 in Figure 6.2 is the structural response under healthy condition, and dataset *j* is the response under unhealthy condition. The question is how to effectively identify and quantify them. Let $y_1, \ldots, y_n$ be the structural response in dataset *j*, which follow normal distribution, that is $y \sim N(\mu, \sigma^2)$. In this study, the variance σ^2 is assumed the same as in healthy status, and the hypothesis testing is made

only on the mean of the observed response. The structure is healthy if the mean of the responses (here it refers to dataset *j*-1) is zero, while it is damaged if otherwise. Hence, the null hypothesis H_0 and alternative hypothesis H_1 are as follows

$$\begin{gathered} H_0\text{: No damage } \mu = 0 \\ H_1\text{: Damage } \mu \neq 0 \text{ with } \mu|H_1 \sim N(\rho, \tau^2) \end{gathered} \tag{6.8}$$

where ρ and τ^2 are two parameters of the prior distribution of μ under the alternative hypothesis. If no information is available, $\rho = 0$ and $\tau^2 = \sigma^2$ are suggested (Migon *et al.* 2014). Then the posterior distribution of μ can be calculated as follows (Sankararaman and Mahadevan 2013)

$$\begin{gathered} \text{Posterior mean of } \mu = \frac{\frac{\rho}{\tau^2} + \frac{y_1 + y_2 \ldots + y_n}{\sigma^2}}{\frac{1}{\tau^2} + \frac{n}{\sigma^2}} \\ \text{Posterior variance of } \mu = \left(\frac{1}{\tau^2} + \frac{n}{\sigma^2}\right)^{-1} \end{gathered} \tag{6.9}$$

Structural damage evaluation can be achieved by means of Bayes factor, which is defined as the ratio of probability of observed data given the null hypothesis to the probability of observed data given the alternate hypothesis

$$B_{10} = \frac{P(D|H_1)}{P(D|H_0)} \tag{6.10}$$

where D refers to the observed data. The logarithm of Bayes factor is derived by Jiang Mahadevan (2008) as

$$\log B_{10} = -\frac{1}{2}\log(n+1) + \frac{n^2 R^2}{2(n+1)\sigma^2} \tag{6.11}$$

where R refers to the mean of observed structural response. If the Bayes factor B_{10} is

greater than 1, it implies that the data favor the hypothesis H_1 and hence suggests that there is damage. Another advantage is that the uncertainty in damage detection can be quantitatively assessed on the basis of Bayes factor. The probability for damage is

$$p(H_1|D) = \frac{p(D|H_1)p(H_1)}{p(D|H_0)p(H_0) + p(D|H_1)p(H_1)} \tag{6.12}$$

where $p(H_1)$ and $p(H_0)$ denote the prior probabilities of acceptance at the hypothesis H_1 and H_0. If each of these prior probabilities is assigned as 0.5, then Equation (6.12) is simplified as

$$p(H_1|D) = \frac{B_{10}}{B_{10} + 1} \tag{6.13}$$

$B_{10} \to 0$ indicates 0% confidence in accepting the alternative hypothesis, and $B_{10} \to \infty$ indicates 100% confidence.

In order to facilitate real-time continuous damage detection, a moving window along with data forward is used to cover the recent data for conducting hypothesis testing. Taking Figure 6.2 as an example, the predefined window moves along dataset *j* from TOC1 to TOC2 and the data covered by the window are selected to conduct hypothesis testing. After dataset *j* is finished, same procedure is applied to dataset *j*+1 for hypothesis testing. Based on the results of Bayesian hypothesis testing, we can make a judgement on whether the structure is healthy and the damage extent in unhealthy case.

6.3 Illustrations of Damage Detection

6.3.1 Application 1: in-service monitoring data from a high-speed train

An in-service passenger train running on a high-speed railway in China has been instrumented with an array of optical fiber sensors to monitor the strain/stress variations in different structural components of the train (Figure 6.3). The strain sensors are mainly mounted on 4 measurement zones of bogies: (i) the zone with high loads imposed, (ii) stress transmission zone, (iii) the zone with high predicted responses by FEM calculation, and (iv) welded joints (Figure 6.4).

Onboard monitoring made during the routine operation of the train has lasted for an entire month from December 2015 to January 2016. During the monitoring period, the train ran at its normal speed around 160 to 200 km/h. The high speed railway is longer than 1,000 km in total. Sampling rate for all the sensors was set as 5,000 Hz.

Pre-processing of the acquired strain data is conducted in order to obtain the average amplitudes of stress ranges at different time intervals. It consists of the following steps: (i) multiplying the strain data with elasticity modulus E of steel to obtain stress time histories; (ii) applying the rainflow counting method (Wang and Ni 2016) to extract the stress range in each of stress cycles. From one stress cycle, the stress range S_a is obtained by calculating the difference between the maximum stress σ_{max} and the minimum stress σ_{min} measured in that stress cycle, i.e., $S_a = \sigma_{max} - \sigma_{min}$; (iii) eliminating those stress

ranges with their amplitudes smaller than 1 MPa (the majority of them are caused by noise); and (iv) calculating the average amplitude of the stress ranges at each time interval.

The data used in this study are the stress ranges collected at one point when the train ran through two railway sections before and after lathing the wheels (lathing is a process to make wheels perfectly rounded). The dataset of the first example illustrated in Figure 6.6 consists of three parts (named as dataset 1 dataset 2 and dataset 3), where the dataset 1 and dataset 3 are the stress ranges before lathing, and dataset 2 is the stress ranges after lathing (Figure 6.5). The dataset of the second example illustrated in Figure 6.8 contains only two parts (named as dataset 1 and dataset 2), where dataset 1 is the stress ranges before lathing and dataset 2 is the stress ranges after lathing (Figure 6.7).

The results of the first example by the proposed method are shown in Figure 6.6. Figure 6.6(a) compares the Bayes factor with the threshold $H_{min} = 10$. Throughout the entire process, all Bayes factor values are below the warning line except at time $t = 30$, which means the occurrence of only one outlier. Figure 6.6(b) presents the maximum cumulative Bayes factor for change detection. It is seen that the maximum cumulative Bayes factor is larger than 10 at times $t = 31$ and 81, which means that two notifications of change are issued separately at the two moments. Both run lengths are $l_t = 2$. So the real time of occurrence is at $t = 30$ and 80 respectively, which are well coincident with the time point of lathing the wheels. Then the monitoring stress ranges after the time $t =$

30 and $t = 80$ are used for damage identification and the results of logarithm of Bayes factor are shown in Figure 6.6(c). It is clear that most of values of logarithm of Bayes factor between $t = 30$ and $t = 80$ are larger than 100, exceeding the given threshold of $H_{min} = 10$, and their corresponding probabilities are approximately 100%, which give decisive evidence that the monitoring stress ranges during this time period are not in the same category as the stress ranges measured before lathing. While the values of logarithm of Bayes factor after time $t = 80$ are below than the threshold, which indicates the monitoring stress range during this period are in the same category as the stress ranges measured before lathing. The proposed algorithm satisfactorily detects the change of stress ranges and identifies the different patterns of stress ranges after the wheels are lathed.

The results of the second example by the proposed method are shown in Figure 6.8. Figure 6.8(a) compares the Bayes factor with the threshold $H_{min} = 10$. Throughout the entire process, all Bayes factors are below the warning line, which means no outlier occurrence. Figure 6.8(b) illustrates the maximum cumulative Bayes factor for change detection. It is seen that the maximum cumulative Bayes factor is larger than 10 at time $t = 57$, which means a notification of change is issued at this moment. The run length is $l_t = 2$. So the real time of occurrence is at $t = 56$, which is well coincident with the time point of lathing the wheels. Figure 6.8(c) shows the results of logarithm of Bayes factor.

It is clear that the values after time $t = 56$ are larger than 100, exceeding threshold of $H_{min} = 10$, and their corresponding probabilities are approximately 100%, which offer decisive evidence that the monitoring stress ranges after time $t = 56$ are not in the same category as the stress ranges measured before lathing. The state of the train wheels has changed at time $t = 56$. The proposed method effectively identifies the differences of monitoring data from the different structural states.

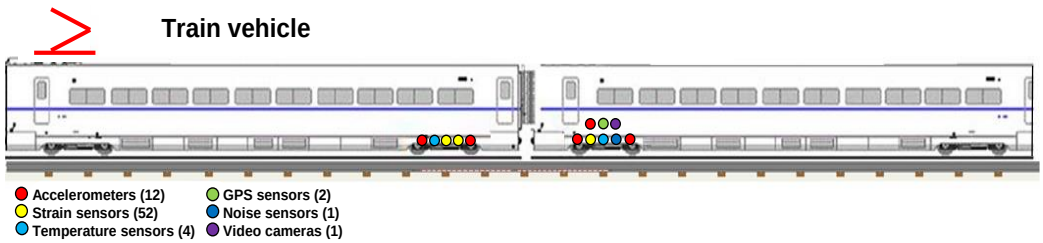

Figure 6.3 Onboard monitoring of an in-service high speed train

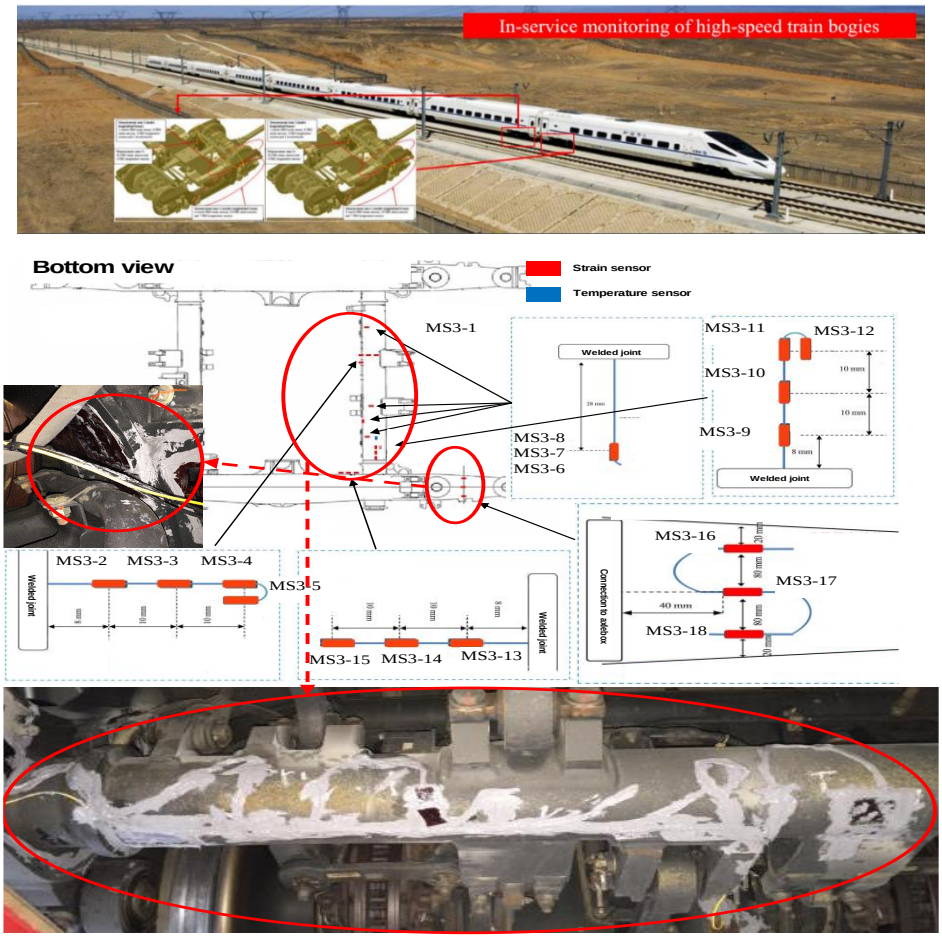

Figure 6.4 Locations of optical fiber strain sensors deployed on a bogie

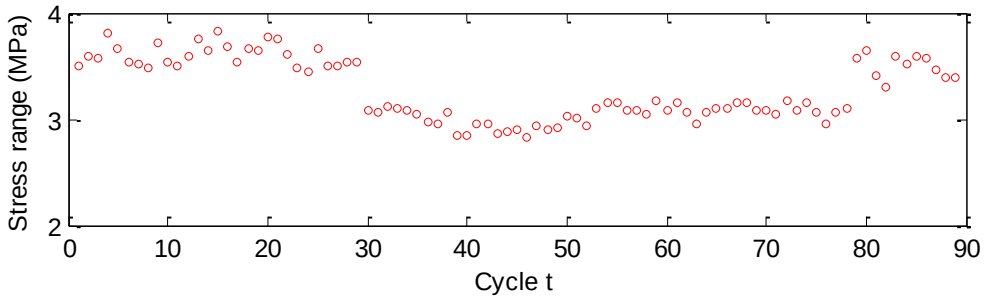

Figure 6.5 Time history of stress ranges (1st example)

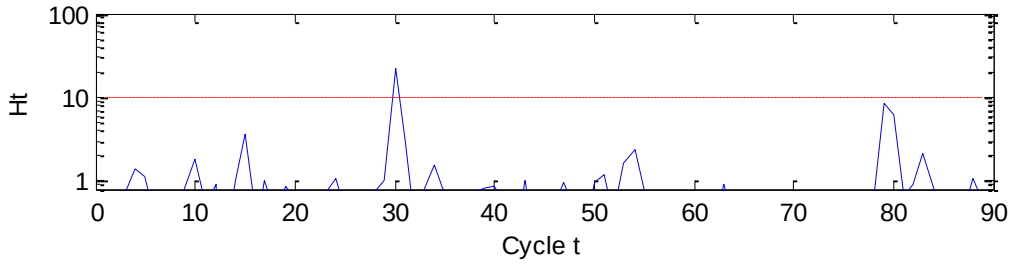

(a) Bayes factor

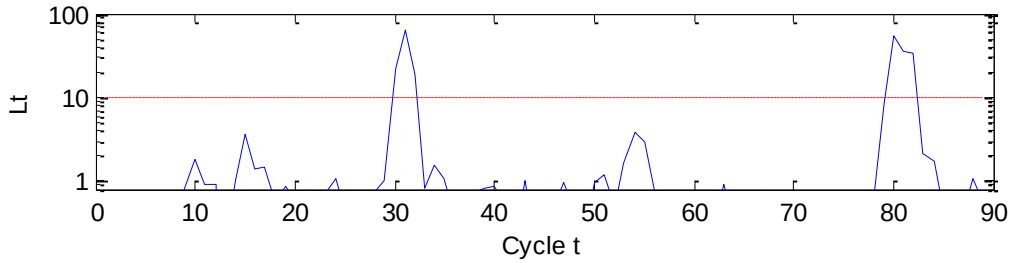

(b) Maximal cumulative Bayes factor

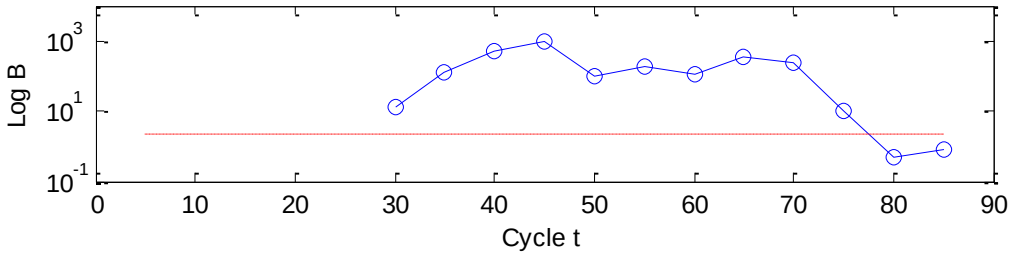

(c) Bayesian hypothesis testing

Figure 6.6 Bayes factor for outlier/change detection and damage assessment (1st example)

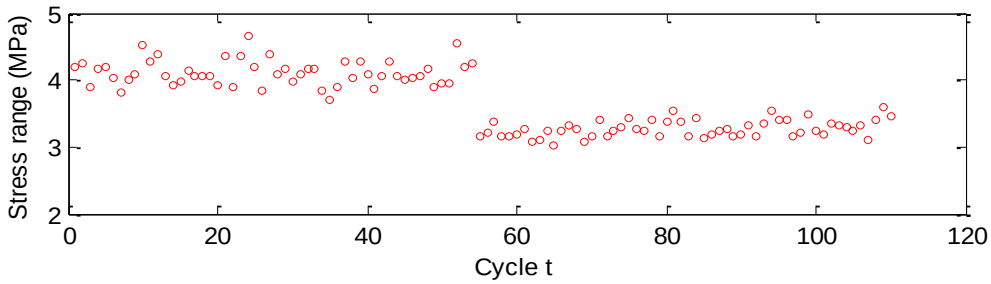

Figure 6.7 Time history of stress ranges (2nd example)

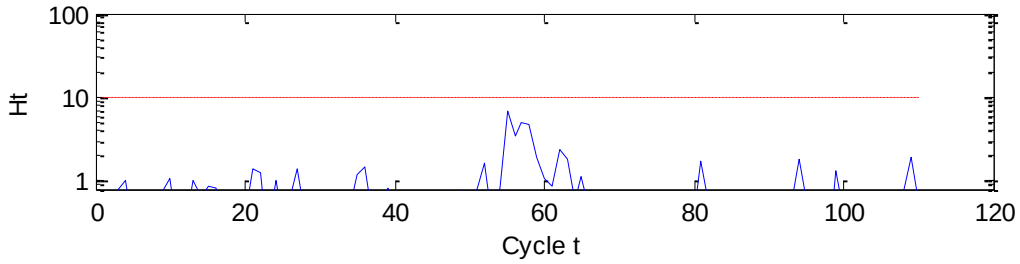

(a) Bayes factor

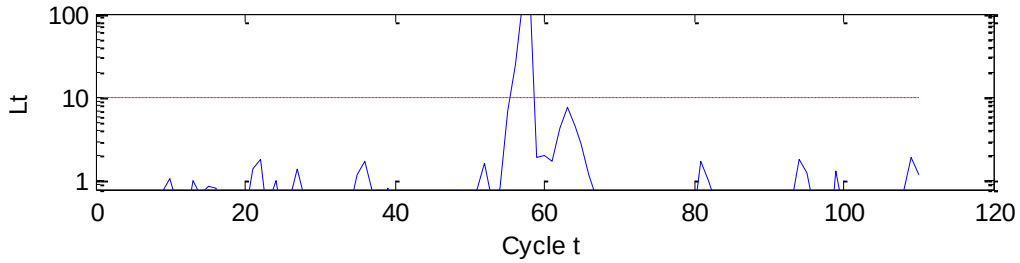

(b) Maximal cumulative Bayes factor

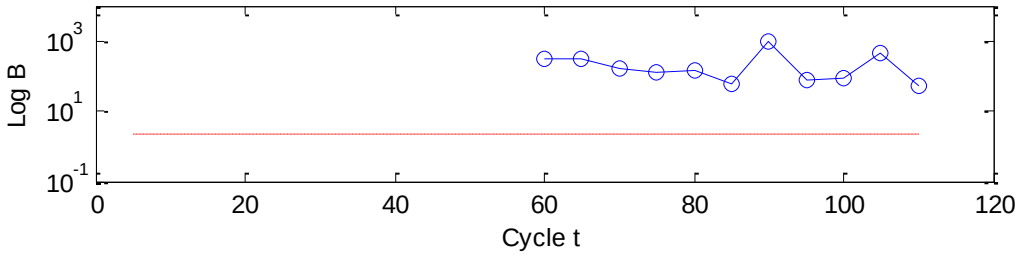

(c) Bayesian hypothesis testing

Figure 6.8 Bayes factor for outlier/change detection and damage assessment (2nd example)

6.3.2 Application 2: SMC benchmark bridge

The proposed damage detection method is then applied to a cable-stayed bridge with several observed damage patterns. All the data used in this section come from the 'SMC benchmark problem for condition assessment and damage detection' proposed by the Center of Structure Monitoring and Control (SMC) at the Harbin Institute of Technology, China. This benchmark structure is a cable-stayed bridge witnessing the bridge deck from health to damage and an SHM system recorded this process. The detailed information of the benchmark problem can be found at the benchmark homepage and relevant papers (Li *et al.* 2010, 2011, 2012, 2014). In the study here only acceleration data recorded by the SHM system from the bridge healthy status to damaged status are used to validate the proposed method. There are 14 accelerometers installed on the bridge deck of main span and two side spans, the sensor locations as shown in Figure 6.9.

Two sets of acceleration time history measured from the side span and the mid-main span are applied to validate the proposed damage detection method, as shown in Figures 6.10 and 6.12. The datasets covering 12 days witness the bridge deck from health to damage. To start with, the acceleration data are pre-processed to obtain the root mean square (RMS) of acceleration per hour.

The damage detection results for the RMS acceleration of side span (Acc 2) are shown in Figure 6.11. Figure 6.11(a) compares the Bayes factor with the threshold

$H_{min} = 10$. Throughout the entire process, all Bayes factors are below the warning line, which means no outlier occurrence. Figure 6.11(b) illustrates the maximum cumulative Bayes factor for change detection. It is seen that the maximum cumulative Bayes factor is larger than 10 at time $t = 147$, which means that a notification of change is issued at this moment. As the run length is $l_t = 4$, the real time of occurrence is at $t = 144$ which is exactly the time moment when the bridge was observed as being damaged (Li *et al.* 2014). Figure 6.11(c) shows the results of logarithm of Bayes factor. It is clear that the values of Bayes factor after TOC $t = 144$ exceed the given threshold of $H_{min} = 10$ and their corresponding probabilities are approximately 100%, which given very strong evidence that the acceleration responses of side span after TOC are not in the same category as before, and hence it is highly likely that damage occurred at that time moment.

Figure 6.13 shows the application of the proposed method to the RMS acceleration of mid-main span (Acc 8). Similar to the previous case, the maximum cumulative Bayes factor exceeds the specified threshold at the turning point $t = 144$. The logarithms of Bayes factor for damage signature are also greater than the specified threshold after the turning point $t = 144$, implying that the data favor the hypothesis H_1 and suggesting that there is damage.

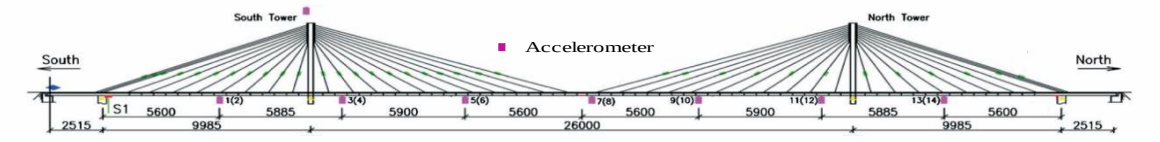

Figure 6.9 Layout of accelerometers in the benchmark bridge

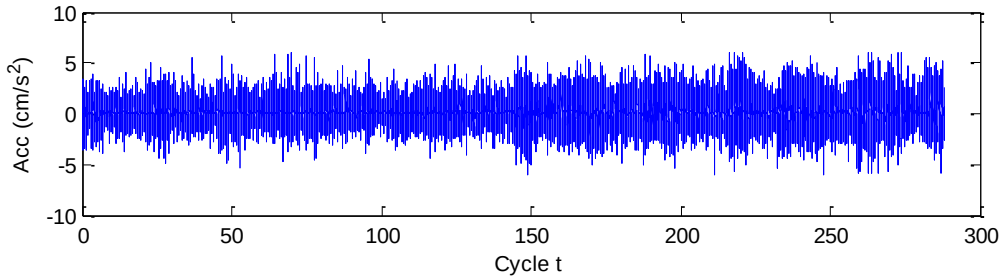

Figure 6.10 Time history of acceleration (side span)

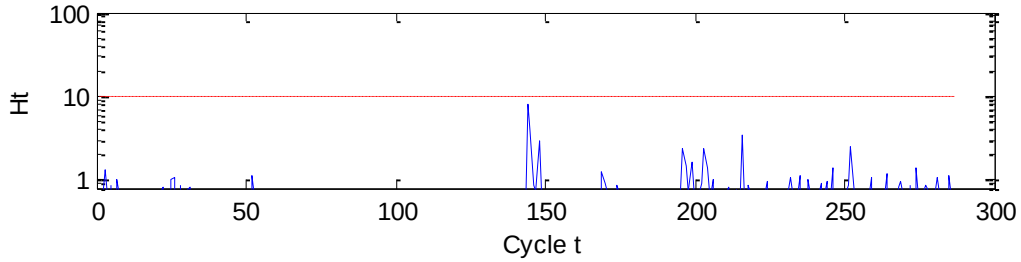

(a) Bayes factor

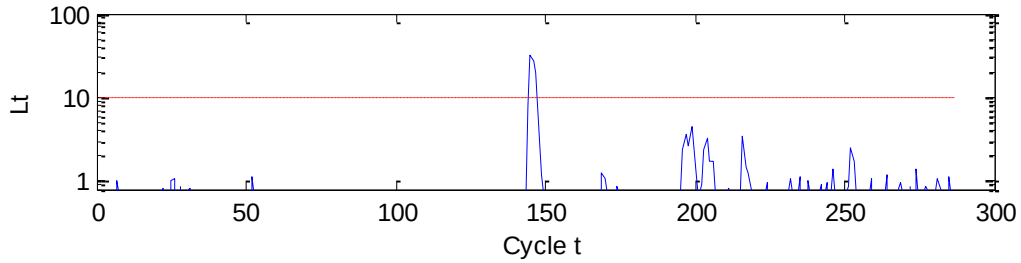

(b) Maximal cumulative Bayes factor

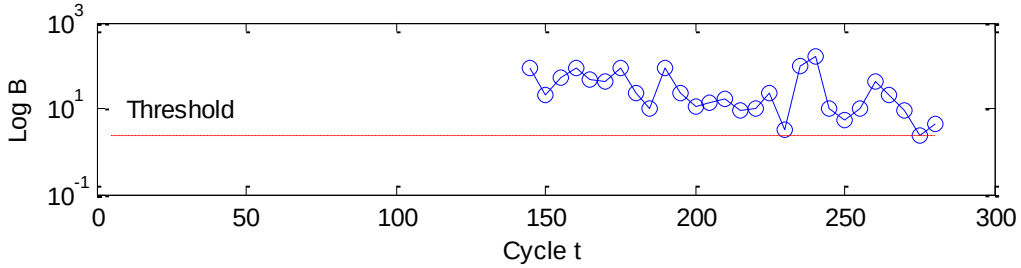

(c) Bayesian hypothesis testing

Figure 6.11 Bayes factor for outlier/change detection and damage detection (side span)

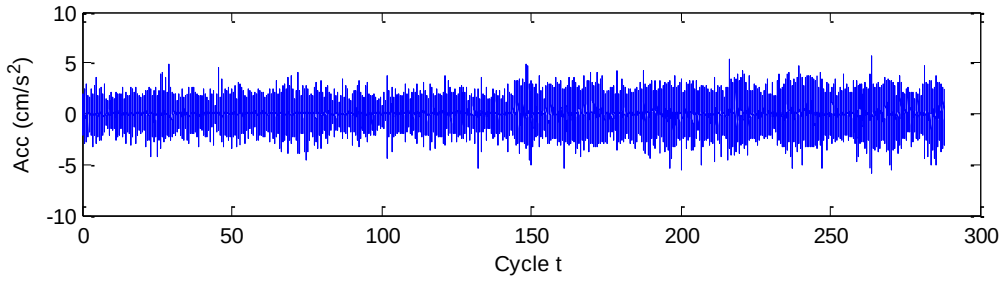

Figure 6.12 Time history of acceleration (mid-main span)

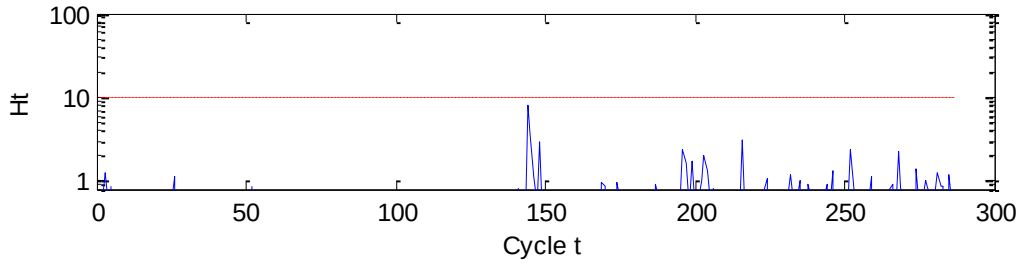

(a) Bayes factor

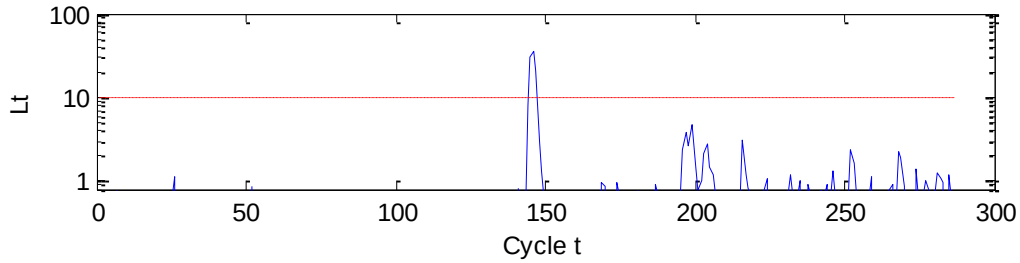

(b) Maximal cumulative Bayes factor

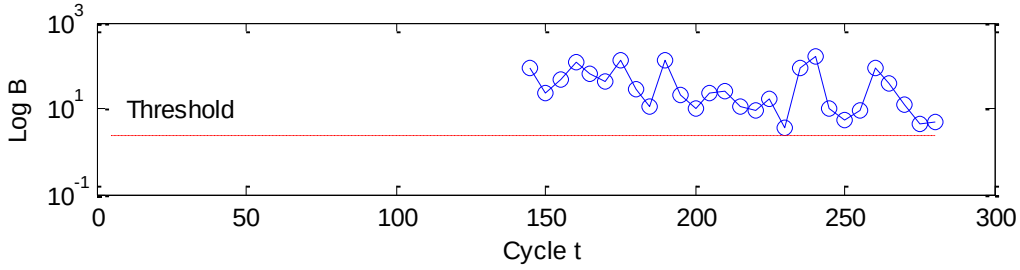

(c) Bayesian hypothesis testing

Figure 6.13 Bayes factor for outlier/change detection and damage detection (mid-main span)

6.4 Summary

A real-time damage detection algorithm based on Bayesian approach is developed and validated in this chapter. This algorithm consists two steps: outlier/change detection and damage assessment. The dynamic process is modeled by BDLM, where the order can be adjusted to satisfy the prognostic needs. The outlier/change detection is carried out by comparing the routine model (forecast distribution generated by the BDLM) with an alternative model (whose mean value is shifted by a prescribed offset). If the alternative model better fits the actual observation, a potential outlier/change is detected. To determine whether the current observation is an outlier or the beginning of a change, a judgement criterion based on Bayes factor and maximum cumulative Bayes factors is developed. The damage detection is conducted based on Bayesian hypothesis testing, which compares the structural response before and after the change point. The damage detection algorithm is investigated with the data collected from an in-service high-speed train and the SMC benchmark bridge. With the maximum cumulative Bayes factor, the exact time of lathing the train wheels is identified. The results of Bayesian hypothesis testing make clear that the two sets of stress ranges measured before and after lathing are not in the same category, indicating that the structure state has changed. Similarly, a signal of change is accurately triggered according to the maximum cumulative Bayes factor when damage occurs in the bridge. The results of Bayesian hypothesis testing also

indicate that the status of bridge has changed after TOC.

Chapter 7

Conclusions and Recommendations

7.1 Conclusions

In this PhD study, two methodologies including SHM-based structural condition assessment using Bayesian linear model (BLM) and Bayesian generalized linear model (BGLM), and structural condition prognosis and damage detection using Bayesian dynamical linear model (BDLM) are developed. The major findings from this study are summarized in the following:

(1) Bayesian linear model (BLM) is well suited for modeling the relationship between the displacement of expansion joints and the effective temperature of bridge deck. By using MCMC simulation analysis, the model parameters associated with their uncertainties are successfully estimated which are close to the analytical results. Based on the formulated BLM, an anomaly index is proposed for evaluating the probability of failure of expansion joints. The predicted mean displacements at the maximum and minimum temperatures are found close to the design values, but the upper bound of the predicted displacement ranges with 95% confidence interval exceeds the design criterion. It is suggested to increase the design values for the sake of expansion joint safety.

(2) An extended BLM termed as Bayesian generalized linear model (BGLM) is

proposed for assessing wind-induced displacement responses of bridges. Among a set of candidate models where each model considers different explanatory variables and orders of variables, the Bayesian model class selection technique is applied to choose the optimal model for capturing the true relationship between the wind-induced displacement and wind speed/direction. Both Log-ML and RMSE values show that Model M4 containing one order of the two explanatory variables, wind speed and direction, is the optimal one to fit the wind-induced displacement response. However, for predicting the displacement response under strong winds, Model M2 with quadratic term of wind speed performs better. This is because the quadratic term plays an important role in assessing wind-induced displacement when the wind speed is very large (such as 50m/s or above). The predicted maximum wind-induced displacement responses and the corresponding confidence interval under the design wind speed in serviceability limit state (SLS) are less than the design value.

(3) Bayesian dynamic linear model (BDLM) performs well in modeling the time-dependent responses of structures subject to external effects by superposing generic components, including baseline response, seasonal component, and regression component. In contrast to classical time series models, BDLM does not require the data series to be stationary and can provide structural response prediction along with their associated confidence interval to account for the response dynamics and uncertainty.

Moreover, the state space method directly contains a model error term, which makes the analysis more robust to mis-specification of the model. The effectiveness and robustness of the proposed method are illustrated and validated using the strain response acquired from an in-service cable-stayed bridge. According to three criteria, the selected optimal model performs well in one or several steps ahead prediction.

(4) A real-time damage detection method based on BDLM is developed and validated in two case studies. This method consists of two steps: outlier/change detection and damage detection. First the time-dependent responses of a structure are modelled by BDLM, where the generic components are adjusted to satisfy the prognostic needs. The outlier/change detection is carried out by comparing the routine model (forecast distribution generated by the BDLM) with an alternative model (whose mean value is shifted by a prescribed offset). If the alternative model better fits the actual observation, a potential outlier/change is detected. To determine whether the current observation is an outlier or the beginning of a change, a judgement criterion based on Bayes factor and maximum cumulative Bayes factor is developed. The damage detection is conducted by means of Bayesian hypothesis testing, which compares the structural response before and after the potential change point. The damage detection algorithm is illustrated with the monitoring data collected from an in-service high-speed train and from the SMC benchmark bridge. The signal of change is accurately triggered according to the

maximum cumulative Bayes factor when the structural damage/anomaly occurs. Then Bayesian hypothesis testing further confirm the extent of structural damage. The state change of the train before and after wheel lathing, and the damage of bridge deck are both successfully detected at the turning point.

7.2 Recommendations for Further Research

The development methods for structural health evaluation and prediction are still preliminary and in its infancy. To improve the proposed methods for more effective and practical applications, the following research issues are suggested to be pursued in the future:

(1) In most situations, the observed response may not be just a single value, but rather multiple responses. The Bayesian linear model and Bayesian generalized linear model can be generalized to multiple responses models, where the correlation in responses should be considered.

(2) The proposed BDLM in Chapter 5 for modeling the time-dependent responses of structure can handle multiple structural responses simultaneously. This dissertation only focuses on one response variable. To accommodate multiple responses cases, the model error covariance matrix should be redefined.

(3) To provide more reliable damage detection, a logic for interaction of detections

of multiple measurements could be implemented. At present, every measurement is run by the detection method separately and the signal of damage is also separately triggered. An enhanced logic would be to issue the damage warning when a certain percentage of all observed measurements signal anomaly.

(4) In proposed Bayesian dynamic linear model, the observational noise and system noise are assumed as Gaussian. However, in some applications, such as detection of structural changes of time series models, the necessity of non-Gaussian hypothesis becomes apparent. The proposed model can be extended to non-Gaussian state space model.

References

AASHTO. (2014). *LRFD Bridge Design Specifications (7th edition)*. American Association of State Highway and Transportation Officials, USA.

Akaike, H. (1974). "Markovian representation of stochastic processes and its application to the analysis of autoregressive moving average processes." *Annals of the Institute of Statistical Mathematics*, 26(1), 363-387.

Akgül, F., and Frangopol, D. M. (2003). "Rating and reliability of existing bridges in a network." *Journal of Bridge Engineering*, 8(6), 383-393.

Akgül, F., and Frangopol, D. M. (2004). "Bridge rating and reliability correlation: Comprehensive study for different bridge types." *Journal of Structural Engineering*, 130(7), 1063-1074.

Alston, C. L., Mengersen, K. L., and Pettitt, A. N. (2012). *Case Studies in Bayesian Statistical Modelling and Analysis*. John Wiley & Sons, New York, USA.

Ando, T. (2007). "Bayesian predictive information criterion for the evaluation of hierarchical Bayesian and empirical Bayes models." *Biometrika*, 94(2), 443-458.

Ando, T. (2010). *Bayesian Model Selection and Statistical Modeling*. CRC Press, New York, USA.

Annamdas, V. G. M., Bhalla, S., and Soh, C. K. (2017). "Applications of structural health

monitoring technology in Asia". *Structural Health Monitoring*, 16(3), 324-346.

Aoki, M. (1987). *State Space Modeling of Time Series*. Springer-Verlag, Heidelberg, Germany.

Arangio, S., and Beck, J. L. (2012). "Bayesian neural networks for bridge integrity assessment." *Structural Control and Health Monitoring*, 19(1), 3-21.

Arangio, S., and Bontempi, F. (2015). "Structural health monitoring of a cable-stayed bridge with Bayesian neural networks." *Structure and Infrastructure Engineering*, 11(4), 575-587.

Ashkenazi, V., and Roberts, G. W. (1997). "Experimental monitoring of the Humber Bridge using GPS." *Proceedings of the Institution of Civil Engineers - Civil Engineering*, 120 (4), 177-182.

Au, S. K. (2011). "Fast Bayesian FFT method for ambient modal identification with separated modes." *Journal of Engineering Mechanics*, 137(3), 214-226.

Au, S. K. (2012a). "Fast Bayesian ambient modal identification in the frequency domain, part I: posterior most probable value." *Mechanical Systems and Signal Processing*, 26, 60-75.

Au, S. K. (2012b). "Fast Bayesian ambient modal identification in the frequency domain, part II: posterior uncertainty." *Mechanical Systems and Signal Processing*, 26, 76-90.

Au, S. K., Ni, Y. C., Zhang, F. L., and Lam, H. F. (2012). "Full-scale dynamic testing and

modal identification of a coupled floor slab system." *Engineering Structures*, 37, 167-178.

Au, S. K., and Zhang, F. L. (2011). "On assessing the posterior mode shape uncertainty in ambient modal identification." *Probabilistic Engineering Mechanics*, 26(3), 427-434.

Au, S. K., Zhang, F. L., and Ni, Y. C. (2013). "Bayesian operational modal analysis: theory, computation, practice." *Computers & Structures*, 126, 3-14.

Barrish Jr, R. A., Grimmelsman, K. A., and Aktan, A. E. (2000). "Instrumented monitoring of the Commodore Barry bridge." *Proceedings of SPIE 3995, Nondestructive Evaluation of Highways, Utilities, and Pipelines IV,* Newport Beach, CA, USA.

Bayes, T. (1763). "An essay towards solving a problem in the doctrine of chances." *Philosophical Transactions of the Royal Society of London*, 53(1), 370–418.

Beck, J. L. (1989). "Statistical system identification of structures." *Proceedings of the International Conference on Structural Safety and Reliability*, San Francisco, USA.

Beck, J. L., Au, S. K., and Vanik, M. W. (2001). "Monitoring structural health using a probabilistic measure." *Computer-Aided Civil and Infrastructure Engineering*, 16(1), 1-11.

Beck, J. L., and Katafygiotis, L. S. (1998). "Updating models and their uncertainties. I:

Bayesian statistical framework." *Journal of Engineering Mechanics*, 124(4), 455-461.

Benchmark homepage. "SMC benchmark problems for conditions assessment and damage detection." http://smc.hit.edu.cn/index.php?option=com_content&view=article&id= 156&Itemid=81 (09 March 2013).

Bergermann, R., and Schlaich, M. (1996). "Ting Kau Bridge, Hong Kong." *Structural Engineering International*, 6(3), 152-154.

Bhattacharya, B., Li, D., Chajes, M., and Hastings, J. (2005). "Reliability-based load and resistance factor rating using in-service data." *Journal of Bridge Engineering*, 10(5), 530-543.

Brownjohn, J. M., and Moyo, P. (2001). "Monitoring of Singapore-Malaysia second link during construction." *Proceedings of SPIE 4317, 2nd International Conference on Experimental Mechanics*, Singapore.

Brownjohn, J. M., Pan, T. C., Mita, A., and Chow, K. F. (1998). "Dynamic and static response of Republic Plaza." *Journal-Institution of Engineers Singapore*, 38, 35-41.

Cardini, A. J., and DeWolf, J. T. (2009). "Long-term structural health monitoring of a multi-girder steel composite bridge using strain data." *Structural Health Monitoring*, 8(1), 47-58.

Casella, G., and George, E. I. (1992). "Explaining the Gibbs sampler." *The American Statistician*, 46(3), 167-174.

Catbas, F. N., Brown, D. L., and Aktan, A. E. (2006). "Use of modal flexibility for damage detection and condition assessment: case studies and demonstrations on large structures." *Journal of Structural Engineering*, 132(11), 1699-1712.

Catbas, F. N., Gul, M., and Burkett, J. L. (2007). "Damage assessment using flexibility and flexibility-based curvature for structural health monitoring." *Smart Materials and Structures*, 17(1), Paper No. 015024.

Cawley, P., and Adams, R. D. (1979). "The location of defects in structures from measurements of natural frequencies." *The Journal of Strain Analysis for Engineering Design*, 14(2), 49-57.

Chan, W. S. (2009). *Application of GPS for Monitoring Long-Span Cable-Supported Bridges under High Winds*. PhD thesis, The Hong Kong Polytechnic University, Hong Kong.

Chang, L. M., and Lee, Y. J. (2002). "Evaluation of performance of bridge deck expansion joints." *Journal of Performance of Constructed Facilities*, 16(1), 3-9.

Chang, P. C., Flatau, A., and Liu, S. C. (2003). "Health monitoring of civil infrastructure." *Structural Health Monitoring*, 2(3), 257-267.

Chen, X. (2012). "Prediction of buffeting response of long span bridges to transient nonstationary winds." *Proceedings of the 7th International Colloquium on Bluff Body Aerodynamics and Applications,* Shanghai, China.

Chen, X., and Kareem, A. (2001). "Equivalent static wind loads for buffeting response of bridges." *Journal of Structural Engineering*, 127(12), 1467-1475.

Cheng, J., and Xiao, R. C. (2006). "A simplified method for lateral response analysis of suspension bridges under wind loads." *Communications in Numerical Methods in Engineering*, 22(8), 861-874.

Cheung, M. S., Tadros, G. S., Brown, T., Dilger, W. H., Ghali, A., and Lau, D. T. (1997). "Field monitoring and research on performance of the Confederation Bridge." *Canadian Journal of Civil Engineering*, 24(6), 951-962.

Chib, S. (1995). "Marginal likelihood from the Gibbs output." *Journal of the American Statistical Association*, 90(432), 1313-1321.

Ching, J., and Leu, S. S. (2009). "Bayesian updating of reliability of civil infrastructure facilities based on condition-state data and fault-tree model." *Reliability Engineering & System Safety*, 94(12), 1962-1974.

Ching, J., Muto, M., and Beck, J. L. (2005). "Bayesian linear structural model updating using Gibbs sampler with modal data." *Proceedings of the 9th International Conference on Structural Safety and Reliability*, Rotterdam, Netherlands.

Cigada, A., Moschioni, G., Vanali, M., and Caprioli, A. (2010). "The measurement network of the San Siro Meazza Stadium in Milan: origin and implementation of a new data acquisition strategy for structural health monitoring." *Experimental*

Techniques, 34(1), 70-81.

Coelho, B. Z., Vervuurt, A. H. J. M., Peelen, W. H. A., and Leendertz, J. S. (2013). "Dynamics of modular expansion joints: the Martinus Nijhoff bridge." *Engineering Structures*, 48, 144-154.

Congdon, P. (2003). *Applied Bayesian Modelling*. John Wiley & Sons, London, UK.

Congdon, P. (2007). *Bayesian Statistical Modelling*. John Wiley & Sons, London, UK.

Cowles, M. K., and Carlin, B. P. (1996). "Markov chain Monte Carlo convergence diagnostics: a comparative review." *Journal of the American Statistical Association*, 91(434), 883-904.

Cox, R. T. (1961). *The Algebra of Probable Inference*. Johns Hopkins Press, Baltimore, USA.

Davids, W. G., Poulin, T. J., and Goslin, K. (2012). "Finite-element analysis and load rating of flat slab concrete bridges." *Journal of Bridge Engineering*, 18(10), 946-956.

Depaoli, S., and Boyajian, J. (2014). "Linear and nonlinear growth models: Describing a Bayesian perspective." *Journal of Consulting and Clinical Psychology*, 82(5), 784-802.

De Roeck, G., and Reynders, E. (2008). "Vibration monitoring as a diagnosis tool for structural condition assessment." *Computational Structural Dynamics and Earthquake Engineering (edited by Papadrakakis et al.)*, 2, 203-220.

Ding, Y., and Li, A. (2011). "Assessment of bridge expansion joints using long-term displacement measurement under changing environmental conditions." *Frontiers of Architecture and Civil Engineering in China*, 5(3), 374.

Dirbaz, M. (2013). *A Bayesian Updating Approach in Structural Health Monitoring for Damage Detection and Assessment*. PhD thesis, Illinois Institute of Technology, USA.

Doebling, S. W., Hemez, F. M., Peterson, L. D., and Farhat, C. (1997). "Improved damage location accuracy using strain energy-based mode selection criteria." *AIAA Journal*, 35(4), 693-699.

Dzunic, Z., Chen, J. G., Mobahi, H., Büyüköztürk, O., and Fisher, J. W. (2017). "A Bayesian state-space approach for damage detection and classification." *Mechanical Systems and Signal Processing*, 96, 239-259.

Enright, M. P., and Frangopol, D. M. (1998). "Service-life prediction of deteriorating concrete bridges." *Journal of Structural Engineering*, 124(3), 309-317.

Enright, M. P., and Frangopol, D. M. (1999). "Condition prediction of deteriorating concrete bridges using Bayesian updating." *Journal of Structural Engineering*, 125(10), 1118-1125.

Farrar, C. R., Baker, W. E., Bell, T. M., Cone, K. M., Darling, T. W., Duffey, T. A., and Migliori, A. (1994). *Dynamic Characterization and Damage Detection in the I-40 Bridge over the Rio Grande.* Report No. LA--12767-MS, Los Alamos National

Laboratory, NM, USA.

Farrar, C. R., and Jauregui, D. A. (1998). "Comparative study of damage identification algorithms applied to a bridge: II. numerical study." *Smart Materials and Structures*, 7(5), 720.

Farrar, C. R., and Lieven, N. A. (2007). "Damage prognosis: the future of structural health monitoring." *Philosophical Transactions of the Royal Society of London A: Mathematical, Physical and Engineering Sciences*, 365(1851), 623-632.

Farrar, C. R., and Worden, K. (2007). "An introduction to structural health monitoring." *Philosophical Transactions of the Royal Society of London A: Mathematical, Physical and Engineering Sciences*, 365(1851), 303-315.

Feinberg, S. E., and van der Linden, W. J. (2005). *Statistics for Social and Behavioral Sciences*. Springer, New York, USA.

Figueiredo, E., Radu, L., Worden, K., and Farrar Charles, R. (2014). "A Bayesian approach based on a Markov-chain Monte Carlo method for damage detection under unknown sources of variability." *Engineering Structures*, 80, 1-10.

Frangopol, D. M. (2011). "Life-cycle performance, management, and optimisation of structural systems under uncertainty: accomplishments and challenges." *Structure and Infrastructure Engineering*, 7(6), 389-413.

Frangopol, D.M., and Soliman, M. (2013). "Integration of structural health monitoring in

system based life-cycle infrastructure management under uncertainty." *Proceedings of the 6th International Conference on Structural Health Monitoring of Intelligent Infrastructure*, Hong Kong.

Frangopol, D. M., Strauss, A., and Kim, S. (2008). "Bridge reliability assessment based on monitoring." *Journal of Bridge Engineering*, 13(3), 258-270.

Frans, R., Arfiadi, Y., and Parung, H. (2017). "Comparative study of mode shapes curvature and damage locating vector methods for damage detection of structures." *Procedia Engineering*, 171, 1263-1271.

Fujino, Y., Murata, M., Okano, S., and Takeguchi, M. (2000). "Monitoring system of the Akashi Kaikyo Bridge and displacement measurement using GPS." *Proceedings of SPIE 3995, Nondestructive Evaluation of Highways*, *Utilities, and Pipelines IV*, Newport Beach, CA, USA.

Gelfand, A. E., and Smith, A. F. (1990). "Sampling-based approaches to calculating marginal densities." *Journal of the American Statistical Association*, 85(410), 398-409.

Geyskens, P., Kiureghian, A. D., and Monteiro, P. (1998). "Bayesian prediction of elastic modulus of concrete." *Journal of Structural Engineering*, 124(1), 89-95.

Gill, J. (2014). *Bayesian Methods: A Social and Behavioral Sciences Approach.* CRC Press, New York, USA.

Green, D., and Unruh, W. G. (2004). “Tacoma Bridge failure--a physical model.” a*rXiv Preprint Physics*, Paper No. 0408101.

Guan, H., Karbhari, V. M., and Sikorsky, C. S. (2006). “Web-based structural health monitoring of an FRP composite bridge.” *Computer-Aided Civil and Infrastructure Engineering,* 21(1), 39-56.

Guo, J., Xu, L., Dai, L., McDonald, M., Wu, J., and Li, Y. (2005). “Application of the real-time kinematic global positioning system in bridge safety monitoring.” *Journal of Bridge Engineering*, 10(2), 163-168.

Guo, T., Liu, J., Zhang, Y., and Pan, S. (2014). “Displacement monitoring and analysis of expansion joints of long-span steel bridges with viscous dampers.” *Journal of Bridge Engineering*, 20(9), Paper No. 04014099.

Hajializadeh, D., OBrien, E. J., and OConnor, A. (2017). “Virtual structural health monitoring and remaining life prediction of steel bridges.” *Canadian Journal of Civil Engineering*, 44, 264-273.

Harrison, J., and West, M. (1999). *Bayesian Forecasting & Dynamic Models (2nd edition)*. Springer-Verlag, New York, USA.

Harvey, A. C. (1990). *Forecasting, Structural Time Series Models and the Kalman Filter*. Cambridge University Press, Cambridge, UK.

Henrik, L. J., and Denmark, S. E. (2002). “Analyzing Europe’s largest suspension bridge.”

Proceedings of FIG XXII International Congress, Washington, USA.

Hoff, P. D. (2009). *A First Course in Bayesian Statistical Methods*. Springer, New York, USA.

Hong Kong Observatory. (2013). *Report of Tropical Cyclones in 2011*. Hong Kong.

Hong, W., Cao, Y., and Wu, Z. (2016). "Strain-based damage-assessment method for bridges under moving vehicular loads using long-gauge strain sensing." *Journal of Bridge Engineering*, 21(10), Paper No. 04016059.

Huang, Y., and Beck, J. L. (2015). "Hierarchical sparse Bayesian learning for structural health monitoring with incomplete modal data." *International Journal for Uncertainty Quantification*, 5(2), 139-169.

Jang, S., Jo, H., Cho, S., Mechitov, K., Rice, J. A., Sim, S. H., and Agha, G. (2010). "Structural health monitoring of a cable-stayed bridge using smart sensor technology: deployment and evaluation." *Smart Structures and Systems*, 6(5-6), 439-459.

Jang, S. A., Sim, S. H., and Spencer Jr, B. F. (2007). "Structural damage detection using static strain data." *Proceedings of the World Forum on Smart Materials and Smart Structures Technology*, Nanjing, China.

Jaynes, E. T. (1968). "Prior probabilities." *IEEE Transactions on Systems Science and Cybernetics*, 4(3), 227-241.

Jaynes, E. T. (1974). *Probability Theory with Applications in Science and Engineering*.

Washington University Press, USA.

Jaynes, E. T. (2003). *Probability Theory: the Logic of Science*. Cambridge University Press, Cambridge, UK.

Jeffreys, H. (1961). *Theory of Probability (3rd edition)*. Oxford Clarendon Press, Oxford, UK.

Jiang, X., Mahadevan, S., and Guratzsch, R. (2009). "Bayesian wavelet methodology for damage detection of thermal protection system panels." *AIAA Journal*, 47(4), 942-952.

Kalman, R. E. (1960a). "A new approach to linear filtering and prediction problems." *Journal of Basic Engineering*, 82(1), 35-45.

Kalman, R. E. (1960b). "Contributions to the theory of optimal control." *Boletin de la Sociedad Matematical Mexicana*, 5(2), 102-119.

Kalman, R. E., and Bucy, R. S. (1961). "New results in linear filtering and prediction theory." *Journal of Basic Engineering*, 83(1), 95-108.

Kaloop, M. R., Elbeltagi, E., and Elnabwy, M. T. (2015). "Bridge monitoring with wavelet principal component and spectrum analysis based on GPS measurements: case study of the Mansoura Bridge in Egypt." *Journal of Performance of Constructed Facilities*, 29 (3), Paper No. 04014071.

Kashima, S., Yanaka, Y., Suzuki, S., and Mori, K. (2001). "Monitoring the Akashi Kaikyo

bridge: first experiences." *Structural Engineering International*, 11(2), 120-123.

Kato, M., and Shimada, S. (1986). "Vibration of PC bridge during failure process." *Journal of Structural Engineering*, 112(7), 1692-1703.

Kim, J. T., and Stubbs, N. (2003). "Nondestructive crack detection algorithm for full-scale bridges." *Journal of Structural Engineering*, 129(10), 1358-1366.

Ko, J. M., and Ni, Y. Q. (2005). "Technology developments in structural health monitoring of large-scale bridges." *Engineering Structures*, 27(12), 1715-1725.

Koop, G. (2003). *Bayesian Econometric Methods*. John Wiley & Sons, New York, USA.

Koshiba, A., Abe, M., Sunaga, T., and Ishii, H. (2001). "Bridge inspection in steel road bridge based on real measurement." *Current and Future Trends in Bridge Design Construction and Maintenance* 2, 268-273.

Kullaa, J. (2003). "Damage detection of the Z24 bridge using control charts." *Mechanical Systems and Signal Processing*, 17(1), 163-170.

Kwon, S. D., Lee, H., Lee, S., and Kim, J. (2013). "Mitigating the effects of wind on suspension bridge catwalks." *Journal of Bridge Engineering*, 18(7), 624-632.

Laine, M., Latva-Pukkila, N., and Kyrölä, E. (2014). "Analysing time-varying trends in stratospheric ozone time series using the state space approach." *Atmospheric Chemistry and Physics*, 14(18), 9707-9725.

Lam, H. F., and Ng, C. T. (2008). "The selection of pattern features for structural damage

detection using an extended Bayesian ANN algorithm." *Engineering Structures*, 30(10), 2762-2770.

Lam, H. F., Yang, J., and Au, S. K. (2015). "Bayesian model updating of a coupled-slab system using field test data utilizing an enhanced Markov chain Monte Carlo simulation algorithm." *Engineering Structures*, 102,144-155.

Lam, H. F., Yuen, K. V., and Beck, J. L. (2006). "Structural health monitoring via measured Ritz vectors utilizing artificial neural networks." *Computer-Aided Civil and Infrastructure Engineering*, 21(4), 232-241.

Lee, L. S., Karbhari, V. M., and Sikorsky, C. (2007). "Structural health monitoring of CFRP strengthened bridge decks using ambient vibrations." *Structural Health Monitoring*, 6(3), 199-214.

Lee, S. Y. (2007). *Structural Equation Modeling: a Bayesian Approach*. John Wiley and Sons, England, UK.

Li, H., Lan, C. M., Ju, Y., and Li, D. S. (2011) "Experimental and numerical study of the fatigue properties of corroded parallel wire cables." *Journal of Bridge Engineering*, 17(2), 211-220.

Li, H., Li, S., Ou, J., and Li, H. (2010). "Modal identification of bridges under varying environmental conditions: temperature and wind effects." *Structural Control and Health Monitoring*, 17(5), 495-512.

Li, H., Li, S., Ou, J., and Li, H. (2012). "Reliability assessment of cable-stayed bridges based on structural health monitoring techniques." *Structure and Infrastructure Engineering*, 8(9), 829-845.

Li, H. N., Yi, T. H., Ren, L., Li, D. S., and Huo, L. S. (2014). "Reviews on innovations and applications in structural health monitoring for infrastructures." *Structural Monitoring and Maintenance*, 1(1), 1-45.

Li, S., Li, H., Liu, Y., Lan, C., Zhou, W., and Ou, J. (2014). "SMC structural health monitoring benchmark problem using monitored data from an actual cable-stayed bridge." *Structural Control and Health Monitoring*, 21(2), 156-172.

Li, J., and Hao, H. (2016). "A review of recent research advances on structural health monitoring in Western Australia." *Structural Monitoring and Maintenance*, 3(1), 33-49.

Lima, J. M., and de Brito, J. (2009). "Inspection survey of 150 expansion joints in road bridges." *Engineering Structures*, 31(5), 1077-1084.

Lin, M. W., and Thaduri, J. (2005). "Structural damage detection using an embedded ETDR distributed strain sensor." *Sensing and Imaging*, 6(4), 315-336.

Lindley, D. V., and Smith, A. F. (1972). "Bayes estimates for the linear model." *Journal of the Royal Statistical Society. Series B (Methodological)*, 1-41.

Lipowsky, H., Staudacher, S., Bauer, M., and Schmidt, K. J. (2010). "Application of

Bayesian forecasting to change detection and prognosis of gas turbine performance." *Journal of Engineering for Gas Turbines and Power*, 132(3), 031602.

Ma, Y., Wang, L., Zhang, J., Xiang, Y., and Liu, Y. (2014). "Bridge remaining strength prediction integrated with Bayesian network and in situ load testing." *Journal of Bridge Engineering*, 19(10), Paper No. 04014037.

Ma, Y., Zhang, J., Wang, L., and Liu, Y. (2013). "Probabilistic prediction with Bayesian updating for strength degradation of RC bridge beams." *Structural Safety*, 44, 102-109.

Magalhães, F., Cunha, Á., and Caetano, E. (2008). "Dynamic monitoring of a long span arch bridge." *Engineering Structures*, 30(11), 3034-3044.

Magalhães, F., Cunha, A., and Caetano, E. (2010). "Continuous dynamic monitoring of an arch bridge: strategy to eliminate the environmental and operational effects and detect damages." *Proceedings of 24th International Conference on Noise and Vibration Engineering*, Leuven, Belgium.

Mekjavić, I. (2015). "Identification of structural damage in bridges using high-frequency vibrational responses." *Shock and Vibration,* 2015, Paper No. 906062.

Migon, H. S., Gamerman, D., and Louzada, F. (2014). *Statistical Inference: An Integrated Approach (2nd edition)*. CRC Press, New York, USA.

Miyata, T., Yamada, H., Katsuchi, H., and Kitagawa, M. (2002). "Full-scale measurement

of Akashi–Kaikyo Bridge during typhoon." *Journal of Wind Engineering and Industrial Aerodynamics*, 90(12), 1517-1527.

Moradipour, P., Chan, T. H., and Gallage, C. (2015). "An improved modal strain energy method for structural damage detection, 2D simulation." *Structural Engineering and Mechanics*, 54(1), 105-119.

Nakamura, S. I. (2000). "GPS measurement of wind-induced suspension bridge girder displacements." *Journal of Structural Engineering*, 126(12), 1413-1419.

Ni, Y. Q., Ko, J. M., Zhou, H. F., and Hua, X. G. (2004). "Challenges in developing structural health monitoring system for a long-span cable-stayed bridge." *Proceedings of the US–Korea Joint Seminar/Workshop on Smart Structures Technologies*, Seoul, Korea.

Ni, Y. Q., Hua, X. G., Wong, K. Y., and Ko, J. M. (2007). "Assessment of bridge expansion joints using long-term displacement and temperature measurement." *Journal of Performance of Constructed Facilities*, 21(2), 143-151.

Ni, Y. Q., Wong, K. Y., and Xia, Y. (2011). "Health checks through landmark bridges to sky-high structures." *Advances in Structural Engineering*, 14(1), 103-119.

Ni, Y. Q., Xia, H. W., Wong, K. Y., and Ko, J. M. (2012). "In-service condition assessment of bridge deck using long-term monitoring data of strain response." *Journal of Bridge Engineering*, 17(6), 876-885.

Ni, Y. Q., Xia, Y., Liao, W. Y., and Ko, J. M. (2009). "Technology innovation in developing the structural health monitoring system for Guangzhou New TV Tower." *Structural Control and Health Monitoring*, 16(1), 73-98.

Ni, Y. Q., Zhou, H. F., Chan, K. C., and Ko, J. M. (2008). "Modal flexibility analysis of cable-stayed Ting Kau Bridge for damage identification." *Computer-Aided Civil and Infrastructure Engineering*, 23(3), 223-236.

O'Hagan, A. (2004). "Bayesian statistics: principles and benefits." *Frontis*, 3, 31-45.

Pandey, A. K., and Biswas, M. (1994). "Damage detection in structures using changes in flexibility." *Journal of Sound and Vibration*, 169(1), 3-17.

Pandey, A. K., and Biswas, M. (1995). "Experimental verification of flexibility difference method for locating damage in structures." *Journal of Sound and Vibration*, 184(2), 311-328.

Peeters, B., Maeck, J., and De Roeck, G. (2001). "Vibration-based damage detection in civil engineering: excitation sources and temperature effects." *Smart Materials and Structures*, 10(3), 518.

Petris, G., Petrone, S., and Campagnoli, P. (2009). *Dynamic Linear Models with R.* Springer, New York, USA.

Phares, B., Lu, P., Wipf, T., Greimann, L., and Seo, J. (2013a). "Evolution of a bridge damage-detection algorithm." *Transportation Research Record: Journal of the*

Transportation Research Board, 2331, 71-80.

Phares, B., Lu, P., Wipf, T., Greimann, L., and Seo, J. (2013b). "Field validation of a statistical-based bridge damage-detection algorithm." *Journal of Bridge Engineering*, 18(11), 1227-1238.

Pole, A., West, M., and Harrison, J. (1994). *Applied Bayesian Forecasting and Time Series Analysis*. CRC Press, New York, USA.

Rachev, S. T., Hsu, J. S., Bagasheva, B. S., and Fabozzi, F. J. (2008). *Bayesian Methods in Finance*. John Wiley & Sons, New York, USA.

Rafiq, M. I., Chryssanthopoulos, M. K., and Sathananthan, S. (2015). "Bridge condition modelling and prediction using dynamic Bayesian belief networks." *Structure and Infrastructure Engineering*, 11(1), 38-50.

Raftery, A. E., and Lewis, S. (1992). "How many iterations in the Gibbs sampler." *Bayesian Statistics*, 4(2), 763-773.

Raiffa, H. (2000). *Applied Statistical Decision Theory*. John Wiley & Son, New York, USA.

Raziq, N., and Collier, P. (2007). "GPS deflection monitoring of the West Gate Bridge." *Journal of Applied Geodesy*, 1(1), 35-44.

Roberts, G. O., and Smith, A. F. (1994). "Simple conditions for the convergence of the Gibbs sampler and Metropolis-Hastings algorithms." *Stochastic Processes and Their*

Applications, 49(2), 207-216.

Roberts, G. W., Brown, C., and Meng, X. (2005). "Deflection monitoring of the Forth Road Bridge by GPS." *Proceedings of 18th International Technical Meeting of the Satellite Division*, Long Beach, CA, USA.

Roeder, C. W. (1998). "Fatigue and dynamic load measurements on modular expansion joints." *Construction and Building Materials*, 12(2), 143-150.

Rossi, P. E., Allenby, G. M., and McCulloch, R. (2012). *Bayesian Statistics and Marketing*. John Wiley & Sons, New York, USA.

Sankararaman, S., and Mahadevan, S. (2013). "Bayesian methodology for diagnosis uncertainty quantification and health monitoring." *Structural Control and Health Monitoring*, 20(1), 88-106.

Scianna, A., and Jang, S. (2011). "Model-free modal flexibility-based damage detection strategy for in-service highway bridges." *Proceedings of SPIE 7981, Sensors and Smart Structures Technologies for Civil, Mechanical, and Aerospace Systems,* San Diego, California, USA.

Seo, J., Hu, J. W., and Lee, J. (2015). "Summary review of structural health monitoring applications for highway bridges." *Journal of Performance of Constructed Facilities*, 30(4), Paper No. 04015072.

Seo, J., Phares, B., Lu, P., Wipf, T., and Dahlberg, J. (2013). "Bridge rating protocol using

ambient trucks through structural health monitoring system." *Engineering Structures*, 46, 569-580.

Shi, Z., Law, S. S., and Zhang, L. M. (1998). "Structural damage localization from modal strain energy change." *Journal of Sound and Vibration*, 218(5), 825-844.

Shi, Z. Y., Law, S. S., and Zhang, L. M. (2000). "Structural damage detection from modal strain energy change." *Journal of Engineering Mechanics*, 126(12), 1216-1223.

Sohn, H. (1997). "A Bayesian probabilistic approach for structure damage detection." *Earthquake Engineering and Structural Dynamics*, 26, 1259-1281.

Sohn H., and Law K. H. (2001). "Damage diagnosis using experimental Ritz vectors." *Journal of Engineering Mechanics*, 127(11), 1184-1193.

Stone, J. V. (2013). *Bayes' Rule: A Tutorial Introduction to Bayesian Analysis*. Sebtel Press, Sheffield, UK.

Sung, S. H., Koo, K. Y., and Jung, H. J. (2014). "Modal flexibility-based damage detection of cantilever beam-type structures using baseline modification." *Journal of Sound and Vibration*, 333(18), 4123-4138.

Takao, M., and Takao, N. (2015). "Health monitoring of high-rise building with fiber optic sensor (SOFO)." *International Journal of High Rise Buildings*, 4(1), 27-37.

Teughels, A., and De Roeck, G. (2004). "Structural damage identification of the highway bridge Z24 by FE model updating." *Journal of Sound and Vibration*, 278(3), 589-610.

Turer, A., and Shahrooz, B. M. (2011). "Load rating of concrete-deck-on-steel-stringer bridges using field-calibrated 2D-grid models." *Engineering Structures*, 33(4), 1267-1276.

van Dijk, R., and van den Boom, H. (2007). "Full scale monitoring Marco Polo tension leg platform." *Proceedings of the 26th International Conference on Offshore Mechanics and Arctic Engineering*, San Diego, California, USA.

Vanik, M. W., Beck, J. L., and Au, S. (2000). "Bayesian probabilistic approach to structural health monitoring." *Journal of Engineering Mechanics*, 126(7), 738-745.

Wahab, M. A., and De Roeck, G. (1999). "Damage detection in bridges using modal curvatures: application to a real damage scenario." *Journal of Sound and Vibration*, 226(2), 217-235.

Wang, G. X., and Ding, Y. L. (2014). "Mathematical modeling for lateral displacement induced by wind velocity using monitoring data obtained from main girder of Sutong cable-stayed bridge." *Mathematical Problems in Engineering*, Paper No. 723152.

Wang, X., and Ni, Y. Q. (2016). "Analysis of influence of mean stress on fatigue life of in-service high-speed train bogies using monitoring data." *Proceedings of the 3rd International Conference on Railway Technology: Research, Development and Maintenance*, Cagliari, Sardinia, Italy.

Wang, Z., and Ong, K. C. G. (2009). "Multivariate statistical approach to structural

damage detection." *Journal of Engineering Mechanics*, 136(1), 12-22.

Wong, K. Y. (2004). "Instrumentation and health monitoring of cable-supported bridges." *Structural Control and Health Monitoring*, 11(2), 91-124.

Wong, K. Y. (2007). "Design of a structural health monitoring system for long-span bridges." *Structure and Infrastructure Engineering*, 3(2), 169-185.

Wong, K. Y., Man, D. K. L., and Chan, W. Y. K. (2001). "Application of global positioning system to structural health monitoring of cable-supported bridges." *Proceedings of SPIE 4337, Health Monitoring and Management of Civil Infrastructure Systems*, Newport Beach, CA, USA.

Wong, K. Y., Man, D. K. L., and Chan, K. W. Y. (2002). "Thermal load and response monitoring of Ting Kau cable-stayed Bridge." *Proceedings of International Conference. on Innovation and Sustainable Development of Civil Engineering in the 21st Century*, China Civil Engineering Society, Beijing, China.

Woodworth, G. G. (2004). *Biostatistics: A Bayesian Introduction*. John Wiley & Sons, New York, USA.

Xu, L., Guo, J. J., and Jiang, J. J. (2002). "Time-frequency analysis of a suspension bridge based on GPS." *Journal of Sound and Vibration*, 254(1), 105-116.

Xu, Y. L., and Chan, W. S. (2009). "Wind and structural monitoring of long span cable-supported bridges with GPS." *Proceedings of the 7th Asia-Pacific Conference on*

Wind Engineering, Taipei, Taiwan.

Xu, Z. D., Zeng, X., and Li, S. (2013). "Damage detection strategy using strain-mode residual trends for long-span bridges." *Journal of Computing in Civil Engineering*, 29(5), Paper No. 04014064.

Yan, W. J., Ren, W. X., and Huang, T. L. (2012). "Statistic structural damage detection based on the closed-form of element modal strain energy sensitivity." *Mechanical Systems and Signal Processing*, 28, 183-194.

Yan, Y. J., Yang, H. F., Wu, Z. Y., and Ge, X. (2010). "Damage detection method for composite structures based on a combined technique of cross modal strain energy and niche genetic algorithms." *Journal of Vibration and Control*, 16(11), 1673-1683.

Yao, Y., and Glisic, B. (2015). "Detection of steel fatigue cracks with strain sensing sheets based on large area electronics." *Sensors*, 15(4), 8088-8108.

Yuen, K. V. (2010). *Bayesian Methods for Structural Dynamics and Civil Engineering*. John Wiley & Sons, New York, USA.

Yuen, K. V., and Kuok, S. C. (2010). "Modeling of environmental influence in structural health assessment for reinforced concrete buildings." *Earthquake Engineering and Engineering Vibration*, 9(2), 295-306.

Zellner, A. (1996). *An Introduction to Bayesian Inference in Econometrics*. John Wiley & Sons, New York, USA.

Zellner, A., and Chetty, V. K. (1965). "Prediction and decision problems in regression models from the Bayesian point of view." *Journal of the American Statistical Association*, 60(310), 608-616.

Zhang, Q., Yang, B., Liu, T., Li, H., and Lv, J. (2015). "Structural health monitoring of Shanghai tower considering time-dependent effects." *International Journal of High Rise Buildings*, 4(1), 39-44.

Zhang, R., and Mahadevan, S. (2000). "Model uncertainty and Bayesian updating in reliability-based inspection." *Structural Safety*, 22(2), 145-160.

Zhu, B., and Frangopol, D. M. (2013). "Reliability assessment of ship structures using Bayesian updating." *Engineering Structures*, 56, 1836-1847.